Economic time-lapse seismic acquisition and imaging—Reaping the benefits of randomized sampling with distributed Compressive Sensing

by

Felix Onovughe Oghenekohwo

B.Sc., (Physics) University of Ibadan, Nigeria, 2007

M.Sc., (Geology) University of Cape Town, South Africa, 2010

A THESIS SUBMITTED IN PARTIAL FULFILLMENT
OF THE REQUIREMENTS FOR THE DEGREE OF

Doctor of Philosophy

in

THE FACULTY OF GRADUATE AND POSTDOCTORAL STUDIES
(Geophysics)

The University of British Columbia
(Vancouver)

August 2017

Abstract

This thesis presents a novel viewpoint on the implicit opportunities randomized surveys bring to time-lapse seismic - which is a proven surveillance tool for hydrocarbon reservoir monitoring. Time-lapse (4D) seismic combines acquisition and processing of at least two seismic datasets (or vintages) in order to extract information related to changes in a reservoir within a specified time interval. The current paradigm places stringent requirements on replicating the 4D surveys, which is an expensive task often requiring uneconomical dense sampling of seismic wavefields. To mitigate the challenges of dense sampling, several advances in seismic acquisition have been made in recent years including the use of multiple sources firing at near simultaneous random times, and the adaptation of Compressive Sensing (CS) principles to design practical acquisition engines that improve sampling efficiency for seismic data acquisition. However, little is known regarding the implications of these developments for time-lapse studies. By conducting multiple experiments modelling surveys adhering to the principles of CS for 4D seismic, I propose a model that demonstrates the feasibility of randomized acquisitions for time-lapse seismic. The proposed joint recovery model (JRM), which derives from distributed CS, exploits the common information in time-lapse data during recovery of dense wavefields from measured subsampled data, providing highly repeatable and high-fidelity vintages. I show that we obtain better vintages when randomized surveys are not replicated, in contrast to standard practice, paving the way for an opportunity to relax the rigorous requirement to replicate surveys precisely. We assert that the vintages obtained using our proposed model are of sufficient quality to serve as inputs to processes that extract time-lapse attributes from which subsurface changes are deduced. Additionally, I show that recovery with the JRM is robust with respect to errors due to differences between actual and recorded postplot information. Finally, I present an opportunity to adapt our model to problems related to time-lapse seismic imaging where the main finding is that we can better delineate time-lapse changes by adapting the joint recovery model to wave-equation based inversion methods.

Lay Summary

Time-lapse seismic technology, used for hydrocarbon reservoir monitoring, involves processing at least two seismic surveys acquired over a specified time interval in order to deduce changes within the reservoir in that time. In order to make reliable deductions, the current practice requires repeating the seismic surveys as much as possible - a task that is both expensive and technically challenging for a variety of reasons. Compressive sensing (CS) is a new sampling paradigm that has been adapted to reduce cost of seismic surveys; however, its application to time-lapse seismic raises concerns as well as possibilities. By leveraging insights from distributed CS, I propose the use of a joint recovery model (JRM) to process data acquired based on ideas from CS. Interestingly, I find that we obtain high-quality time-lapse data when the surveys are not repeated, providing an opportunity to relax the current strict requirement to repeat surveys precisely.

Preface

This thesis consists of both my sole and collaborative research projects, conducted under the supervision of Professor Felix Herrmann in the Seismic Laboratory for Imaging and Modelling (SLIM) at the University of British Columbia, Vancouver, Canada. My supervisor was extensively involved in all my projects as the supervisory author, from topic formalism to manuscript revisions. The thesis comprises chapters containing previously published or submitted work.

A version of Chapter 2 was published in (Oghenekohwo et al., 2017), which significantly extends earlier conference proceedings in (Oghenekohwo et al., 2014a). I was the principal investigator, sourcing the relevant literature, preparing the original manuscript including providing background information on the theoretical and practical aspects of the subject area. I set up, conducted and analyzed the results of the stylized experiments based on compressive sensing and I also wrote the section on stylized experiments. Ernie Esser was involved in the algorithm evaluation from the outset. Haneet Wason setup and conducted the seismic experiments, contributed to and wrote the seismic experiment sections. Felix Herrmann was extensively involved in writing the discussion and conclusion sections. Given the equivalent significant contributions made by Haneet and me, we mutually agreed to include this chapter in our respective PhD dissertations. This chapter appears verbatim as chapter 5 in Haneet Wason's PhD dissertation. I granted permission for this chapter to also appear in Haneet Wason's dissertation.

A version of Chapter 3 was published in (Wason et al., 2017), which significantly extends earlier conference proceedings in (Wason et al., 2014a) and (Wason et al., 2015a). Haneet Wason was the lead investigator and primary contributor in this chapter, conducting the seismic experiments and composing the original manuscript. This chapter is a necessary extension of Chapter 2 where I started investigating the research idea at the advise of Felix Herrmann. I also contributed to a SEAM time-lapse model simulation in the experiments as well as evaluation of the results and conclusions. Felix Herrmann was largely involved in the theoretical, discussion and conclusion sections. This chapter also appears verbatim as chapter 6 in Haneet Wason's PhD dissertation. Since this chapter is a necessary extension of Chapter 2, Haneet has granted permission for this chapter to also appear in my dissertation.

A version of Chapter 4 has been published as [Oghenekohwo, F. and F.J. Herrmann, 2017, Highly repeatable time-lapse seismic with distributed Compressive Sensing—mitigating effects of calibration errors] to a special section on Compressive Sensing in The Leading Edge journal publication. This article significantly extends the conference proceedings in (Oghenekohwo and Herrmann, 2017). I was the lead investigator, formulated the concept, composed the manuscript subject to some editorial corrections from Felix Herrmann.

A version of Chapter 5 was published as two separate extended abstracts — (Oghenekohwo et al., 2014c) and (Oghenekohwo et al., 2015) — in different conference proceedings. I was the lead investigator in these projects. In the first abstract, Rajiv Kumar contributed to the concept formation. In the second abstract, both Rajiv Kumar and Ernie Esser contributed to the concept formation and algorithm development. I composed both manuscripts, simulated the experiments and presented the findings at the respective meetings. Felix Herrmann edited the respective papers.

Table of Contents

List of Tables

List of Figures

Acknowledgments

Firstly, I wish to extend unreserved gratitude to my PhD advisor, Dr. Felix Herrmann, who is also the director of the Seismic Laboratory for Imaging and Modelling (SLIM) at UBC. Felix ensured my research was of the highest standard and not only has this practice made me a smarter person today, it continues to enhance my critical thinking ability. I am thankful for the opportunities Felix provided me to gain exposure on several occasions at various international conferences. In addition, the financial support I received from Felix through the sponsors of SLIM has come in quite handy, making living in Vancouver possible. For these and many more, I am thankful.

I am equally thankful to my PhD supervisory committee comprising Dr. Erik Eberhardt and Dr. Roger Beckie whose availability and pieces of advice during committee meetings and at random times, made the PhD process at UBC less daunting.

Adapting to my new environment when I first arrived Vancouver for my PhD would have been really challenging if not for the warm welcome and homely atmosphere provided by Prof. Douw Steyn, and his lovely family (Margaret and Jo-Hanna). Douw's recommendation made my UBC dream a reality and his constant guidance over the years has been tremendous.

Past and current members of SLIM have played diverse roles in the course of my studies at UBC. I appreciate the time spent here discussing several interesting projects that has led to fruitful collaborations with a few colleagues including Rajiv Kumar and Haneet Wason. The support I received from Henryk Modzelewski and Miranda Joyce has been extremely valuable. I miss Ernie Esser who unfortunately passed away in March 2015, and whose valuable contributions culminated in my first published journal article. Sadly, Ernie was not able to witness this work and a few notable publications at SLIM.

Finding a safe haven where I can share my concerns with brethren has been a constant part of my academic journey. At UBC, I found my safe haven in fellowship with friends I made at both Christ Embassy and The Restored House Chapel. My friends and pastors have been extremely encouraging and supportive. I am very thankful for this.

I am blessed to be born into a family that loves me unconditionally. I value and appreciate the love, encouragement and prayers of my mother (Agnes Oghenekohwo) and siblings (Alex, Tega, Ejiro, Ogaga, Silas, Akpevwe) back at home in Nigeria. Several members of my extended family have also been supportive and are duly acknowledged. This thesis is dedicated to my late dad (Francis Oghenekohwo) who sadly passed away in November 2015. It was my wish to have him grace my PhD graduation ceremony.

Pursuing my dream of a PhD at UBC, at first away from my beloved wife Zubeida, and children (Liam, Noah, Rukevwe), was one of the most difficult decisions I had to make. Thankfully, I am blessed with the most understanding and patient wife and family including our newest addition, Fejiro. I love you all dearly and I thank you for your endurance while I completed my studies.

Finally, all praise be to my maker who made my PhD dream a reality.

Chapter 1

Introduction

1.1 Principle of time-lapse seismic

In order to optimize production from hydrocarbon reservoirs, practitioners monitor the reservoir for changes in some physical properties of interest (e.g., fluid saturation, temperature, pressure). A tool used for this monitoring is time-lapse (4D) seismic technology whereby seismic data are acquired at specified time intervals over an area of interest followed by data processing to extract information related to the changes in the constituent rock and fluid properties of the reservoir within the survey area. Basically, time-lapse seismic technology involves (1) the acquisition of at least two seismic datasets — the first survey is called the baseline while subsequent surveys are called monitors or *repeat* surveys — over an area where the subsurface reservoir properties change with time; (2) processing of the datasets (or vintages) to obtain time-lapse images; (3) comparison of the images in order to quantify dynamic changes in some physical properties of the reservoir.

Although 4D seismic has been successfully applied for reservoir monitoring (Koster et al., 2000; Lumley, 2001; Fanchi, 2001) and CO_2 sequestration (Lumley, 2010; Chadwick et al., 2010), the technology remains challenging due to its reliance on dense sampling and requirement for replicated surveys each of which have their challenges that will be reviewed later. Before I discuss these challenges, I will describe the basics of seismic acquisition and the link to time-lapse seismic.

1.1.1 Seismic acquisition

Conventional method of acquiring seismic data entails firing seismic sources or shots at regular time intervals while receivers (sensors) record the pressure wavefield reflected from the interfaces in the earth's subsurface. Seismic surveys can either be done on land (onshore) or in a marine environment (offshore). Figure 1.1 illustrates a typical marine survey with receivers (streamers) towed behind a survey vessel with

a source array (two or more airguns). Ocean bottom seismic surveys have receivers (nodes or cables) placed at the sea floor.

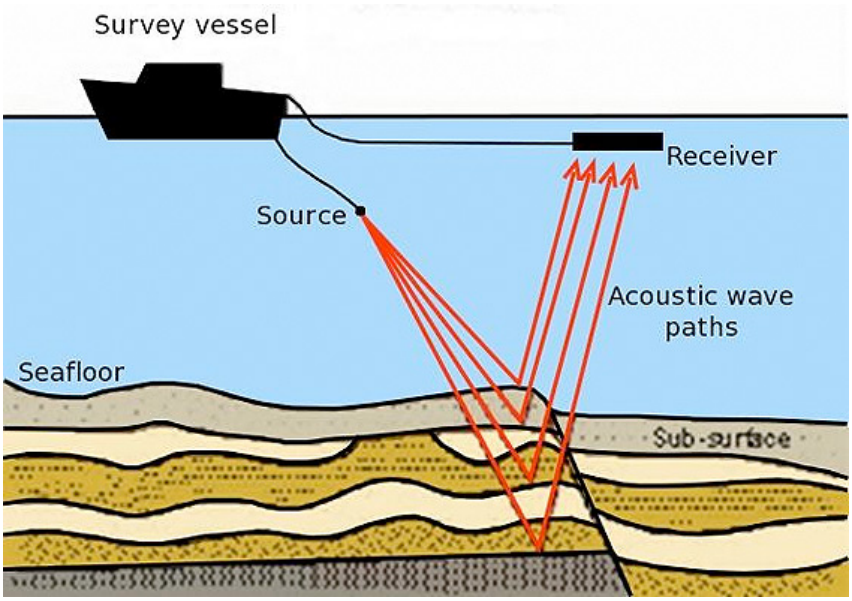

Figure 1.1 A cartoon illustrating how 2-D seismic surveys are performed. An airgun source fires at intervals while a receiver array records reflected wavefields coming from the subsurface. Image courtesy of ZIGZAG (https://www.zigzag.co.za).

Seismic surveys produce data volumes that are a collection of seismic traces at the locations of the receivers. A seismic trace represents the response of the elastic wavefield to velocity and density contrasts across interfaces of layers of rock or sediments as energy travels from a source through the subsurface to a receiver or receiver array [Schlumberger Oilfield Glossary]. To illustrate seismic data acquisition in the field, I modeled a simple example of these data. For example, a 2-D survey generates a common receiver gather (e.g. see Figure 1.2a) as a function of different shot positions from the receiver, called source-receiver offset. To gain an insight to the geology of the subsurface, standard processing of the seismic line — normal move out (NMO) plus summation of events along the offset direction — generates a stack section as shown in Figure 1.2b. In these grayscale images, the troughs (white events) represent a decrease in acoustic impedance with negative polarity and the peaks (dark events) represent an increase in acoustic impedance with positive polarity. The vertical axis is the two-way travel time, which is the time it takes a sound wave from a fired shot to travel through the medium below the sea surface, down to the subsurface and reflected back to the location of the receiver.

Ideally, synthetic finite-difference modeling of time-lapse data with exactly the same acquisition and modeling parameters generates a baseline data (Figure 1.3a) and monitor data (Figure 1.3b). In this example, the difference (Figure 1.3c) between the baseline and monitor is the true time-lapse signal; it shows events directly related to the subsurface changes in the synthetic model used in the modeling. Note

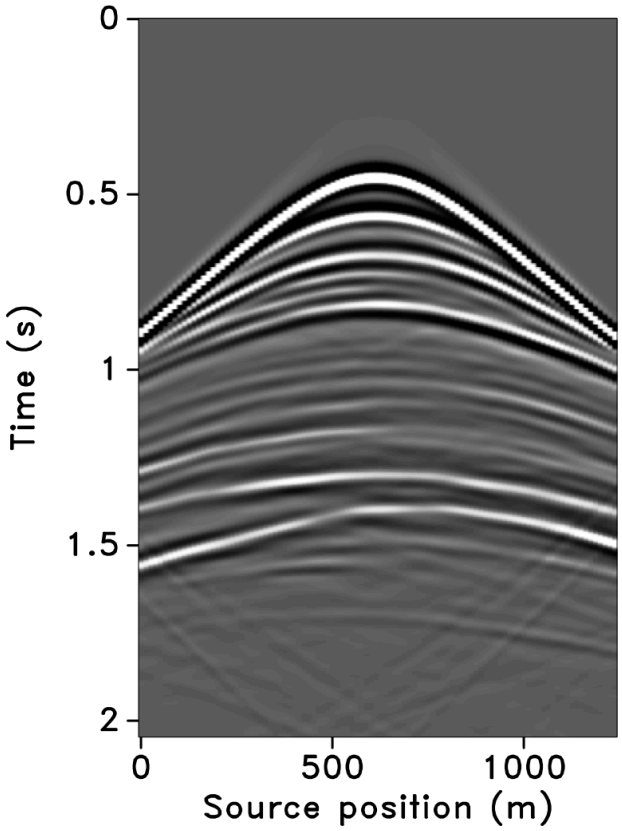

(a)

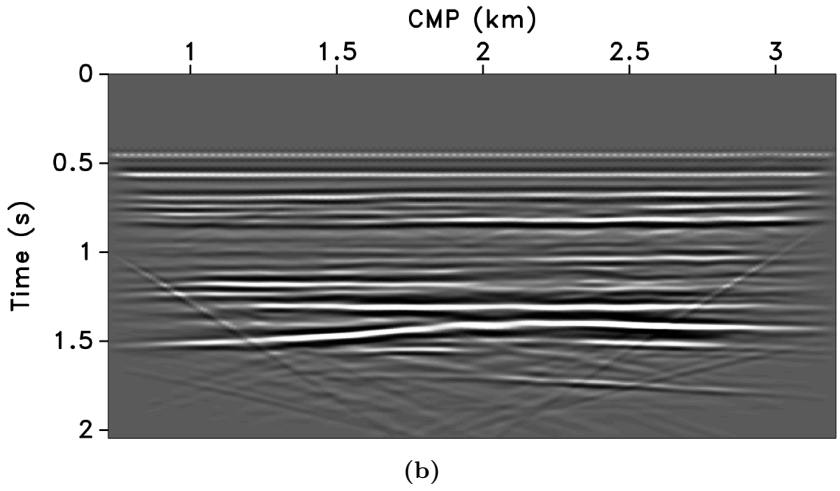

(b)

Figure 1.2 Seismic data. (a) An example of a common receiver gather as a function of source positions from the receiver. (b) A stack section as a function of common midpoint (CMP) — halfway point between source and receiver that is shared by numerous source-receiver pairs — depicting the geology of the subsurface.

that the time-lapse signal is plotted at a scale equal to one-tenth of the vintages because it is weak in magnitude compared to the vintages.

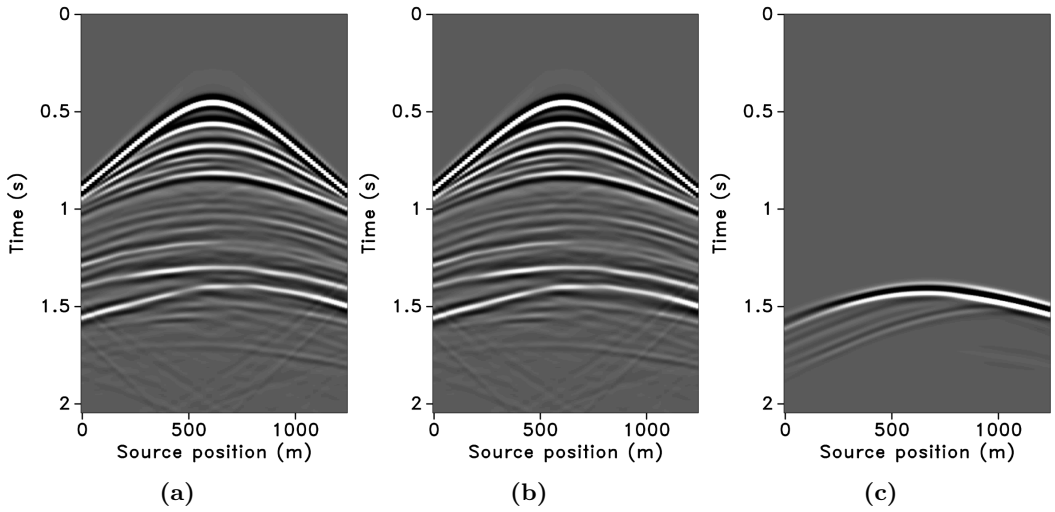

Figure 1.3 Idealized time-lapse data. (a) baseline, (b) monitor and (c) time-lapse (difference between (a) and (b)). The time-lapse scale is one-tenth the scale of the vintages (baseline and monitor).

1.1.2 Time-lapse seismic acquisition

To obtain high resolution images of the Earth subsurface, conventional imaging algorithms such as reverse time migration (RTM) require regularly and densely sampled shots/receivers from seismic surveys. The cost of acquiring densely sampled surveys is prohibitively expensive, and when time-lapse is of interest, this cost increases since time-lapse surveys comprise at least a baseline and monitor survey each of which is expensive. To resolve the high cost of seismic surveys, researchers (Hennenfent and Herrmann, 2008; Herrmann, 2010; Mansour et al., 2012; Wason and Herrmann, 2013) adapted ideas from the field of compressive sensing (CS, Donoho, 2006; Candes and Tao, 2006) to design surveys that sample seismic data at a cost significantly lower than conventional approaches. However, little is known about the implications of this approach for time-lapse seismic data acquisition and processing. This knowledge gap and the recent success of actual field demonstration (Mosher et al., 2014) of the feasibility of CS-inspired seismic surveys motivated me to investigate the challenges and opportunities of extending the approach of compressive sensing to time-lapse seismic. Before discussing details on the applications of compressive sensing to (time-lapse) seismic data acquisition, I introduce the concept of survey replication and repeatability in relation to time-lapse seismic.

1.1.3 Repeatability and survey replicability

To ensure that the 4D image difference between the baseline and monitor surveys reflects only true subsurface reservoir changes and not the result of seismic acquisition and processing differences, repeatability of the images and/or vintages is an important requirement (Lumley et al., 1997; Johnston, 2013). Repeatability quantifies the similarity or likeness of two vintages of seismic data, and a foremost goal of time-lapse seismic acquisition and processing is to minimize non-repeatability effects in order to make credible interpretation of changes in reservoir properties extracted or reaped from the final processed vintages. Maximizing repeatability, however, can be both technically challenging and expensive because repeatability is affected by several factors including requirement for dense sampling of sources/receivers, unavoidable differences in acquisition (Moldoveanu et al., 1996; Beasley et al., 1997; Landrø, 1999), processing techniques (Ross and Altan, 1997; Lumley et al., 2003), and signal-to-noise ratio (Landrø, 2008). To mitigate errors arising from differences in acquisitions and minimize non-repeatability effects caused by non-replicated surveys, the current paradigm requires strict replication of time-lapse surveys. This means that practitioners attempt to make the baseline and monitor(s) survey geometries as similar as possible, an approach that is technically challenging for a variety of reasons. Landrø (1999) showed how repeatability degrades as a function of increasing deviations between shot positions, demonstrating the sensitivity of repeatability to differences in survey geometries. As a result, various approaches have been proposed (Eiken et al., 2003; Day et al., 2010; Brown and Paulsen, 2011) that aim to produce highly replicable surveys, albeit at a relatively expensive acquisition cost. Therefore, finding innovative ways to replicate time-lapse surveys in order to maximize repeatability is an active area and continues to be the subject of many studies (Roach et al., 2014; Eggenberger et al., 2014; White et al., 2015; Shulakova et al., 2015).

1.2 Compressive sensing in seismic acquisition

Before ideas from compressive sensing were adapted to seismic acquisition, the requirement for dense sampling necessitated surveys with simultaneous sources whereby single and/or multiple source vessels fire sources at near-simultaneous random times, resulting in overlapping (blended) shot records (Beasley et al., 1998; de Kok and Gillespie, 2002; Beasley, 2008; Hampson et al., 2008a; Berkhout, 2008; Moldoveanu et al., 2010; Abma et al., 2013; Mosher et al., 2014). Simultaneous source acquisitions are economically viable and lower acquisition costs since overall acquisition time becomes compressed and it improves acquisition efficiency. In practice, simultaneous source surveys with dynamic acquisition geometry (towed streamers) incorporate low variability in the shot firing times since both the sources and receivers are moving, whereas surveys with static receiver geometries such as ocean bottom nodes (OBNs) or ocean bottom cables (OBCs) permit low to high variability in the shot firing times.

Figure 1.4 illustrates the differences in the random firing times of the shots in different acquisition settings. Because simultaneous source acquisition results in blended shot records, an appropriate source separation technique is required to unravel (deblend) the overlapping shots into sequential shots. The source separation step is necessary for subsequent data processing and imaging algorithms that require data volumes with dense sequential shots in order to produce high-resolution images of the subsurface.

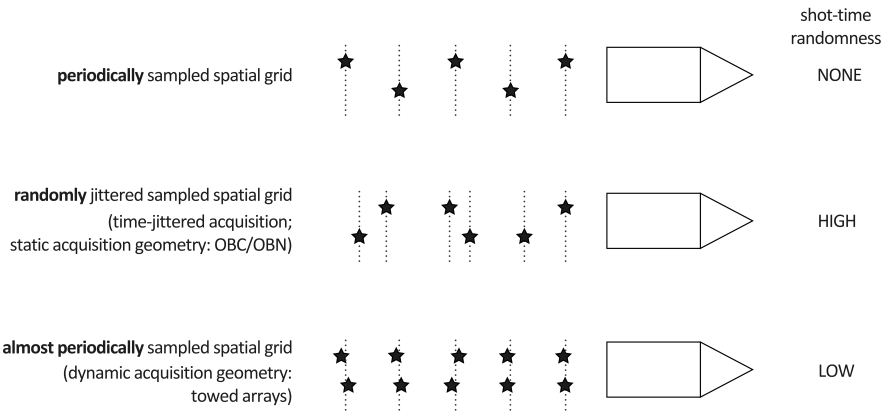

Figure 1.4 Periodic versus randomized (jittered) marine survey showing scenarios for low and high variability in shot firing times of the simultaneous sources.

A practically feasible way to render marine seismic survey more economically viable is to fire at random time-jittered compressed-in-time firing times (Mansour et al., 2012; Wason and Herrmann, 2013), which is an instance of simultaneous-source acquisition. In this *time-jittered marine* scheme, which leverages ideas from compressive sensing (CS, Donoho, 2006; Candes and Tao, 2006), a single source vessel sails across an ocean-bottom array of receivers (nodes or cables) constantly firing airgun arrays at "jittered" source locations and time instances with receivers recording continuously. Figure 1.5 illustrates how the proposed CS-inspired acquisition scheme compresses the survey time and how we aim to recover dense data onto a fine periodic grid with increased source sampling. This sampling scheme generates surveys with overlapping shot records (as in Figure 1.6) and coarse source sampling that are subsequently unraveled (separated) and interpolated to finely-sampled grid yielding sequentially sampled shots with improvements in spatial sampling. Recently, Mosher et al. (2014) demonstrated the potential of CS-based acquisition design in actual field surveys reporting up to ten fold improvements in economics.

In seismic applications, adherence to three key principles of CS are critical, namely we need to

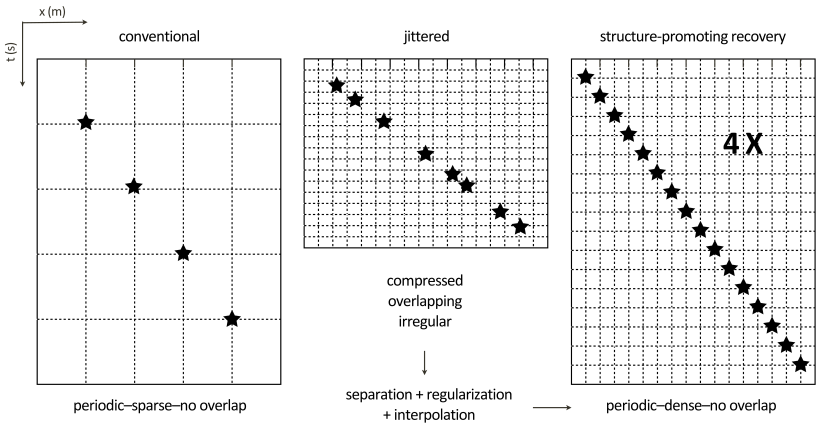

Figure 1.5 Schematic of sampling schemes and recovery. Left: conventional survey with non-overlapping shots. Middle: compressed survey time with overlapping shots. Right: recovery of non-overlapping dense periodic shots with improved source sampling. [Adapted from Wason et al. (2017)]

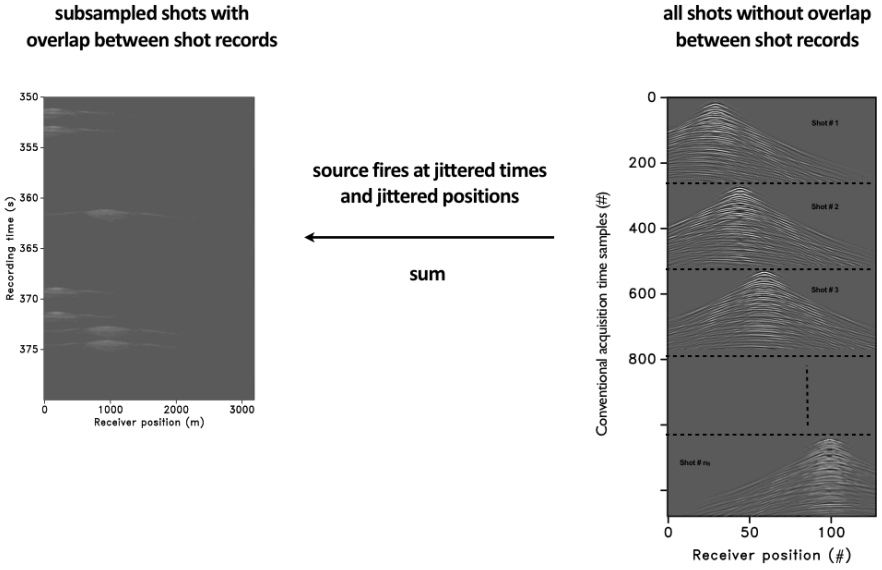

Figure 1.6 Simultaneous source acquisition and source separation. (a) Subset of data extracted from a continuous record of overlapping shots on a fixed receiver spread (b) Recovered data after source separation showing non-overlapping shots.

(i) find a compressible representation, e.g. via transform-domain sparsity; *(ii)* design a physically realizable randomized subsampling scheme, which turns subsampling related artifacts into incoherent noise that is not compressible; *(iii)* restore densely sampled data by promoting structure—i.e., by mapping incoherent artifacts to coherent signal.

Finding an appropriate representation for seismic wavefields requires seeking transform-domains that concentrate the wavefield's energy in as few as possible significant coefficients. To meet this objective, we use the curvelet transform (Candes et al., 2006), which is multiscale (splits the Fourier spectrum into dyadic frequency bands) and multidirectional (splits the Fourier spectrum into different angular wedges). In other words, curvelets decompose seismic data into multiscale and multi-angular localized waveforms, and they have been successfully adapted to various seismic applications (e.g. Herrmann et al., 2008; Hennenfent et al., 2010a). Furthermore, Herrmann (2010) demonstrated the improvements in wavefield reconstruction when curvelets are used for representing seismic data compared to other transforms such as wave atoms (Demanet and Ying, 2007). Therefore, we find curvelets adequate in representing seismic data for our application to time-lapse seismic.

For our implementation of these principles of CS (especially incorporating randomness) to time-lapse seismic acquisition, we consider the more favorable case of large variability in the shot firing times (ocean bottom seismic surveys), supported by good recovery results (Mansour et al., 2012; Wason and Herrmann, 2013). This scheme has the advantage of good replicability in the receiver positions since the receiver array is static and relatively unchanged between time-lapse surveys; however, we still have to address the implications of randomness in the source firing times and positioning of the sources between compressively sampled time-lapse surveys. Therefore, the challenging problem is how this CS-based acquisition design and subsequent recovery (source separation, regularization and interpolation) affects the quality of time-lapse vintages, time-lapse signal and repeatability of both the vintages and images obtained after recovery of the prestack vintages.

1.2.1 Compressive time-lapse seismic acquisition

While the potential advantages of randomized subsampling (compressively sampled surveys) on individual surveys (e.g., Mosher et al., 2014) are relatively well understood, the significance of this approach for time-lapse seismic data acquisition and its implication for repeatability raises important questions such as :

1. Should we replicate randomized surveys that are based on ideas from compressive sensing ?
2. How does imposing randomness in CS-based time-lapse surveys impact degrees of seismic repeatability ?

3. Can we expect high-fidelity time-lapse vintages and high-grade 4D signals from surveys acquired via randomized subsampling ideas from compressive sensing?

Finding answers to these questions has significant benefits for the economics of time-lapse seismic because it can potentially mitigate, if not resolve, the challenges related to expensive dense survey replication. Therefore, one of the objectives of this thesis is to provide answers to these important questions by exploring the feasibility of randomized subsampling for time-lapse surveys focusing on how these economic surveys impact repeatability.

To begin answering these questions, I consider compressive time-lapse acquisition of a baseline ($j = 1$) and monitor ($j = 2$) data as

$$\mathbf{y}_j = \mathbf{A}_j \mathbf{x}_j \quad \text{for} \quad j = \{1, 2\}. \tag{1.1}$$

In this formulation, which can be extended to $j > 2$ monitor surveys, the vectors $\mathbf{y}_1$ and $\mathbf{y}_2$ represent the corresponding subsampled measurement vectors. As described in Hennenfent and Herrmann (2008), Herrmann (2010), and Mansour et al. (2012), the flat measurement matrices $\mathbf{A}_j$ encapsulate specifics on the survey geometry for each vintage and the sparsifying transform, namely, curvelets. Note that the matrices are not necessarily equal ($\mathbf{A}_1 \neq \mathbf{A}_2$). In practice, finely sampled vintages can in principle be recovered under the right CS conditions by solving Equation 1.1 with the following sparsity-promoting optimization program

$$\widetilde{\mathbf{x}} = \underset{\mathbf{x}}{\operatorname{argmin}} \|\mathbf{x}\|_1 := \sum_{i=1}^{N} |x_i| \quad \text{subject to} \quad \mathbf{y} = \mathbf{A}\mathbf{x}, \tag{1.2}$$

yielding vectors $\widetilde{\mathbf{x}}_j$'s from which estimates for densely sampled vintages $\widetilde{\mathbf{d}}_j$, that live on one and the same fine periodic grid can be derived. To obtain the prestack time-lapse signal, I simply subtract the recovered vintages.

1.2.2 Insights from distributed compressive sensing

Baron et al. (2009a) proposed and presented a mathematical analysis of a joint recovery model (JRM) for distributed CS whereby jointly sparse signals are recovered simultaneously in one optimization program. Aside from permitting sparse representations individually, jointly sparse signals share information. As we will see later, time-lapse vintages have an intrinsic property i.e. they share a lot of information especially when viewed in a transform domain such as curvelets, allowing us to adapt the ideas from distributed CS to time-lapse seismic. There are several ways to integrate this shared information between the different vintages. We found that we get the best recovery result if we exploit the common component amongst the baseline and monitor data explicitly. This means that for two-vintage surveys we end up with three unknown vectors: one for the common component, denoted by $\mathbf{z}_0$, and two for the innovations $\mathbf{z}_j$ for $j \in 1, 2$ with respect to this common component that

is shared amongst the vintages. In this JRM, the vectors representing the vintages are given by

$$\mathbf{x}_j = \mathbf{z}_0 + \mathbf{z}_j, \qquad j \in 1, 2. \tag{1.3}$$

As we can see, the vintages contain the common component $\mathbf{z}_0$ and the time-lapse difference is contained within the difference between the innovations $\mathbf{z}_j$ for $j \in 1, 2$. We can further exploit this complementary structure during time-lapse recovery from randomized subsampling in order to improve the repeatability by solving

$$\widetilde{\mathbf{z}} = \arg\min_{\mathbf{z}} \|\mathbf{z}\|_1 \quad \text{subject to} \quad \mathbf{y} = \mathbf{A}\mathbf{z} \tag{1.4}$$

with

$$\underbrace{\begin{bmatrix}\mathbf{y}_1\\ \mathbf{y}_2\end{bmatrix}}_{\mathbf{y}} = \underbrace{\begin{bmatrix}\mathbf{A}_1 & \mathbf{A}_1 & \mathbf{0}\\ \mathbf{A}_2 & \mathbf{0} & \mathbf{A}_2\end{bmatrix}}_{\mathbf{A}} \underbrace{\begin{bmatrix}\mathbf{z}_0\\ \mathbf{z}_1\\ \mathbf{z}_2\end{bmatrix}}_{\mathbf{z}} \tag{1.5}$$

Compared to recovering the vintages separately as in Equation 1.2, the joint recovery model inverts for the coefficient vectors of the common component ($\widetilde{\mathbf{z}}_0$) and *innovations* ($\widetilde{\mathbf{z}}_j$) that encode the time-lapse. By construction, the common component benefits from sensing by both surveys (first column of $\mathbf{A}$ in Equation 1.5). Estimates for the finely sampled vintages are readily derived via Equation 1.4 with the recovered $\widetilde{\mathbf{z}}$ while the time-lapse difference is computed via $\widetilde{\mathbf{z}}_1 - \widetilde{\mathbf{z}}_2$.

Since the different surveys sense the common component and their respective innovations, the question is how the proposed joint recovery model performs on the vintages and the time-lapse differences, and what is the consequence of non-replicated randomized time-lapse surveys particularly with respect to achievable degrees of repeatability.

1.3 Objectives

The primary focus of this thesis is to present a practical strategy that allows for the implementation of low-cost randomized acquisitions in time-lapse seismic without compromising repeatability by leveraging ideas from distributed compressive sensing. The main objectives of this work are:

1. to address challenges related to requirements for dense sampling in time-lapse surveys by evaluating the opportunities inherent in low-cost randomized survey designs including simultaneous-source acquisitions;

2. to investigate the implications of replicated and non-replicated randomized surveys — based on ideas from compressive sensing — on attainable degrees of repeatability in time-lapse seismic;

3. to evaluate the effects of recovering time-lapse surveys in situations where the acquisition information (e.g. shot positions) are not precise because according

to CS, accurate recovery of signals relies on having accurate sampling matrices or operators;

4. to investigate the potential of estimating time-lapse models or images by incorporating the joint recovery model in wave-equation based inversion formulations.

1.4 Contributions

To the best of my knowledge, this work represents the first instance to cast time-lapse survey acquisition and recovery (or processing) as an inverse problem that produces densely sampled vintages from randomly (compressively) subsampled observations. I propose the application of a joint recovery model, which derives from distributed compressive sensing, to recover densely sampled prestack time-lapse vintages from randomized surveys that adhere to the principles of compressive sensing. More importantly, I propose to not replicate compressive randomized time-lapse surveys and discovered that we obtain better and improved vintages when the observed randomly under-sampled data are recovered (processed) with our joint recovery model. Because independent non-replicated surveys provide extra information that we exploit during our joint recovery, we obtain vintages with better quality compared to vintages obtained from processing the surveys separately. Furthermore, the recovered prestack vintages using our proposed model are of high-fidelity, exhibit improved seismic repeatability, and can serve as inputs to processes that derive poststack time-lapse attributes from the vintages. The results of this study are of great significance since it provides options that circumvents current requirements to replicate conventional expensive and dense time-lapse surveys.

In order to accurately recover signals acquired using CS, the sampling matrix or operator needs to be accurate. For applications to seismic acquisition, this implies having precise information about the acquisition geometry because this information is encapsulated in the CS matrix that is used during sparsity-promoting recovery. Therefore, using the proposed joint recovery model, I also evaluate the attainable degrees of repeatability from compressive time-lapse surveys in situations where the postplot acquisitions are not accurate. I show that moderate deviations between the true and recorded postplot shot positions — for marine surveys with static receiver configuration — do not degrade repeatability when the non-replicated baseline and monitor surveys are recovered with our proposed joint recovery model. This result is truly remarkable and further boosts our confidence in the practical implementation of these techniques in realistic field surveys, where errors between actual and recorded postplot positions are inevitable.

Finally, I investigate the performance of the joint recovery model for time-lapse imaging where my objective is to compare the quality of time-lapse images obtained using the proposed JRM to images obtained from performing separate imaging or linearized inversions on the vintages. While separate inversions result in artifacts that

smear true time-lapse changes in the images, inversion with our joint recovery model attenuates these artifacts in the time-lapse difference images, delineating true time-lapse changes. This result is significant because it further demonstrates improved repeatability with our joint recovery model, suggesting that we can minimize the risk in interpreting time-lapse changes by performing joint inversions, which adapt our model. As with our observations in the data-domain implementation described in the last two paragraphs, the key to our successful results on time-lapse seismic is the fact that our joint recovery model explicitly exploits the common information shared amongst time-lapse vintages and images.

1.5 Thesis overview

The main body of this thesis comprises five chapters following the present introduction.

Chapter 2 presents the origin of our approach towards addressing some of the current acquisition-related problems faced in time-lapse seismic with respect to difficulty in survey replication and requirements for dense sampling. To understand the relevance and benefits of the proposed joint recovery model, I first conduct a series of stylized experiments for thousands of random realizations of signal vectors that capture the essential features of randomized seismic acquisition. From these experiments, I compute recovery probabilities as a function of the number of measurements and increasing degrees of survey replicability, the two main factors that determine the cost of seismic acquisitions. I confirm that the joint recovery method model, which exploits common information among jointly sparse vectors (e.g. time-lapse vintages), leads to significant improvements in recovery quality compared to an independent recovery approach that does not leverage this shared information. In the seismic implementation, we show that under controlled survey conditions and by ignoring errors related to recording data off the grid, we obtain high-quality and highly repeatable prestack data from randomized (compressively) subsampled measurements that are observed from non-replicated surveys via the time-jittered marine scheme. We posit that the recovered vintages can be used to extract post-stack time-lapse attributes, which gives information on subsurface changes.

In Chapter 3, we demonstrate the feasibility of the joint recovery model in a more practical acquisition scenario where we no longer ignore errors related to sampling off the grid i.e., by collecting irregular samples that do not lie on a discrete regular periodic grid. We conduct several synthetic experiments that recover full prestack vintages from subsampled measurements (continuous recording) via time-jittered sources in marine. We include an operator that maps measurements from an irregular to a regular grid, thereby making the time-lapse data recovery issue a combined shot separation, regularization and interpolation problem. Furthermore this study analyzes the implications of repeatability of time-lapse vintages in situations where the spatial locations of the sources differ from the sampling grid by a small fraction of the fine sampling grid. Overall, our claims from Chapters 2 and

3 are : *(i)* non-replicated randomized surveys and recovery with the joint recovery model yields better data compared to independently recovering the surveys, and *(ii)* instead of aiming for randomized time-lapse seismic surveys with high degrees of replicability, it will be beneficial to know the postplot acquisition parameters (e.g. shot firing times and source/receiver positions) to a high degree of accuracy.

Chapter 4 demonstrates the feasibility of our joint recovery model for more realistic acquisitions with a specific issue, namely, surveys whose actual acquisition parameters do not exactly match the recorded postplots. Because it is the postplot information that is used in processing, I analyse the performance of the joint recovery model for mitigating effects of such errors in the positioning of sources for a fixed receiver array. Using standard measures of quantifying repeatability, I investigate two scenarios that allow us to measure attainable levels of repeatability. I confirm that recovery of the vintages does not decrease rapidly as the size of errors increases. Measured values of repeatability also suggest that the joint recovery model is robust to these difficult to control position errors in realistic field surveys.

In Chapter 5, we consider the time-lapse image domain implementation of our proposed joint recovery model. This means we consider an inversion problem where the dimension of the output (model/image) is less than that of the input (observed data). To this end, we seek to investigate two seismic inversion problems : least-squares migration (see e.g. Herrmann and Li, 2012; Tu and Herrmann, 2015) and full-waveform inversion (FWI) (see e.g. Virieux and Operto, 2009). In the first part of this chapter, rather than demonstrate the application of our proposed JRM to least-squares migration (or linearized imaging), we present recovery of stacked time-lapse data volumes from randomly under-sampled prestack data. Assuming stacking is a cheap proxy for migration, we expect our findings to hold when our joint recovery model is directly applied to actual time-lapse imaging experiments. The second part of this chapter directly explores nonlinear inversion (or FWI) of time-lapse data. We show how the joint recovery model can be integrated with a standard FWI algorithm (Li et al., 2012b), allowing us to obtain better models and difference compared to performing independent inversions of the vintages.

Finally in Chapter 6, I summarize the findings in this thesis. Because the conclusions drawn from this research are by no means exhaustive with regards to tackling the challenges related to time-lapse seismic technology, I discuss some limitations of my work and present an overview of future possible directions.

Chapter 2

Low-cost time-lapse seismic with distributed Compressive Sensing—exploiting common information amongst the vintages

2.1 Summary

Time-lapse seismic is a powerful technology for monitoring a variety of subsurface changes due to reservoir fluid flow. However, the practice can be technically challenging when one seeks to acquire colocated time-lapse surveys with high degrees of replicability amongst the shot locations. We demonstrate that under "ideal" circumstances, where we ignore errors related to taking measurements off the grid, high-quality prestack data can be obtained from randomized subsampled measurements that are observed from surveys where we choose not to revisit the same randomly subsampled on-the-grid shot locations. Our acquisition is low cost since our measurements are subsampled. We find that the recovered finely sampled prestack baseline and monitor data actually improve significantly when the same on-the-grid shot locations are not revisited. We achieve this result by using the fact that different time-lapse data share information and that nonreplicated (on-the-grid) acquisitions can add information when prestack data are recovered jointly. Whenever the time-lapse data exhibit joint structure—i.e., are compressible in some transform domain and share information—sparsity-promoting recovery of the "common component" and "innovations", with respect to this common component, outperforms independent recovery of both the prestack baseline and monitor data. The recovered time-lapse data are of high enough quality to serve as input to extract poststack attributes used to compute time-lapse differences. Without joint recovery, artifacts—due to the randomized subsampling—lead to deterioration of the degree of repeatability

of the time-lapse data. We support our claims by carrying out experiments that collect reliable statistics from thousands of repeated experiments. We also confirm that high degrees of repeatability are achievable for an ocean-bottom cable survey acquired with time-jittered continuous recording.

2.2 Introduction

Time-lapse (4-D) seismic techniques involve the acquisition, processing and interpretation of multiple 2-D or 3-D seismic surveys, over a particular time period of production (Lumley, 2001). While this technology has been applied successfully for reservoir monitoring (Koster et al., 2000; Fanchi, 2001) and CO_2 sequestration (Lumley, 2010), it remains a challenging and expensive technology because it relies on finely sampled and replicated surveys each of which have their challenges (Lumley and Behrens, 1998). To improve repeatability of the combination of acquisition and processing, various approaches have been proposed varying from more repeatable survey geometries (Beasley et al., 1997; Porter-Hirsche and Hirsche, 1998; Eiken et al., 2003; Brown and Paulsen, 2011; Eggenberger et al., 2014) to tailored processing techniques (Ross and Altan, 1997) such as cross equalization (Rickett and Lumley, 2001), curvelet-domain processing (Beyreuther et al., 2005) and matching (Tegtmeier-Last and Hennenfent, 2013).

We present a new approach that addresses these acquisition- and processing-related issues by explicitly exploiting common information shared by the different time-lapse vintages. To this end, we consider time-lapse acquisition as an inversion problem, which produces finely sampled colocated data from randomly subsampled baseline and monitor measurements. The presented joint recovery method, which derives from distributed compressive sensing (DCS, Baron et al., 2009a), inverts for the "common component" and "innovations" with respect to this common component. As during conventional compressive sensing (CS, Donoho, 2006; Candes and Tao, 2006), which has successfully been adapted and applied to various seismic settings (Hennenfent and Herrmann, 2008; Herrmann, 2010; Mansour et al., 2012; Wason and Herrmann, 2013) including actual field surveys (see e.g., Mosher et al., 2014), the proposed method exploits transform-based (curvelet) sparsity in combination with the fact that randomized acquisitions break this structure and thereby create favorable recovery conditions.

While the potential advantages of randomized subsampling on individual surveys are relatively well understood (see e.g., Wason and Herrmann, 2013), the implications of these randomized subsampling schemes on time-lapse seismic have not yet been studied, particularly regarding achievable repeatability of the prestack data after recovery and processing. Since the different surveys contain the common component and their respective innovations, the question is how the proposed joint recovery model performs on the vintages and the time-lapse differences, and what is the importance of replicating the surveys. Our analyses will be carried out assuming our observations lie on a discrete grid so that exact survey replicability

is in principle achievable. In this situation, we ignore any errors associated with taking measurements from an irregular grid. Our approach makes our time-lapse acquisition low-cost since our measurements are always subsampled and we do not necessarily replicate the surveys. In chapter 3, we demonstrate how we deal with the effects of non-replicability of the surveys, particularly when we take measurements from an irregular grid. Since the observations are subsampled and on the grid for this chapter (off the grid for chapter 3), the aim is to recover vintages on a colocated fine grid.

We also ignore complicating factors—such as tidal differences and seasonal changes in water temperature—that may adversely affect repeatability of the time-lapse surveys. We focus here on recovering high quality prestack vintages rather than the prestack time-lapse differences, since a foremost goal of 4-D seismic is to obtain poststack attributes from the vintages using various methods (Lumley, 2001; Landrø, 2001; Spetzler and Kvam, 2006; Yang et al., 2014, 2015; Asnaashari et al., 2015; Oghenekohwo et al., 2015; Maharramov et al., 2016; Kamei and Lumley, 2017).

The rest of the chapter is organized as follows. First, we summarize the main findings of CS, its governing equations, and its main premise that structured signals can be recovered from randomized measurements sampled at a rate below Nyquist. Next, we set up the CS framework for time-lapse surveys, and we discuss an independent recovery strategy, where the baseline and monitor data are recovered independently. We juxtapose this approach with our joint recovery method, which produces accurate estimates for the common component—i.e., the component that is shared amongst all vintages—and innovations with respect to this common component. To study the performance of these two recovery strategies, we conduct a series of stylized experiments for thousands of random realizations that capture the essential features of randomized seismic acquisition. From these experiments, we compute recovery probabilities as a function of the number of measurements and survey replicability, the two main factors that determine the cost of seismic acquisitions. Next, we conduct a series of synthetic experiments that involve time-lapse ocean-bottom surveys with time-jittered continuous recordings and overlapping shots as recently proposed by (Wason and Herrmann, 2013). Aside from computing signal-to-noise ratios measured with respect to finely sampled true baseline, monitor, and time-lapse differences and their stacks, we also use (Kragh and Christie, 2002)'s root-mean-square (NRMS) metric to quantify the repeatability of the recovered data.

2.3 Methodology

2.3.1 Synopsis of compressive sensing

Compressive sensing (CS) is a sampling paradigm that aims to reconstruct a signal $\mathbf{x} \in \mathbb{R}^N$ (N is the fully sampled ambient dimension) that is *sparse* (only a few of the entries are non-zero) or *compressible* (can be well approximated by a sparse signal)

in some transform domain, from few measurements $\mathbf{y} \in \mathbb{R}^n$, with $n \ll N$. According to the theory of CS (Candes and Tao, 2006; Donoho, 2006), recovery of $\mathbf{x}$ is attained from n linear subsampled measurements given by

$$\mathbf{y} = \mathbf{A}\mathbf{x}, \tag{2.1}$$

where $\mathbf{A} \in \mathbb{R}^{n \times N}$ is the sampling matrix.

Finding a solution to the above underdetermined system of equations involves solving the following sparsity-promoting convex optimization program :

$$\widetilde{\mathbf{x}} = \underset{\mathbf{x}}{\operatorname{argmin}} \|\mathbf{x}\|_1 := \sum_{i=1}^{N} |x_i| \quad \text{subject to} \quad \mathbf{y} = \mathbf{A}\mathbf{x}. \tag{2.2}$$

where $\widetilde{\mathbf{x}}$ is an approximation of $\mathbf{x}$. In the noise-free case, this (ℓ_1-minimization) problem finds amongst all possible vectors $\mathbf{x}$, the vector that has the smallest ℓ_1-norm and that explains the observed subsampled data. To arrive at this solution, we use the software package SPGℓ_1 (Van Den Berg and Friedlander, 2008). The main contribution of CS is to design sampling matrices that guarantee solutions to the recovery problem in Equation 2.2, by providing rigorous proofs in specific settings. Furthermore, a key highlight in CS is that favorable conditions for recovery is attained via randomized subsampling rather than periodic subsampling. This is because random subsampling introduces incoherent, and therefore non-sparse, subsampling related artifacts that are removed during sparsity-promoting signal recovery. Basically, CS is an extension of the anti-leakage Fourier transform (Xu et al., 2005a; Schonewille et al., 2009), where random sampling in the physical domain renders coherent aliases into incoherent noisy crosstalk (leakage) in the spatial Fourier domain. In this case, the signal is sparse in the Fourier basis.

For details on precise recovery conditions in terms of the number of measurements n, allowable recovery error, and construction of measurement/sampling matrices $\mathbf{A}$, we refer to the literature on compressive sensing (Donoho, 2006; Candes and Tao, 2006; Candès and Wakin, 2008). For our application to time-lapse seismic, we follow adaptations of this theory by (Herrmann et al., 2008) and (Herrmann and Hennenfent, 2008), and use curvelets as the sparsifying transform in the seismic examples that involve randomized marine acquisition (Mansour et al., 2012; Wason and Herrmann, 2013; Wason et al., 2015). The latter references involve marine acquisition with ocean-bottom nodes and time-jittered time-compressed firing times with single or multiple source vessels. As shown by (Wason and Herrmann, 2013), this type of randomized acquisition and processing leads to better wavefield reconstructions than the processing of regularly subsampled data. Furthermore, because of the reduced acquisition time, it is more efficient economically (Mosher et al., 2014).

2.3.2 Independent recovery strategy (IRS)

To arrive at a compressive sensing formulation for time-lapse seismic, we describe noise-free time-lapse data acquired from the baseline ($j = 1$) and monitor ($j = 2$) surveys as

$$\mathbf{y}_j = \mathbf{A}_j \mathbf{x}_j \quad \text{for} \quad j = \{1, 2\}. \tag{2.3}$$

In this CS formulation, which can be extended to $J > 2$ surveys, the vectors $\mathbf{y}_1$ and $\mathbf{y}_2$ represent the corresponding subsampled measurement vectors; $\mathbf{A}_1$ and $\mathbf{A}_2$ are the corresponding flat ($n \ll N$) measurement matrices, which are not necessarily equal. As before, finely sampled vintages can in principle be recovered under the right conditions by solving Equation 2.3 with a sparsity-promoting optimization program (cf. Equation 2.2) for each vintage separately. We will refer to this approach as the independent recovery strategy (IRS). In this context, we compute the time-lapse signal by directly subtracting the recovered vintages.

2.3.3 Shared information amongst the vintages

Aside from invoking randomizations during subsampling, CS exploits structure residing within seismic data volumes during reconstruction—the better the compression the better the reconstruction becomes for a given set of measurements. If we consider the surveys separately, curvelets are good candidates to reveal this structure because they concentrate the signal's energy into few large-magnitude coefficients and many small coefficients (see left-hand side plot in Figure 2.1). Curvelets have this ability because they decompose seismic data into multiscale and multi-angular localized waveforms. As the cross plot in Figure 2.1 reveals (right-hand side plot), the curvelet transform's ability to compress seismic data and time-lapse difference (left-hand side plot Figure 2.1) is not the only type of structure that we can exploit. The fact that most of the magnitudes of the curvelet coefficients of two common-receiver gathers from a 2-D OBS time-lapse survey (see Figure 2.8) nearly coincide indicate that the data from the two vintages shares lots of information in the curvelet domain. Therefore, we can further exploit this complementary structure during time-lapse recovery from randomized subsampling in order to improve the repeatability.

2.3.4 Joint recovery method (JRM)

(Baron et al., 2009a) introduced and analyzed mathematically a model for distributed CS where jointly sparse signals are recovered jointly. Aside from permitting sparse representations individually, jointly sparse signals share information. For instance, sensor arrays aimed at the same object tend to share information (see (Xiong et al., 2004) and the references therein) and time-lapse seismic surveys are no exception.

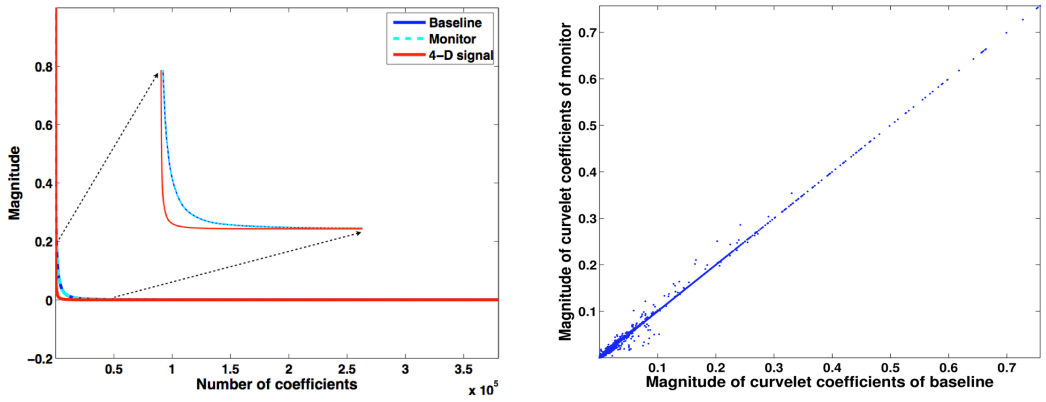

Figure 2.1 Left: Decay of curvelet coefficients of time-lapse data and difference. Right: Scatter plot of curvelet coefficients of the baseline and monitor data indicating that they share significant information.

There are different ways to incorporate this shared information amongst the different vintages. We found that we get the best recovery result if we exploit the common component amongst the baseline and monitor data explicitly. This means that for two-vintage surveys we end up with three unknown vectors. One for the common component, denoted by $\mathbf{z}_0$, and two for the innovations $\mathbf{z}_j$ for $j \in 1, 2$ with respect to this common component that is shared by the vintages. In this model, the vectors for the vintages are given by

$$\mathbf{x}_j = \mathbf{z}_0 + \mathbf{z}_j, \qquad j \in 1, 2. \tag{2.4}$$

As we can see, the vintages contain the common component $\mathbf{z}_0$ and the time-lapse difference is contained within the difference between the innovations $\mathbf{z}_j$ for $j \in 1, 2$. Because $\mathbf{z}_0$ is part of both surveys, the observed measurements are now given by

$$\begin{bmatrix} \mathbf{y}_1 \\ \mathbf{y}_2 \end{bmatrix} = \begin{bmatrix} \mathbf{A}_1 & \mathbf{A}_1 & \mathbf{0} \\ \mathbf{A}_2 & \mathbf{0} & \mathbf{A}_2 \end{bmatrix} \begin{bmatrix} \mathbf{z}_0 \\ \mathbf{z}_1 \\ \mathbf{z}_2 \end{bmatrix}, \quad \text{or} \tag{2.5}$$
$$\mathbf{y} = \mathbf{A}\mathbf{z}.$$

In this expression, we overloaded the symbol $\mathbf{A}$, which from now on refers to the matrix linking the observations of the time-lapse surveys to the common component and innovations pertaining to the different vintages. The above joint recovery model readily extends to $J > 2$ surveys, yielding a $J \times$ (number of vintages $+ 1$) system.

Contrary to the IRS, which essentially corresponds to setting the common component to zero so there is no communication between the different surveys, both vintages share the common component, $\mathbf{z}_0$, in Equation 2.5. As a result correlations amongst the vintages will be exploited if we solve instead

$$\widetilde{\mathbf{z}} = \underset{\mathbf{z}}{\operatorname{argmin}} \|\mathbf{z}\|_1 \quad \text{subject to} \quad \mathbf{y} = \mathbf{A}\mathbf{z}. \tag{2.6}$$

As a result, we seek solutions for the common component and innovations that have the smallest ℓ_1-norm such that the observations explain both the incomplete recordings for both vintages. Estimates for the finely sampled vintages are readily obtained via Equation 2.4 with the recovered $\widetilde{\mathbf{z}}$ while the time-lapse difference is computed via $\widetilde{\mathbf{z}}_1 - \widetilde{\mathbf{z}}_2$.

Albeit recent progress has been made (Li, 2015), precise recovery conditions for JRM are not yet very well studied. Moreover, the JRM was also not designed to compute differences between the innovations. To gain some insight on our formulation, we will first compare the performance of IRS and JRM in cases where the surveys are exactly replicated ($\mathbf{A}_1 = \mathbf{A}_2$), partially replicated ($\mathbf{A}_1$ and $\mathbf{A}_2$ share certain fractions of rows), or where $\mathbf{A}_1$ and $\mathbf{A}_2$ are statistically completely independent. To get reliable statistics on the recovery performance for the different recovery schemes, we repeat a series of small stylized problems thousands of times. These small stylized examples serve as proxies for seismic acquisition problems that we will discuss later.

2.4 Stylized experiments

To collect statistics on the performance of the different recovery strategies, we repeat several series of small experiments many times. Each random time-lapse realization is represented by a vector with $N = 50$ elements that has $k = 13$ nonzero entries with Gaussian distributed weights that are located at random locations such that the number of nonzero entries in each innovation is two—i.e., $k_1 = k_2 = 2$. This leaves 11 nonzeros for the common component. For each random experiment, $n = \{10, 11, \cdots, 40\}$ observations $\mathbf{y}_1$ and $\mathbf{y}_2$ are collected using Equation 2.3 for Gaussian matrices $\mathbf{A}_1$ and $\mathbf{A}_2$ that are redrawn for each repeated experiment. This means we repeat several series of experiments for a given fixed number of observations where $\mathbf{A}_1$ and $\mathbf{A}_2$ are redrawn each time. These Gaussian matrices have independent identically distributed Gaussian entries and serve as a proxy for randomized acquisitions in the field. An example of the vectors $\mathbf{z}_0, \mathbf{z}_1, \mathbf{z}_2, \mathbf{x}_1, \mathbf{x}_2$, and $\mathbf{x}_1 - \mathbf{x}_2$ involved in these experiments is included in Figure 2.2. As stated previously, these vectors only mimic representations of actual seismic traces. In that sense, our goal is to recover estimates for the vintages and time-lapse signals—i.e., we want to obtain the estimates $\widetilde{\mathbf{x}}_1$ and $\widetilde{\mathbf{x}}_2$, and their difference $\widetilde{\mathbf{x}}_1 - \widetilde{\mathbf{x}}_2$ from subsampled measurements $\mathbf{y}_1$ and $\mathbf{y}_2$. When using the joint recovery model, we compute estimates for the jointly sparse vectors via $\widetilde{\mathbf{x}}_1 = \widetilde{\mathbf{z}}_0 + \widetilde{\mathbf{z}}_1$, and $\widetilde{\mathbf{x}}_2 = \widetilde{\mathbf{z}}_0 + \widetilde{\mathbf{z}}_2$, where $\widetilde{\mathbf{z}}$ is found by solving Equation 2.6.

To get reliable statistics on the probability of recovering the vectors representing time-lapse vintages and differences, we choose to perform $M = 2000$ repeated experiments generating M different realizations for $\mathbf{y}_1$ and $\mathbf{y}_2$ from different realizations of $\mathbf{x}_1$ and $\mathbf{x}_2$. Next, we recover $\widetilde{\mathbf{x}}_1$ and $\widetilde{\mathbf{x}}_2$ from these measurements using the IRS or JRM. From these estimates, we compute empirical probabilities of successful recovery via

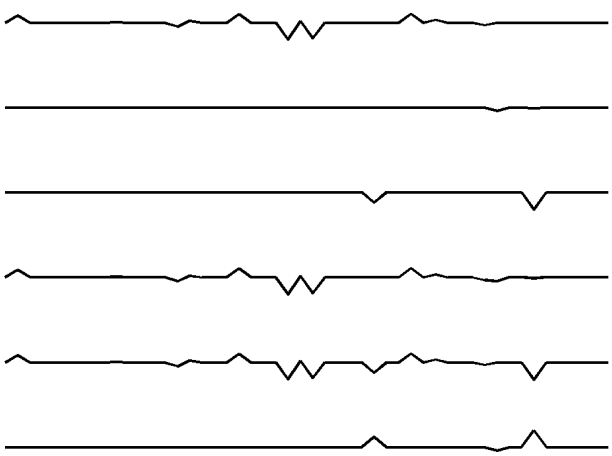

Figure 2.2 From top to bottom: $\mathbf{z}_0, \mathbf{z}_1, \mathbf{z}_2, \mathbf{x}_1, \mathbf{x}_2, \mathbf{x}_1 - \mathbf{x}_2$. We are particularly interested in recovering estimates for $\mathbf{x}_1, \mathbf{x}_2$ and $\mathbf{x}_1 - \mathbf{x}_2$ from $\mathbf{y}_1$ and $\mathbf{y}_2$.

$$P(\mathbf{x}) = \frac{\text{Number of times} \dfrac{\|\mathbf{x} - \tilde{\mathbf{x}}\|_2}{\|\mathbf{x}\|_2} < \rho}{M}. \tag{2.7}$$

We set the relative error threshold to $\rho = 0.1$. The vector $\mathbf{x}$ either represents the vintages or the difference. In case of the vintages, we multiply the probabilities.

2.4.1 Experiment 1 independent versus joint recovery

To reflect current practices in time-lapse acquisition—where people aim to replicate the surveys—we run the experiments by drawing the same random Gaussian matrices of size $n \times N$ for $n = \{10, 11, \cdots, 40\}$ and $N = 50$ for $\mathbf{A}_1$ and $\mathbf{A}_2$—i.e., $\mathbf{A}_1 = \mathbf{A}_2$. We conduct the same experiments where the surveys are not replicated by drawing statistically independent measurement matrices for each repeated experiment, yielding $\mathbf{A}_1 \neq \mathbf{A}_2$. For each series of experiments, we recover estimates $\widetilde{\mathbf{x}}_1$, $\widetilde{\mathbf{x}}_2$, and $\widetilde{\mathbf{x}}_1 - \widetilde{\mathbf{x}}_2$ from which we compute the corresponding recovery probabilities using Equation 2.7. The results are plotted in Figure 2.3 for the recovery of the vintages (Figure 2.3a) and time-lapse difference (Figure 2.3b).

The results of these experiments indicate that regardless of the number of measurements, JRM leads to improved recovery compared to IRS because it exploits information shared by the two jointly sparse vectors representing the vintages. The recovery probabilities for JRM (solid lines in Figure 2.3) show an overall improvement for both the time-lapse vectors and the time-lapse difference vector—all probability

curves are to the left compared to those from IRS meaning that recovery is more likely for fewer measurements. For the time-lapse vectors, this improvement is much more pronounced for measurement matrices that are statistically independent—i.e., not replicated ($\mathbf{A}_1 \neq \mathbf{A}_2$). This observation is consistent with distributed compressive sensing, which predicts significant improvements when the time-lapse vectors share a significant common component. In that case, the shared component benefits most from being observed by both surveys (via the first column of $\mathbf{A}$, cf. Equation 2.5). The IRS results for the time-lapse vectors are much less affected whether the survey is replicated or not, which makes sense because the processing is done in parallel and independently. This suggests that for time-lapse seismic, independent surveys give additional information on the sparse structure of the vintages that is reflected in their improved recovery quality. Another likely interpretation is that time-lapse data obtained via JRM has better repeatability compared to data obtained via IRS.

While independent surveys improve recovery with JRM, the recovery probability of the time-lapse difference vectors improves drastically when the experiments are replicated exactly. The reason for this is that the JRM simplifies to the recovery of the time-lapse differences alone in cases where the time-lapse measurements are exactly replicated. Since these time-lapse differences are sparser than the vintage vectors themselves, the time-lapse difference vectors are well recovered while the time-lapse vectors themselves are not. This result is not surprising since the error in reconstructing the vintages cancels out in the difference. This means that in CS, if one is interested in the time-lapse difference, exact repetition of the survey is preferred. However, this approach does not provide any additional structural information in the vintages. We will revisit this observation in Experiment 2 to see how the recovery performs when we have varying degrees of repeatability in the measurements.

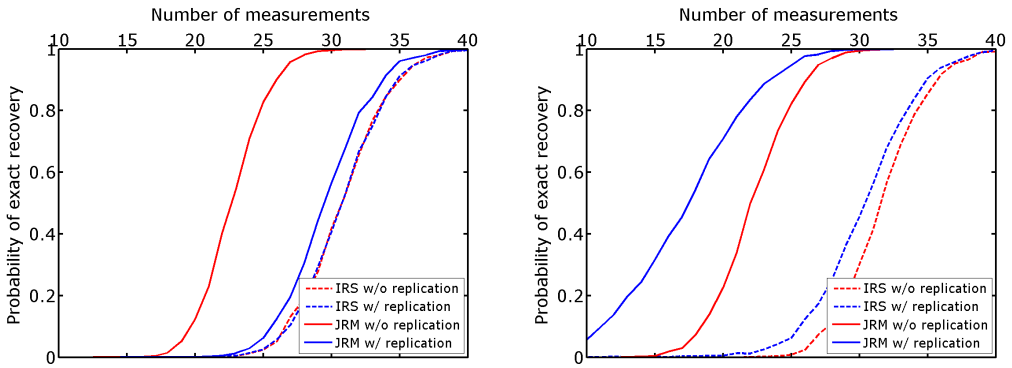

(a) **(b)**

Figure 2.3 Recovery of (a) the jointly sparse signals $\mathbf{x}_1$ and $\mathbf{x}_2$, (b) $\mathbf{x}_1 - \mathbf{x}_2$; with and without repetition of the measurement matrices, using the independent recovery strategy versus the joint recovery method.

2.4.2 Experiment 2 impact of degree of survey replicability

So far, we explored only two extremes, namely recovery of vintages with absolutely no replication ($\mathbf{A}_1 \neq \mathbf{A}_2$ and statistically independent) or exact replication ($\mathbf{A}_1 = \mathbf{A}_2$). To get a better understanding of how replication factors into the recovery, we repeat the experiments where we vary the degree of dependence between the surveys by changing the number of rows the matrices $\mathbf{A}_1$ and $\mathbf{A}_2$ have in common. When all rows are in common, the survey is replicated and the percentage of overlap between the surveys is a measure for the degree of replicability of the surveys. Since JRM clearly outperformed IRS, we only consider recovery with JRM.

As before we compute recovery probabilities from $M = 2000$ repeated time-lapse experiments generating M different realizations for the observations. We summarize the recovery probability curves for varying degrees of overlap in Figure 2.4. These curves confirm that the recovery of the time-lapse vectors, $\mathbf{x}_1$ and $\mathbf{x}_2$, improves when the surveys are not replicated. As soon as the surveys are no longer replicated, the recovery probabilities for the time-lapse vectors improve. These improvements become less prominent when large percentages do not overlap and as expected reaches its maximum when the surveys become independent. Recovery of the time-lapse differences, $\mathbf{x}_1 - \mathbf{x}_2$, on the other hand suffers drastically when the surveys are no longer 100% replicated. When less then 80% of the surveys are no longer replicated, the recovery probabilities no longer benefit from replicating the surveys. Recovery of the time-lapse vectors, on the other hand, already improves significantly at this point.

While these experiments are perhaps too idealized and small to serve as a strict guidance on how to design time-lapse surveys, they lead to the following observations. Firstly, the recovery probabilities improve when we exploit joint sparsity amongst the time-lapse vectors via JRM. Secondly, since the common component is observed by all surveys recovery of the common component and therefore vintages improves if the surveys are not replicated. Thirdly, the time-lapse differences benefit from high degrees of replication of the surveys. In that case, the JRM degenerates to recovery of the time-lapse difference alone and as a consequence the time-lapse vectors are not well recovered.

Even though the quality of the time-lapse difference is often considered as a good means of quality control, we caution the reader to draw the conclusion that we should aim to replicate the surveys. The reason for this is that time-lapse differences are generally computed from poststack attributes computed from finely sampled, and therefore recovered, prestack baseline and monitor data and not from prestack differences. Therefore, recovery of time-lapse difference alone may not be sufficient to draw firm conclusions. Our observations were also based on very small idealized experiments that did not involve stacking and permit exact replication, which may not be realistic in practice.

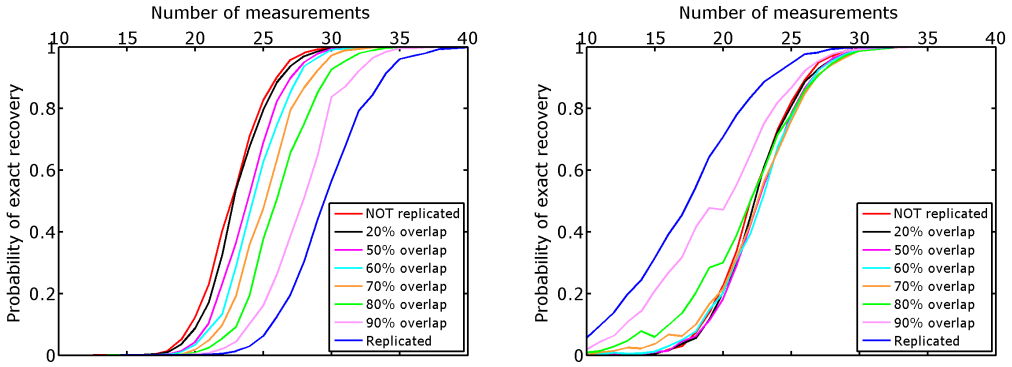

(a) **(b)**

Figure 2.4 Recovery as a function of overlap between measurement matrices. Probability of recovering (a) $\mathbf{x}_1$ and $\mathbf{x}_2$, (b) $\mathbf{x}_1 - \mathbf{x}_2$, with joint recovery method.

2.5 Experimental setup on-the-grid time-lapse randomized subsampling

One of the main parts of the experimental setup for the synthetic seismic case study is how we define the underlying grid on which samples are taken. In context of this chapter, we assume that the samples are taken on a discrete grid—i.e., samples lie "exactly" on the grid. It is also important to note that we randomly subsample the grid only in the source dimension. As mentioned in the compressive sensing section above, randomized subsampling introduces incoherent subsampling related artifacts that are removed during sparsity-promoting signal recovery. Figure 2.5 shows a schematic comparison between different random realizations of a subsampled grid. As illustrated in the schematic, random samples are taken exactly on the grid. We define the term "overlap" as the percentage of on-the-grid shot locations exactly replicated between two (or more) time-lapse surveys. For the synthetic seismic case study, whenever there is an overlap between the surveys (e.g., 50%, 33%, 25%, etc.) the on-the-grid shot locations are exactly replicated for the baseline and monitor surveys. Similarly, for the stylized experiments, when two rows of the Gaussian matrices are the same it can be interpreted as if we hit the same shot location for both the baseline and monitor surveys. Therefore, we either assume that the experimental circumstances are ideal or alternatively we can think of this assumption as ignoring the effects of being off the grid. Chapter 3 analyses the effects of the more realistic off-the-grid sampling. In summary, we consider the case where measurements are exactly replicated whenever we choose to visit the same shot location for the two surveys. However, because we are subsampled we need not choose to revisit all the shot locations of the baseline survey.

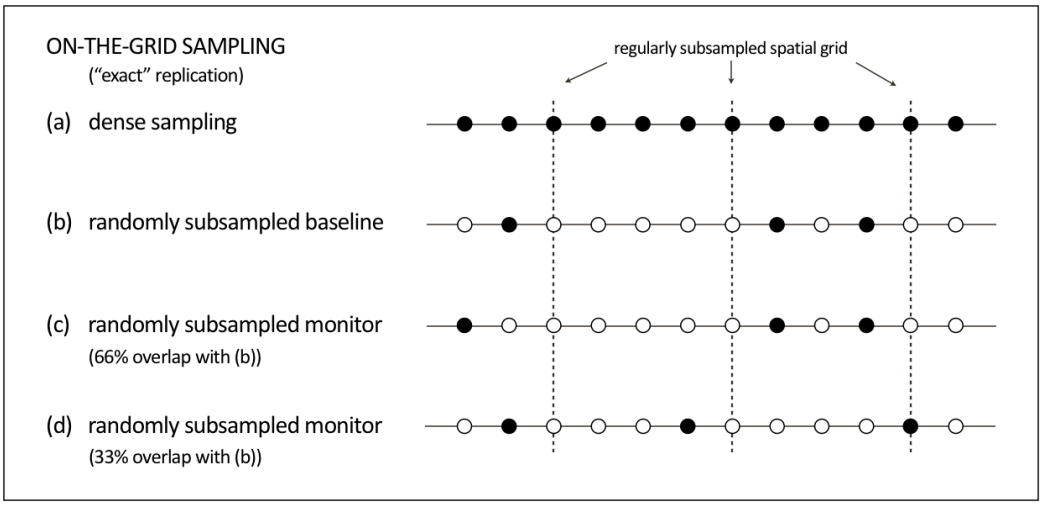

Figure 2.5 Schematic comparison between different random realizations of a subsampled grid. The subsampling factor is 3. As illustrated, random samples are taken exactly on the grid. Moreover, the samples are exactly replicated whenever there is an overlap between the time-lapse surveys.

2.6 Synthetic seismic case study time-lapse marine acquisition via time-jittered sources

To study a more realistic example, we carry out a number of experiments on 2-D seismic lines generated from a synthetic velocity model—the BG COMPASS model (provided by BG Group). To illustrate the performance of randomized subsamplings—in particular the time-jittered marine acquisition—in time-lapse seismic, we use a subset of the BG COMPASS model (Figure 2.6a) for the baseline. We define the monitor model (Figure 2.6b) from the baseline via a fluid substitution resulting in a localized time-lapse difference at the reservoir level as shown in Figure 2.6c.

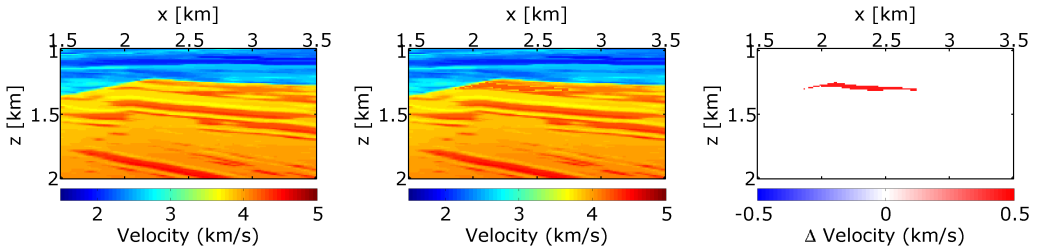

Figure 2.6 Reservoir zoom of the synthetic time-lapse velocity models showing the change in velocity as a result of fluid substitution. (a) Baseline model, (b) monitor model, (c) difference between (a) and (b).

Using IWAVE (Symes, 2010) time-stepping acoustic simulation software, two acoustic datasets with a conventional source (and receiver) sampling of 12.5 m are generated, one from the baseline model and the other from the monitor model. Each dataset has $N_t = 512$ time samples, $N_r = 100$ receivers, and $N_s = 100$ sources. Subtracting the two datasets yields the time-lapse difference, whose amplitude is small in comparison to the two datasets (about one-tenth). Since no noise is added to the data, the time-lapse difference is simply the time-lapse signal. A receiver gather from the simulated baseline data, the monitor data and the corresponding time-lapse difference is shown in Figure 2.7. In order to make the time-lapse difference visible, the color axis for the figures showing the time-lapse difference is one-tenth the scale of the color axis for the figures showing the baseline and the monitor data. This colormap applies for the remainder of the chapter. Also, the first source position in the receiver gathers—labeled as 0 m in the figures—corresponds to 725 m in the synthetic velocity model.

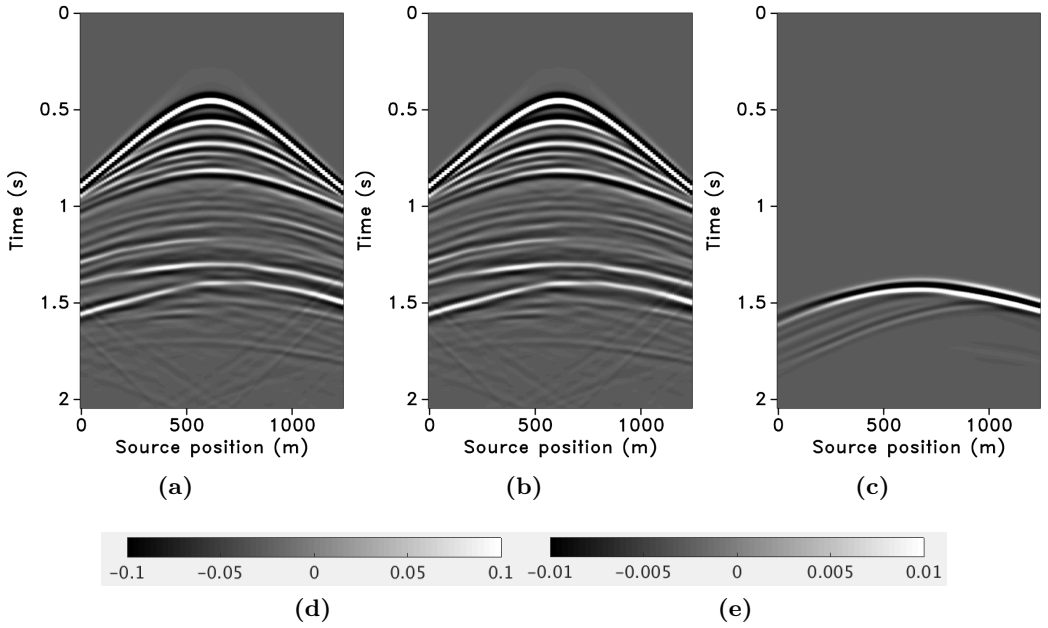

Figure 2.7 A synthetic receiver gather from the conventional (a) baseline survey, (b) monitor survey. (c) The corresponding 4-D signal. (d) Color scale of the vintages. (e) Color scale of the 4-D signal. Note that (e) is one-tenth the scale of (d). These color scales apply to all the corresponding figures for the vintages and the 4-D signal.

2.6.1 Time-jittered marine acquisition

(Wason and Herrmann, 2013) presented a pragmatic single vessel, albeit easily extendable to multiple vessels, simultaneous marine acquisition scheme that leverages CS by invoking randomness in the acquisition via random jittering of the source fir-

ing times. As a result, source interferences become incoherent in common-receiver gathers creating a favorable condition for separating the simultaneous data into conventional nonsimultaneous data (also known as "deblending") via curvelet-domain sparsity promotion. Like missing-trace interpolation, the randomization via jittering turns the recovery into a relatively simple "denoising" problem with control over the maximum gap size between adjacent shot locations (Hennenfent and Herrmann, 2008), which is a practical requirement of wavefield reconstruction with localized sparsifying transforms such as curvelets (Hennenfent and Herrmann, 2008). The basic idea of jittered subsampling is to regularly decimate the interpolation grid and subsequently perturb the coarse-grid sample points on the fine grid. A jittering parameter, dictated by the type of acquisition and parameters such as the minimum distance (or minimum recharge time for the airguns) required between adjacent shots, relates to how close and how far the jittered sampling point can be from the regular coarse grid, effectively controlling the maximum acquisition gap. Since we are still on the grid, this is a case of discrete jittering. In this chapter, we limit ourselves to the discrete case but this technique can relatively easily be taken off the grid as we discuss in chapter 3.

A seismic line with N_s sources, N_r receivers, and N_t time samples can be reshaped into an N dimensional vector $\mathbf{f}$, where $N = N_s \times N_r \times N_t$. For simplicity, we assume that all sources see the same receivers, which makes our method applicable to marine acquisition with ocean-bottom cables or nodes (OBC or OBN). As stated previously, seismic data volumes permit a compressible representation $\mathbf{x}$ in the curvelet domain denoted by $\mathbf{S}$. Therefore, $\mathbf{f} = \mathbf{S}^H\mathbf{x}$, where ^{H} denotes the Hermitian transpose (or adjoint), which equals the inverse curvelet transform. Since curvelets are a redundant frame (an over-complete sparsifying dictionary), $\mathbf{S} \in \mathbb{C}^{P\times N}$ with $P > N$, and $\mathbf{x} \in \mathbb{C}^P$.

With the inclusion of the sparsifying transform, the matrix $\mathbf{A}$ can be factored into the product of a $n \times N$ (with $n \ll N$) acquisition matrix $\mathbf{M}$ and the synthesis matrix $\mathbf{S}^H$. The design of the acquisition matrix $\mathbf{M}$ is critical to the success of the recovery algorithm. From a practical point of view, it is important to note that matrix-vector products with these matrices are matrix free—i.e., these matrices are operators that define the action of the matrix on a vector. Since the marine acquisition is performed in the source-time domain, the acquisition operator $\mathbf{M}$ is a combined jittered-shot selector and time-shifting operator. Note that in this framework it is also possible to randomly subsample the receivers.

Given a baseline data vector $\mathbf{f}_1$ and a monitor data vector $\mathbf{f}_2$, $\mathbf{x}_1$ and $\mathbf{x}_2$ are the corresponding sparse representations—i.e., $\mathbf{f}_1 = \mathbf{S}^H\mathbf{x}_1$, and $\mathbf{f}_2 = \mathbf{S}^H\mathbf{x}_2$. Given the measurements $\mathbf{y}_1 = \mathbf{M}_1\mathbf{f}_1$ and $\mathbf{y}_2 = \mathbf{M}_2\mathbf{f}_2$, and $\mathbf{A}_1 = \mathbf{M}_1\mathbf{S}^H$, $\mathbf{A}_2 = \mathbf{M}_2\mathbf{S}^H$, our aim is to recover sparse approximations $\widetilde{\mathbf{f}}_1$ and $\widetilde{\mathbf{f}}_2$ by solving sparse recovery problems for the scenarios (IRS and JRM) as described above from which the time-lapse signal can be computed.

2.6.2 Acquisition geometry

In time-jittered marine acquisition, source vessels map the survey area firing shots at jittered time-instances, which translate to jittered shot locations for a given speed of the source vessel. Conventional acquisition with one source vessel and two airgun arrays—where each airgun array fires at every alternate periodic location—is called flip-flop acquisition. If we wish to acquire 10.0 s—long shot records at every 12.5 m, the speed of the source vessel would have to be about 1.25 m/s (approximately 2.5 knots). Figure 2.8a illustrates one such conventional acquisition scheme, where each airgun array fires every 20.0 s (or 25.0 m) in a flip-flop manner, traveling at about 1.25 m/s, resulting in nonoverlapping shot records of 10.0 s every 12.5 m. In time-jittered acquisition, Figure 2.8b, each airgun array fires at every 20.0 s jittered time-instances, traveling at about 2.5 m/s (approximately 5.0 knots), with the receivers (OBC) recording continuously, resulting in overlapping (or blended) shot records (Figure 2.9a). Since the acquisition design involves subsampling, the acquired data volume has overlapping shot records and missing shots/traces. Consequently, the jittered flip-flop acquisition might not mimic the conventional flip-flop acquisition where airgun array 1 and 2 fire one after the other—i.e., in Figures 2.8b and 2.8c, a circle (denoting array 1) may be followed by another circle instead of a star (denoting array 2). The minimum interval between the jittered times, however, is maintained at 10.0 s (typical interval required for airgun recharge) and the maximum interval is 30.0 s. For the speed of 2.5 m/s, this translates to jittering a 50.0 m source grid with a minimum (and maximum) interval of 25.0 m (and 75.0 m) between jittered shots. Both arrays fire at the 50.0 m jittered grid independent of each other.

Two realizations of the time-jittered marine acquisition are shown in Figures 2.8b and 2.8c, one each for the baseline and the monitor survey. Acquisition on the 50.0 m jittered grid results in an subsampling factor,

$$\eta = \frac{1}{\text{number of airgun arrays}} \times \frac{\text{jittered spatial grid interval}}{\text{conventional spatial grid interval}} = \frac{1}{2} \times \frac{50.0 \text{ m}}{12.5 \text{ m}} = 2. \tag{2.8}$$

Figures 2.9a and 2.9b show the corresponding randomly subsampled and simultaneous measurements for the baseline and monitor surveys, respectively. Note that only 50.0 s of the continuously recorded data is shown. If we simply apply the adjoint of the acquisition operator to the simultaneous data—i.e., $\mathbf{M}^H\mathbf{y}$, the interferences (or source crosstalk) due to overlaps in the shot records appear as random noise—i.e., incoherent and nonsparse, as illustrated in Figures 2.9c and 2.9d. Our aim is to recover conventional, nonoverlapping shot records from simultaneous data by working with the entire (simultaneous) data volume, and not on a shot-by-shot basis. For the present scenario, since $\eta = 2$, the recovery problem becomes a joint deblending and interpolation problem. In contrast to conventional acquisition at a source sampling grid of 12.5 m (Figure 2.8a), time-jittered acquisition takes half the acquisition time (Figures 2.8b and 2.8c), and the simultaneous data is separated into its individual shot records along with interpolation to the 12.5 m sampling grid.

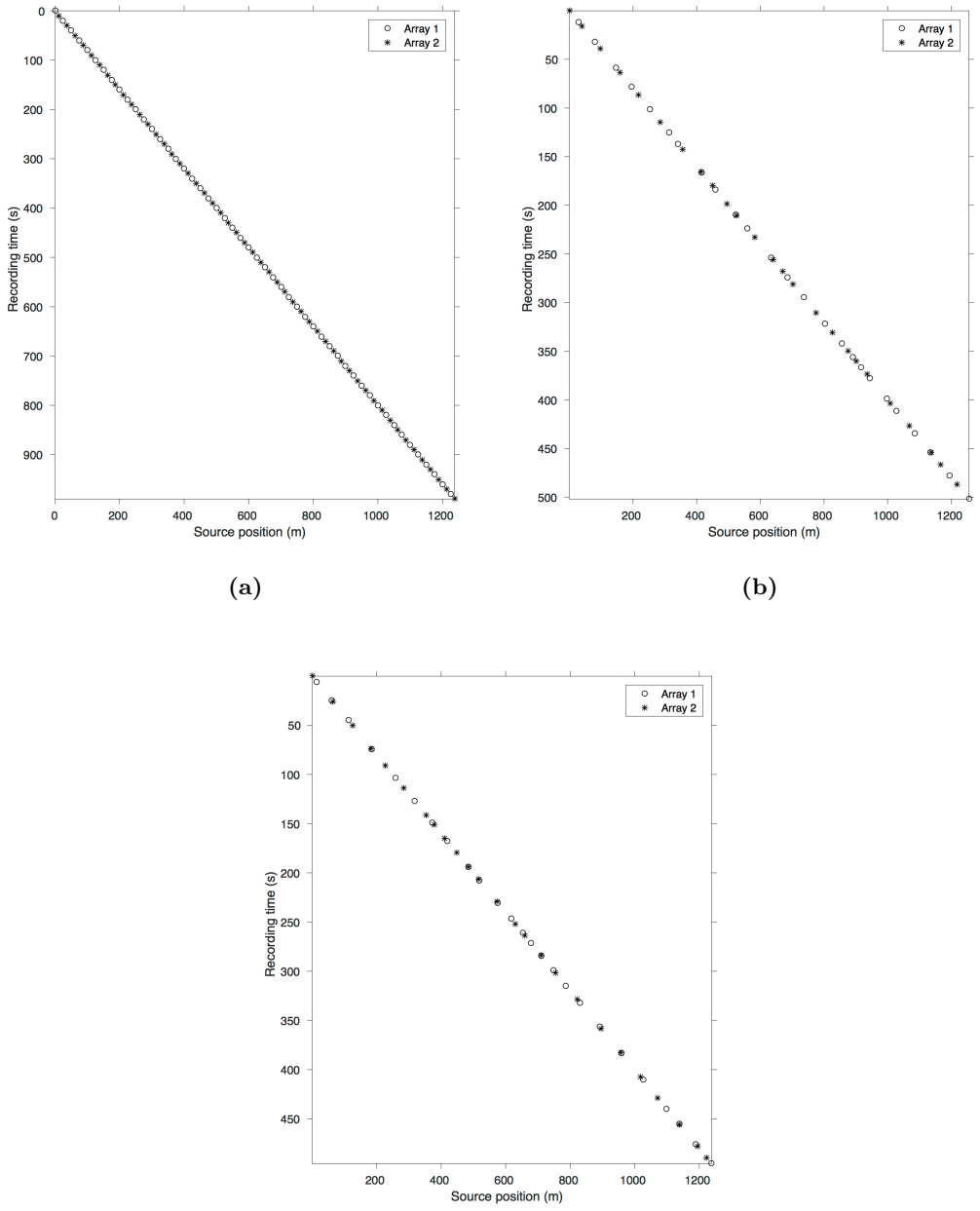

(a) **(b)**

(c)

Figure 2.8 Acquisition geometry: (a) conventional marine acquisition with one source vessel and two airgun arrays; time-jittered marine acquisition (with $\eta = 2$) for (b) baseline, and (c) monitor. Note the acquisition speedup during jittered acquisition, where the recording time is reduced to one-half the recording time of the conventional acquisition. (b) and (c) are plotted on the same scale as (a) in order to make the jittered locations easily visible.

The recovery problem is solved by applying the independent recovery strategy and the joint recovery method, as we will describe in the next section.

2.6.3 Experiments and observations

To analyze the implications of the time-jittered marine acquisition in time-lapse seismic, we follow the same sequence of experiments as conducted for the stylized examples—i.e., we compare the independent (IRS) and joint recovery methods (JRM) for varying degrees of replicability in the acquisition. Given the 12.5 m spatial sampling of the simulated (conventional) time-lapse data, applying the time-jittered marine acquisition scheme results in a subsampling factor, $\eta = 2$ (Equation 2.8). In practice, this corresponds to an improved efficiency of the acquisition with the same factor. Recent work (Mosher et al., 2014) has shown that factors of two or as high as ten in efficiency improvement are achievable in the field. With this subsampling factor, the number of measurements for each experiment is fixed—i.e., $n = N/2$, each for $\mathbf{y}_1$ and $\mathbf{y}_2$ albeit other scenarios are possible.

We simulate different realizations of the time-jittered marine acquisition with 100%, 50%, and 25% overlap between the baseline and monitor surveys. Because we are in a discrete setting, these overlaps translate one-to-one into percentages of replicated on-the-grid shot locations for the surveys. Since $\eta = 2$, and by virtue of the design of the blended acquisition, it is not possible to have two completely different (0% overlap) realizations of the time-jittered acquisition. In all cases, we recover the deblended and interpolated baseline and monitor data from the blended data $\mathbf{y}_1$ and $\mathbf{y}_2$, respectively, using the independent recovery strategy (by solving Equation 2.2) separately and the joint recovery method (by solving Equation 2.6). As stated previously, the inherent time-lapse difference is computed by subtracting the recovered baseline and monitor data.

We perform 100 experiments for the baseline measurements, wherein each experiment has a different random realization of the measurement matrix $\mathbf{A}_1$. Then, for each experiment, we fix the baseline measurement and subsequently work with different random realizations for the monitor survey, each corresponding to the 50% and the 25% overlap. The purpose of doing this is to examine the impact of degree of replicability of acquisition in time-lapse seismic. Table 2.1 summarizes the recovery results for the stacked sections, in terms of the signal-to-noise ratio defined as

$$\mathrm{SNR}(\mathbf{f}, \widetilde{\mathbf{f}}) = -20 \log_{10} \frac{\|\mathbf{f} - \widetilde{\mathbf{f}}\|_2}{\|\mathbf{f}\|_2}, \tag{2.9}$$

for different overlaps between the baseline and monitor surveys—i.e., measurement matrices $\mathbf{A}_1$ and $\mathbf{A}_2$. Each SNR value is an average of 100 experiments including the standard deviation.

Figure 2.10 shows the recovered receiver gathers and difference plots for the monitor survey (for the different overlaps) using the independent recovery strategy (IRS), and Figure 2.11 shows the corresponding result using the joint recovery

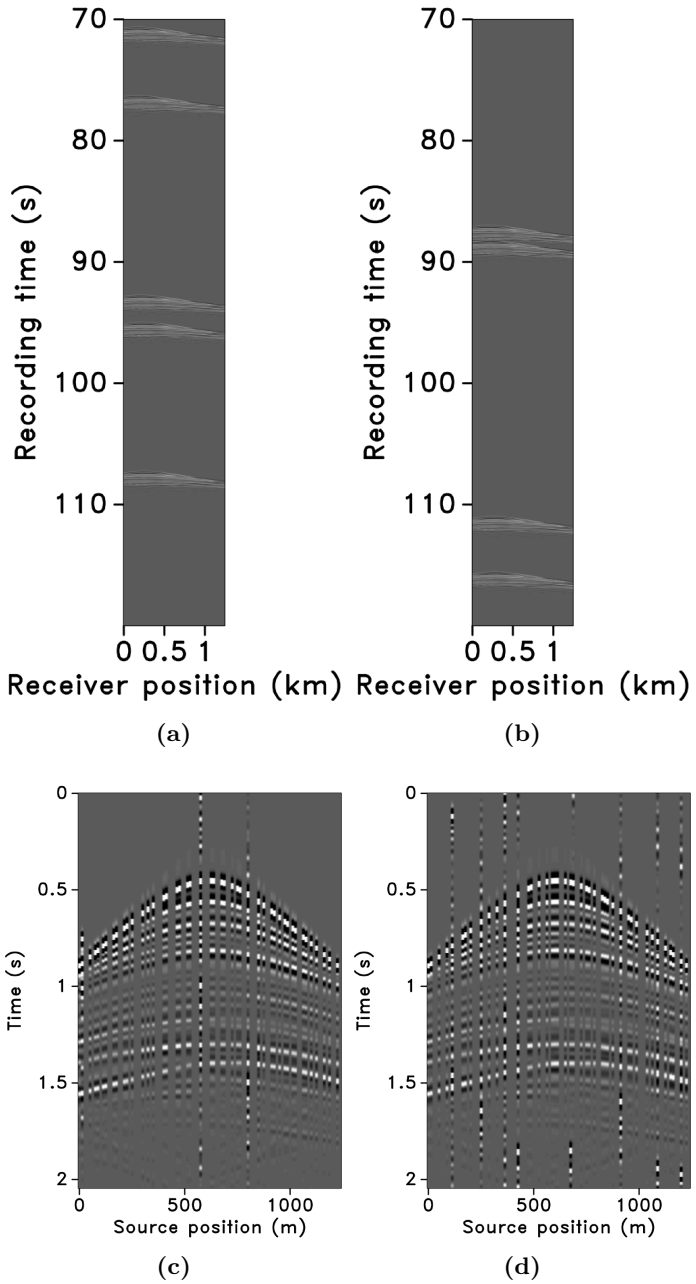

Figure 2.9 Simultaneous data for the (a) baseline and (b) monitor surveys (only 50.0 s of the full data is shown). Interferences (or source crosstalk) in a common-receiver gather for the (c) baseline and (d) monitor surveys, respectively. Since the subsampling factor $\eta = 2$, (c) and (d) also have missing traces. The simultaneous data is separated and interpolated to a sampling grid of 12.5 m.

method (JRM). As illustrated in these figures, JRM leads to significantly improved recovery of the vintage compared to IRS because it exploits the shared information between the baseline and monitor data. Moreover, the recovery improves with decrease in the overlap. The IRS and JRM recovered time-lapse differences for the different overlaps are shown in Figure 2.12, which shows that recovery via JRM is still significantly better than IRS, however, the recovery is slightly improved with increase in the overlap. The edge artifacts in Figures 2.10, 2.11 and 2.12 are related to missing traces near the edges that curvelets are unable to reconstruct.

The SNRs for the stacked sections indicate a similar trend in the observations as made from the stylized experiments—i.e., *(i)* JRM performs better than IRS because it exploits information shared between the baseline and monitor data. Note that the SNR value, which is an average of the 100 experiments, for recovery of the baseline dataset via IRS is repeated for all three cases of overlap because we work with the same 100 realizations of the jittered acquisition throughout. However, for each of the 100 experiments, different realizations are drawn for the monitor survey, which explains the variations in the SNRs for the recovery via IRS. Similar fluctuations were observed by (Herrmann, 2010). *(ii)* Replication of surveys hardly affects recovery of the vintages via IRS (note similar SNRs), since the processing is done in parallel and independently. *(iii)* Recovery of the baseline and monitor data with JRM is better when there is a small degree of overlap between the two surveys, and it decreases with increasing degrees of overlap. As explained earlier, this behavior can be attributed to partial independence of the measurement matrices that contribute additional information via the first column of $\mathbf{A}$ in Equation 2.6, i.e., for time-lapse seismic, independent surveys give additional structural information leading to improved recovery quality of the vintages. *(iv)* The converse is true for recovery of the time-lapse difference, wherein it is better if the surveys are exactly replicated. Again, as stated previously, the reason for this is the increased sparsity of the time-lapse difference itself and apparent cancelations of recovery errors due to the exactly replicated geometry.

In addition to the above observations, we find that for 100% overlap, good recovery of the stacks for IRS and JRM is possible with SNRs that are similar for the time-lapse difference and the vintages themselves. The standard deviations for the two recovery methods are also similar. One could construe that this is the ideal situation but unfortunately it is not easily attained in practice. As we move to more practical acquisition schemes where we decrease the overlap between the surveys, we see a drastic jump downwards in the SNRs for the time-lapse stack obtained with IRS. The results from JRM, on the other hand, decrease much more gradually with standard deviations that vary slightly from those for IRS, however, drops off with decrease in the overlap. In contrast, we actually see significant improvements for the SNRs of the stacks of both the baseline and monitor data with slight variations in the standard deviations.

Remember, that the number of measurements is the same for all experiments and the observed differences can be fully attributed to the performance of the recovery method in relation to the overlap between the two surveys encoded in the measure-

ment matrices. Also, the improvements in SNRs of the vintages are significant as we lower the overlap, which goes at the expense of a relatively small loss in SNR for the time-lapse stack. However, given the context of randomized subsampling, it is important to recover the finely sampled vintages and then the time-lapse difference. In addition, time-lapse differences are often studied via differences in certain poststack attributes computed from the vintages, hence, reinforcing the importance of recovering prestack baseline and monitor data as opposed to recovering the time-lapse difference alone. While some degree of replication seemingly improves the prestack time-lapse difference, we feel that quality of the vintages themselves should prevail in the light of the above discussion. In addition, concentrating on the quality of the vintages gives us the option to compute prestack time-lapse differences in alternative ways (Wang et al., 2008).

Overlap	Baseline		Monitor		4-D signal	
	IRS	JRM	IRS	JRM	IRS	JRM
100%	23.1 ± 1.2	24.8 ± 1.2	23.1 ± 1.3	24.8 ± 1.2	21.4 ± 1.8	23.4 ± 2.1
50%	23.1 ± 1.2	32.8 ± 1.6	23.4 ± 1.2	32.8 ± 1.6	9.1 ± 1.2	20.2 ± 1.3
25%	23.1 ± 1.2	35.3 ± 1.5	22.0 ± 1.1	35.0 ± 1.5	7.8 ± 1.3	18.0 ± 1.1

Table 2.1 Summary of recoveries in terms of SNR (in dB) for the stacked sections.

All these observations are corroborated by the plots of the recovered (monitor) receiver gathers and their differences from the original (idealized) gather in Figures 2.10 and 2.11, and the recovered time-lapse differences in Figure 2.12. Stacked sections of the IRS and the JRM recovered time-lapse difference are shown in Figure 2.13.

2.6.4 Repeatability measure

Aside from measuring SNRs, researchers have introduced repeatability measures expressing the similarity between prestack and poststack time-lapse datasets. One of the most commonly used metrics, which gives an intuitive understanding of the data repeatability, is the normalized root-mean-square (NRMS, Kragh and Christie, 2002):

$$\text{NRMS} = \frac{2\times, \text{RMS}(\widetilde{\mathbf{f}}_2 - \widetilde{\mathbf{f}}_1)}{\text{RMS}(\widetilde{\mathbf{f}}_1) + \text{RMS}(\widetilde{\mathbf{f}}_2)}, \tag{2.10}$$

with $\text{RMS}(\widetilde{\mathbf{f}})$ being the root-mean-square of either vintage. This formula implies that the lower the NRMS, the higher the repeatability between the recovered datasets. Usually, lower levels of NRMS are observed for stacked data compared to prestack data since stacking reduces uncorrelated random noise. A NRMS ratio of 0 is achievable only in a perfectly repeatable world. The lower the NRMS value, the more repeatable the data are. In our studies, we consider NRMS ratios between 0.1 and 0.2 as acceptable and ratios less than 0.1 as excellent. To further evaluate the results

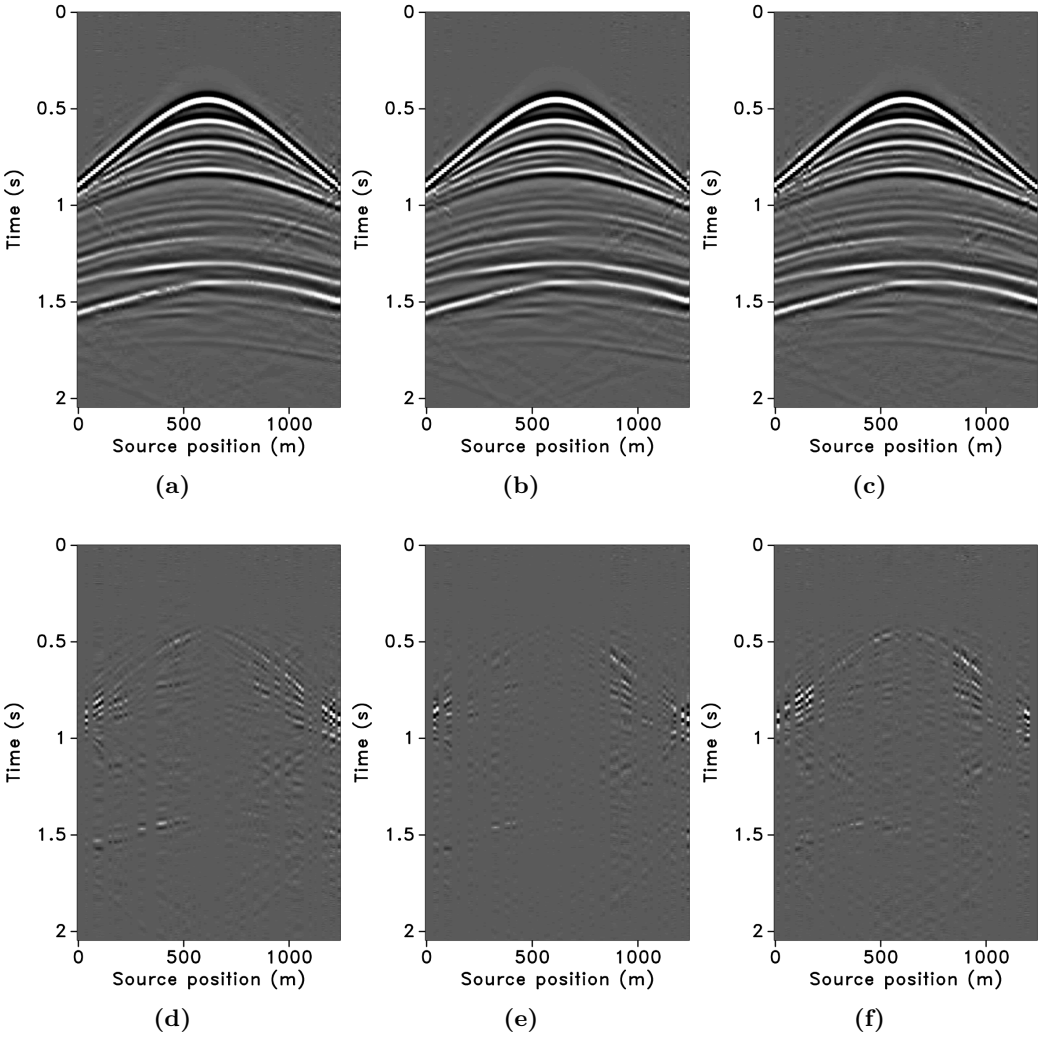

Figure 2.10 Receiver gathers (from monitor survey) recovered via IRS from time-jittered marine acquisition with (a) 100%, (b) 50%, and (c) 25% overlap in the measurement matrices ($\mathbf{A_1}$ and $\mathbf{A_2}$). (d), (e), and (f) Corresponding difference plots from the original receiver gather (2.7b).

of our synthetic seismic experiment, we compute the NRMS ratios from stacked sections before and after recovery via IRS and JRM.

To compute this quantity, we extract time windows from stacked sections around two-way travel time between 0.5 s and 1.3 s, where we know there is no time-lapse signal present. We obtain the stacked sections before and after processing by either applying the adjoint of the sampling matrix (see discussion under Equation 2.8) to the observed data or by solving a sparsity-promoting program. The former serves as a proxy for acquisition scenarios where one relies on the fold to stack out acquisition related artifacts. Results of this exercise for 50% overlap and 25% overlap

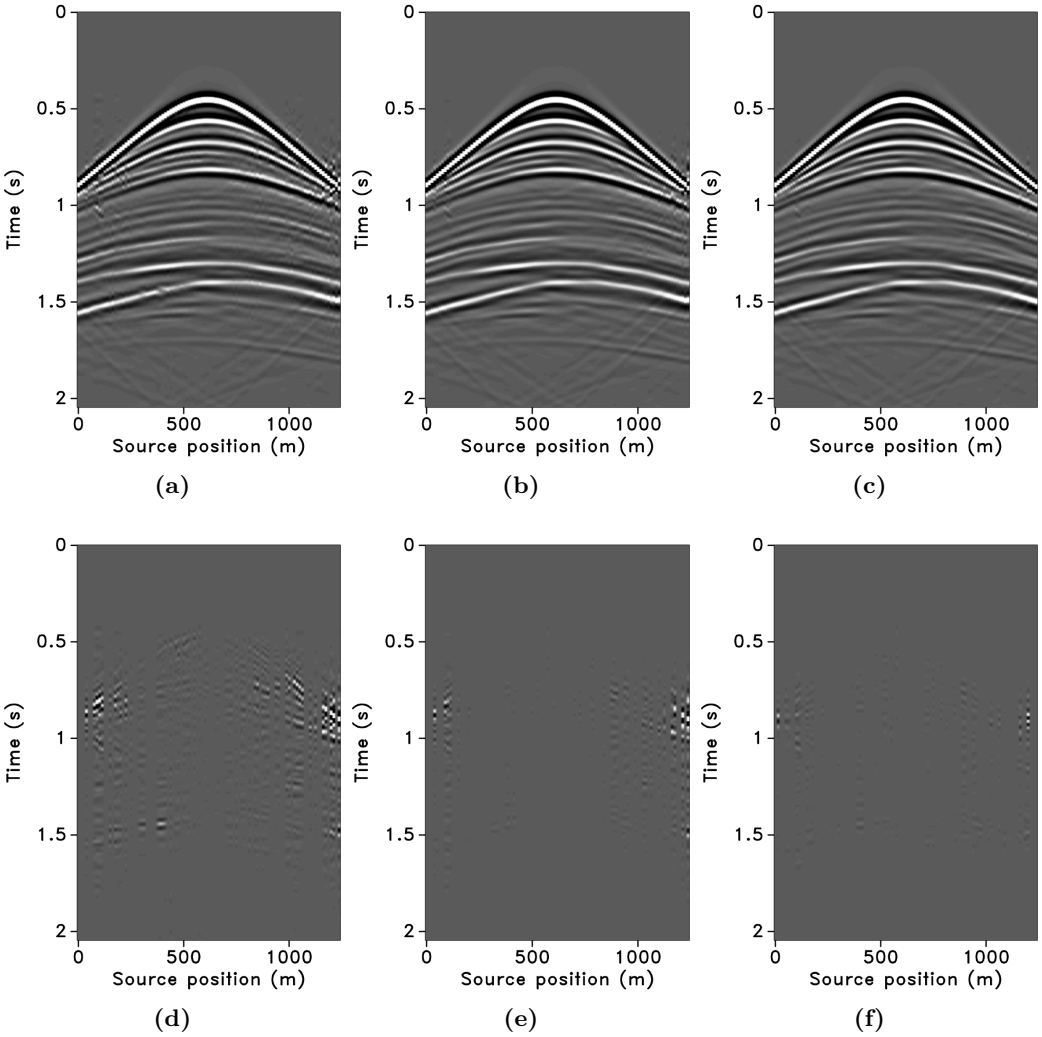

Figure 2.11 Receiver gathers (from monitor survey) recovered via JRM from time-jittered marine acquisition with (a) 100%, (b) 50%, and (c) 25% overlap in the measurement matrices ($\mathbf{A_1}$ and $\mathbf{A_2}$). (d), (e), and (f) Corresponding difference plots from the original receiver gather (2.7b).

are included in Figures 2.14a and 2.14b. These plots clearly show that *(i)* simply applying the adjoint, followed by stacking, leads to poor repeatability, and therefore is unsuitable for time-lapse practices; *(ii)* sparse recovery improves the NRMS; *(iii)* exploiting shared information amongst the vintages leads to near optimal values for the NRMS despite the subsampling; and finally *(iv)* high degrees of repeatability of recovered data are achievable from data collected with small overlaps in the acquisition geometry.

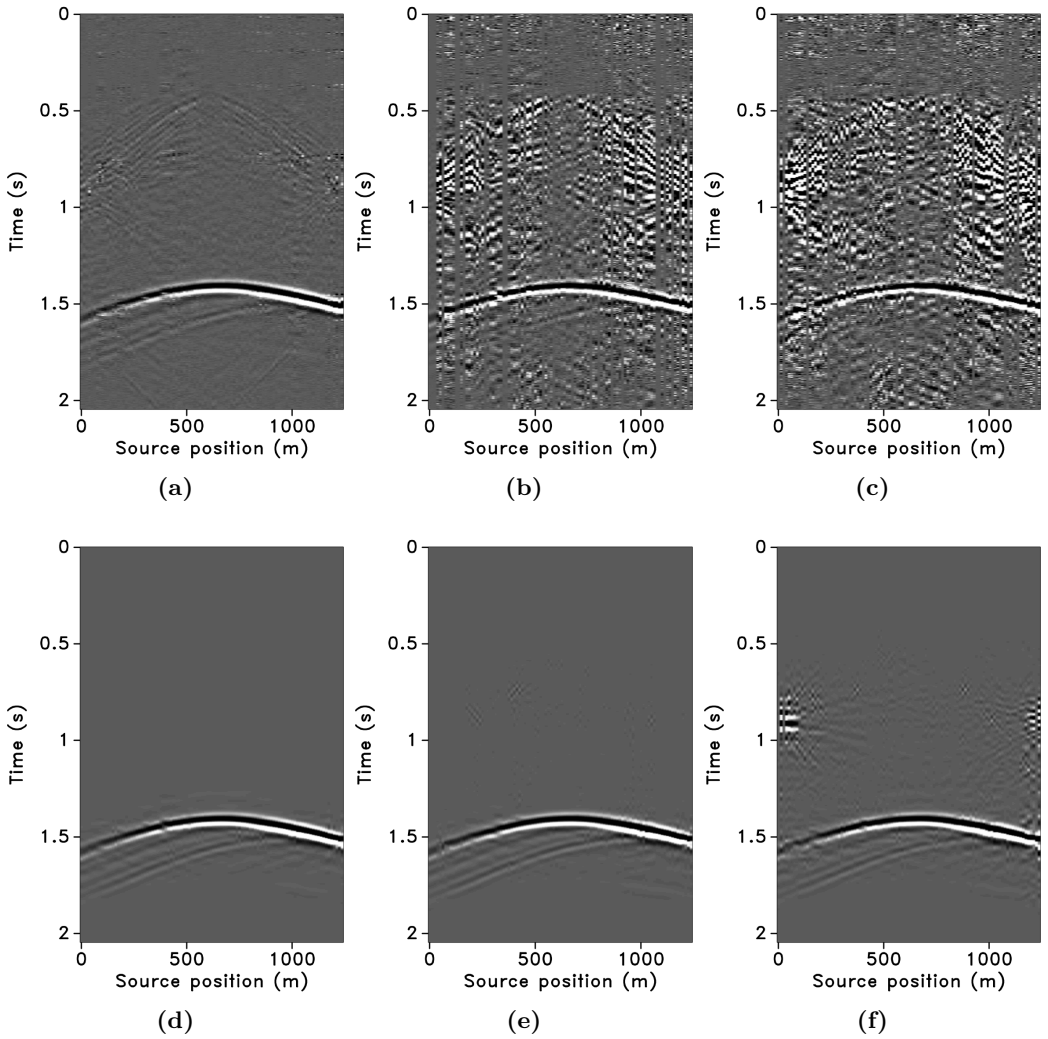

Figure 2.12 Recovered 4-D signal for the (a) 100%, (b) 50%, and (c) 25% overlap. Top row: IRS, bottom row: JRM. Note that the color axis is one-tenth the scale of the color axis for the vintages.

2.7 Discussion

Obtaining useful time-lapse seismic is challenging for many reasons, including cost, the need to calibrate the surveys, and the subsequent processing to extract reliable time-lapse information. Meeting these challenges in the field has resulted in acquisitions which aim to replicate the geometry of the previous survey(s) as precisely as possible. Unfortunately, this replication can be both difficult to achieve and expensive. Post acquisition, processing aims to improve the repeatability of the data such that certain (poststack) attributes can be derived reliably from the baseline and monitor surveys. Within this context, our aim is to reduce the cost and improve the

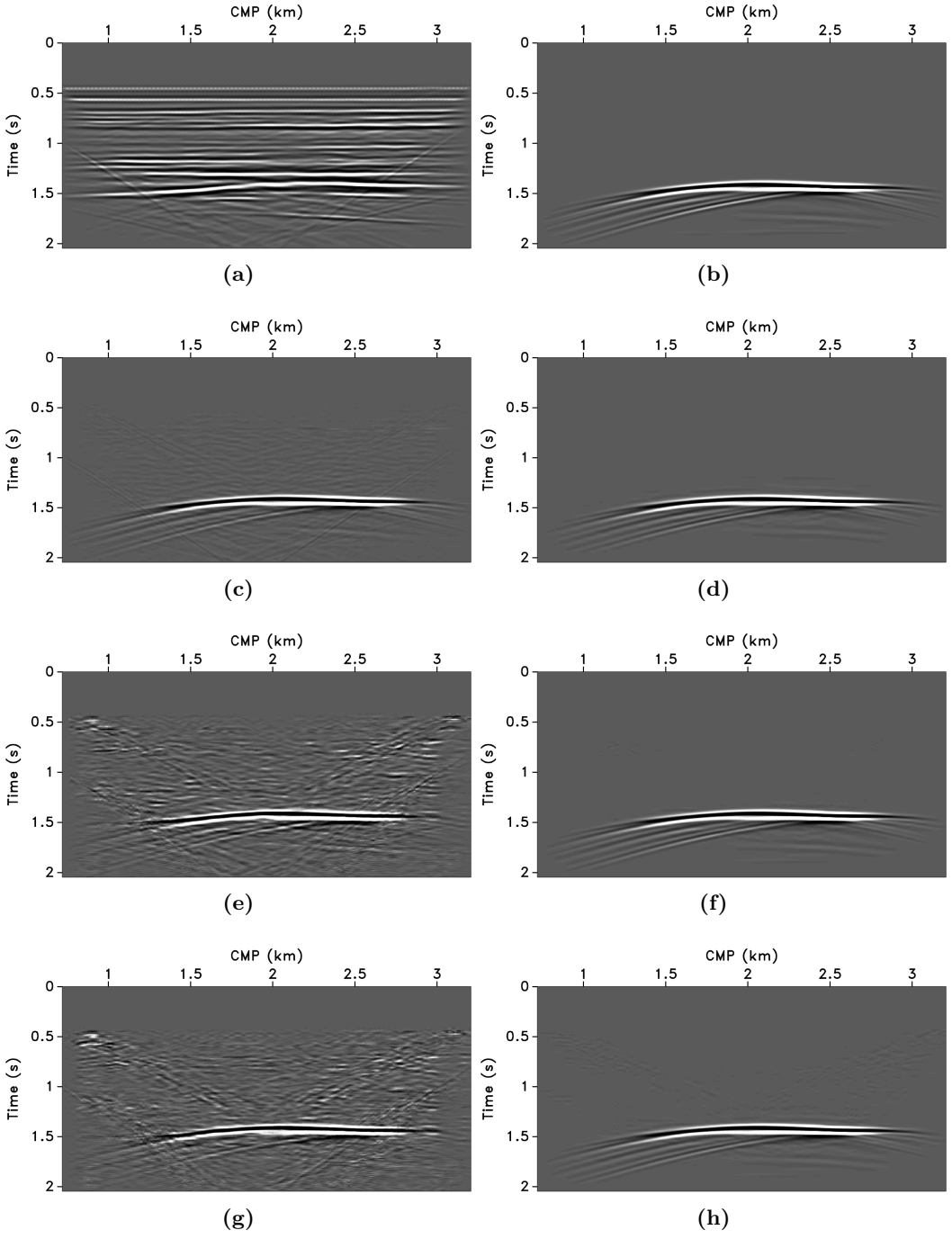

Figure 2.13 Stacked sections. (a) baseline; (b) true 4-D signal; reconstructed 4-D signals via IRS for 100% (c), 50%(e), and 25% (g) overlap; the reconstructed 4-D signals via JRM for 100%(d), 50%(f), and 25% (h) overlap. Notice the improvements for JRM where we see much less deterioration as the overlap between the surveys decreases. Note that the color axis for the time-lapse difference stacks is one-tenth the scale of the color axis for the baseline stack.

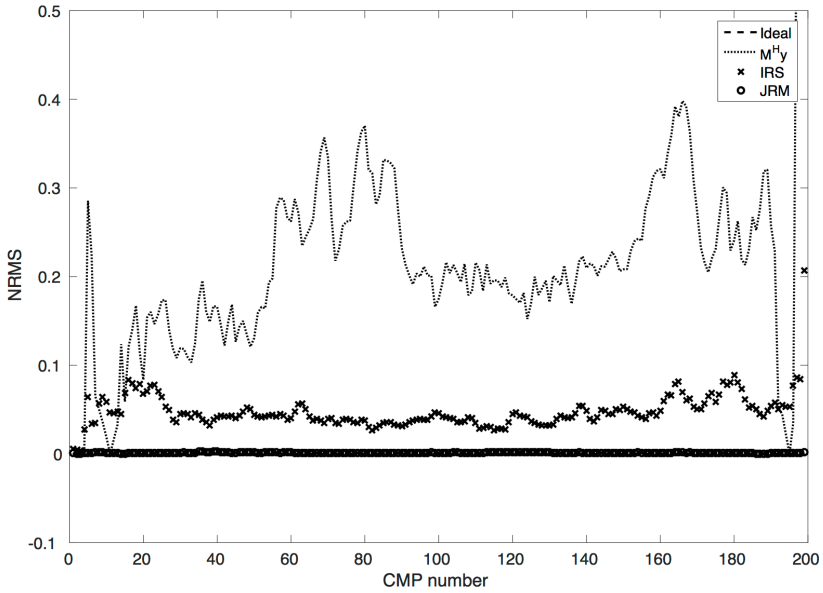

(a)

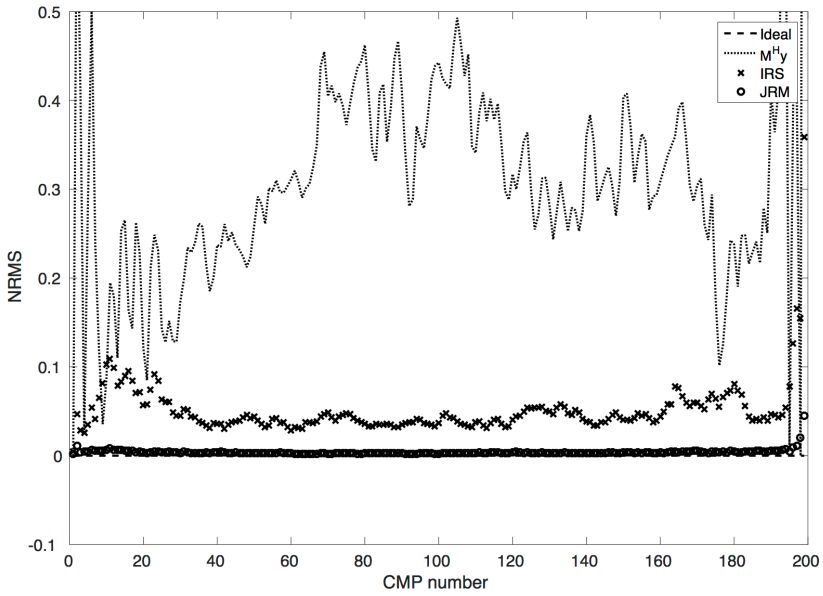

(b)

Figure 2.14 NRMS for each recovered trace of the stacked section for *(a)* 50% and the *(b)* 25% overlap. Vintages obtained with the joint recovery method are more repeatable compared to those obtained via independent recovery and the "unprocessed" stacks. The latter are unsuitable for time lapse.

quality of the prestack baseline and monitor data without relying on expensive fine sampling and high degrees of replicability of the surveys. Our methodology involves a combination of economical randomized samplings and sparsity-promoting data recovery. The latter exploits (curvelet-domain) sparsity and correlations amongst different vintages. To the authors' knowledge, this approach is among the first to address time-lapse seismic problems in which the common component amongst vintages—and innovations with respect to this shared component—is made explicit.

The presented synthetic seismic case study, supported by the findings from the stylized examples and theoretical results from the distributed compressive sensing literature (Baron et al., 2009a), represents a proof of concept for how sharing information amongst the vintages can lead to high-fidelity vintages and 4-D signals (with minor trade-offs) in a cost effective manner. This approach creates new possibilities for meeting modern survey objectives, including cost and environmental impact considerations, and improvements in spatial sampling. In this chapter, even though our measurements are taken on the grid, allowing us to ignore errors related to sampling off the grid, our proposed time-lapse acquisition is low-cost since we are always subsampled in the surveys. Our joint recovery model produces finely sampled data volumes from these subsampled, and not necessarily replicable, randomized surveys. These data volumes exhibit better repeatability levels (in terms of NRMS ratios) compared to independent recovery, where correlations amongst the vintages are not exploited.

In chapter 3, we demonstrate how we deal with the effects of non-replicability of the surveys when we take measurements from an irregular grid. We demonstrate that errors related to being off the grid cannot be ignored. The "bad news" is that replication is unattainable because small inevitable deviations in the shot locations amongst the time-lapse surveys negate the benefit of replication for the time-lapse signal itself. However, the good news is that a slightly deviated measurement already adds information that improves recovery of the vintages. This implies that an argument can be made to not replicate the surveys as long as we know sufficiently accurately where we fired in the field. Please remember that the claims of this paper relate to the unnecessary requirement to visit the same randomly subsampled on-the-grid shot locations during the two, or more, surveys.

Furthermore, we did not consider surveys that have been acquired in situations where there are significant variations in the water column velocities amongst the different surveys. As long as these physical changes can be modeled, we do not foresee problems. As expected using standard CS, our recovery method should be stable with respect to noise (Candes et al., 2006), but this needs to be investigated further. Moreover, recent successes in the application of compressive sensing to actual land and marine field data acquisition (see e.g. (Mosher et al., 2014)) support the fact that these technical challenges with noise and calibration can be overcome in practice. Our future research will also involve working with towed-streamer surveys where other challenges like the sparse and irregular crossline sampling will be investigated.

In this study, we concentrated our efforts on producing high-quality baseline and monitor surveys from economic randomized acquisitions. There are areas of application for the joint recovery model that have not yet been explored in detail, such as imaging and full-waveform inversion problems. Early results on these applications suggest that our joint recovery model extends to sparsity-promoting imaging (Tu et al., 2011; Herrmann and Li, 2012) including imaging with surface-related multiples, and time-lapse full-waveform inversion (Oghenekohwo et al., 2015). In all applications, the use of shared information amongst vintages improves the inversion results even for acquisitions with large gaps.

Finally, we note that several authors use the shared information in time-lapse vintages in inversion formulations that differ from ours. For instance, double difference waveform inversion (Yang et al., 2014, 2015; Asnaashari et al., 2015), total-variation norm minimization on time-lapse earth models (Maharramov and Biondi, 2014; Maharramov et al., 2016), and bootstrap inversion (Kamei and Lumley, 2017) all present alternative ways of extracting 4D changes from time-lapse data.

2.8 Conclusions

We considered the situation of recovering time-lapse data from on-the-grid but randomly subsampled surveys. In this idealized setting, where we ignore the effects of being off the grid, we found that it is better not to revisit the on-the-grid shot locations amongst the time-lapse surveys when the vintages themselves are of prime interest. This result is a direct consequence of introducing a common component, which contains information shared amongst the vintages, as part of our proposed joint recovery method. Compared to independent recoveries of the vintages, we obtain time-lapse data exhibiting a higher degree of repeatability in terms of normalized root-mean-square ratios. Under the above stated idealized setting and ignoring complicating factors such as tidal differences, our proposed method lowers the cost and environmental imprint of acquisition because fewer shot locations are visited. It also allows us to extend the survey area or to increase the data's resolution at the same costs as conventional surveys. Our improvements concern the vintages and not the time-lapse difference itself, which would benefit if we choose to use the same shot locations during the surveys. Because we are generally interested in "post-stack" attributes derived from the vintages, their recovery took prevalence. So, we make the argument not to replicate—i.e., revisit on-the-grid shot locations during randomized surveys in cases where poststack time-lapse attributes are of interest only.

Chapter 3

Low-cost time-lapse seismic with distributed Compressive Sensing—impact on repeatability

3.1 Summary

Irregular or off-the-grid spatial sampling of sources and receivers is inevitable in field seismic acquisitions. Consequently, time-lapse surveys become particularly expensive since current practices aim to replicate densely sampled surveys for monitoring changes occurring in the reservoir due to hydrocarbon production. We demonstrate that under certain circumstances, high-quality prestack data can be obtained from cheap randomized subsampled measurements that are observed from nonreplicated surveys. We extend our time-jittered marine acquisition to time-lapse surveys by designing acquisition on irregular spatial grids that render simultaneous, subsampled and irregular measurements. Using the fact that different time-lapse data share information and that nonreplicated surveys add information when prestack data are recovered jointly, we recover periodic densely sampled and colocated prestack data by adapting the recovery method to incorporate a regularization operator that maps traces from an irregular spatial grid to a regular periodic grid. The recovery method is, therefore, a combined operation of regularization, interpolation (estimating missing fine-grid traces from subsampled coarse-grid data), and source separation (unraveling overlapping shot records). By relaxing the insistence on replicability between surveys, we find that recovery of the time-lapse difference shows little variability for realistic field scenarios of slightly nonreplicated surveys that suffer from unavoidable natural deviations in spatial sampling of shots (or receivers) and pragmatic compressed-sensing based nonreplicated surveys when compared to the "ideal" scenario of exact replicability between surveys. Moreover, the recovered densely sampled prestack baseline and monitor data improve significantly when the

acquisitions are not replicated, and hence can serve as input to extract poststack attributes used to compute time-lapse differences. Our observations are based on experiments conducted for an ocean-bottom cable survey acquired with time-jittered continuous recording assuming source equalization (or same source signature) for the time-lapse surveys and no changes in wave heights, water column velocities or temperature and salinity profiles, etc.

3.2 Introduction

Simultaneous marine acquisition is being recognized as an economic and environmentally more sustainable way to sample seismic data and speedup acquisition, wherein single or multiple source vessels fire shots at random, compressed times resulting in overlapping shot records (de Kok and Gillespie, 2002; Beasley, 2008; Berkhout, 2008; Hampson et al., 2008b; Moldoveanu and Quigley, 2011; Abma et al., 2013), and hence generating compressed seismic data volumes. The aim then is to separate the overlapping shot records into individual shot records, as acquired during conventional acquisition, but with denser source sampling while preserving amplitudes of the late, often weak, arrivals. This leads to recovering densely sampled data economically, which is essential for producing high-resolution images of the subsurface.

(Mansour et al., 2012), (Wason and Herrmann, 2013) and (Mosher et al., 2014) have showed that compressed sensing (CS, Candès et al., 2006; Donoho, 2006) is a viable technology to sample seismic data economically with low environmental imprint—by reducing numbers of shots (or injected energy in the subsurface) or compressing survey times. (Mansour et al., 2012) and (Wason and Herrmann, 2013) proposed an alternate sampling strategy for simultaneous acquisition ("time-jittered" marine), addressing the separation problem through a combination of tailored (simultaneous) acquisition design and sparsity-promoting recovery via convex optimization using ℓ_1 objectives. This separation technique interpolates sub-Nyquist jittered shot positions to a fine regular grid while unraveling the overlapping shots. The time-jittered marine acquisition is designed for continuous recording, fixed-receiver (or "static") geometries, which is different from the case of towed-streamer (or "dynamic") geometries, wherein multiple sources fire shots within a time interval of $(0, 1)$ or $(0, 2)$ s generating overlapping shot records that need to be separated into its constituent sources, i.e., a data volume for each individual source (Kumar et al., 2015). Our approach for conventional data recovery from simultaneous data from static geometries can equally apply to other settings including static land and other static marine geometries.

The implications of randomization in time-lapse (or 4D) seismic, however, are less well-understood since the current paradigm relies on dense sampling and replicability amongst the baseline and monitor surveys (Lumley and Behrens, 1998). These requirements impose major challenges because dense sampling is prohibitively expensive and variations in acquisition geometries (between the surveys) due to

physical constraints do not allow for exact replication of the surveys. In chapter 2, we presented a new approach (the "joint recovery method") that addresses these acquisition- and processing-related issues by explicitly exploiting common information shared by the different time-lapse vintages. Our analyses were carried out assuming that the observations lied on a discrete grid so that exact survey replicability is in principle achievable. We also assume sources to have the same source signature for the time-lapse surveys. While assuming source equalization in this chapter, we extend our work on simultaneous time-jittered marine acquisition to time-lapse surveys for more realistic field acquisitions that lie on irregular spatial grids, where the notion of exact replicability of the surveys is inexistent. This is because the "real" world suffers from unavoidable deviations between pre- and post-acquisition shot (and receiver) positions, rendering regular, periodic spatial grids irregular, and hence exact replication of the surveys impossible. As mentioned later in the chapter, accounting for the irregularity of seismic data is key to recovering densely sampled data. Moreover, while we do not insist that we actually visit pre-designed (irregular) shot positions, but it is important to know these positions to sufficient accuracy after acquisition for high-quality data recovery. Recent successes in the application of compressed sensing to land and marine field data acquisition (see e.g., Mosher et al., 2014) show that this can be achieved in practice.

Simultaneous time-jittered marine acquisition generates compressed and subsampled data volumes, therefore, extending this to time-lapse surveys generates compressed and subsampled baseline and monitor data. Consequently, we are interested in recovering densely sampled vintages and time-lapse difference. Moreover, time-lapse differences are often studied via differences in certain poststack attributes computed from the vintages (Landrø, 2001; Spetzler and Kvam, 2006), hence, we prioritize on recovering the prestack vintages. In this chapter, we push this technology to realistic settings of off-the-grid acquisitions and demonstrate that we actually gain if we relax the insistence to replicate surveys since even the smallest known deviations from the grid can lead to significant improvements in the recovery of the vintages with minimal compromise with the recovery of the time-lapse difference.

3.2.1 Motivation: on-the-grid vs. off-the-grid data recovery

Chapter 2 illustrated that the joint recovery method gives better recoveries of time-lapse data and time-lapse difference than the independent recovery strategy, since the former approach exploits the common information shared by the vintages. It also showed that "exact" replication of the baseline and monitor surveys lead to good recovery of the time-lapse difference but not of the vintages. These analyses, however, were carried out assuming that the observations lied on a discrete grid so that exact survey replicability is achievable. Realistic field acquisitions, on the contrary, lie off the grid—i.e., have irregular spatial sampling—where exact replicability of the surveys is inexistent. Figure 3.1 shows a comparison between conventional periodic acquisition which generates data with nonoverlapping shot records, and simultaneous time-jittered acquisition which generates compressed recordings with

overlapping shots. Note that the sampling grid for conventional acquisition "in the field" would be slightly irregular, however, this in contrast to the jittered acquisition which by virtue of its design is aperiodic and lies on an irregular sampling grid. Since the time-jittered acquisition scheme leverages compressed sensing—the success of which hinges on randomized subsampling—additional and unavoidable deviations in the field add to the randomization of the designed irregular shot positions, and helps in sparsity-promoting inversion as long as we know the final shot positions to sufficient precision.

Figures 3.2a-3.2c show receiver gathers from a conventional (synthetic) time-lapse data set and the corresponding time-lapse difference. To recover periodic densely sampled data from simultaneous, compressed and irregular data, we could implicitly rely on binning, however, failure to account for irregularity of seismic traces can adversely affect the recovery as shown in Figure 3.3. This is because binning does not represent accurate positions of irregular traces. Note that this example corresponds to a time-jittered acquisition scheme for the baseline that is exactly replicated for the monitor. The results show that binning offsets all the gains of exact survey replication and also of the joint recovery method. Figure 3.4 illustrates the importance of regularization of irregular traces for high-quality data recovery. In this chapter, therefore, we extend our work on simultaneous time-jittered acquisition to time-lapse surveys by acknowledging the irregularity of field seismic data and incorporating sparsifying transforms that exploit this irregularity to recover periodic densely sampled time-lapse data.

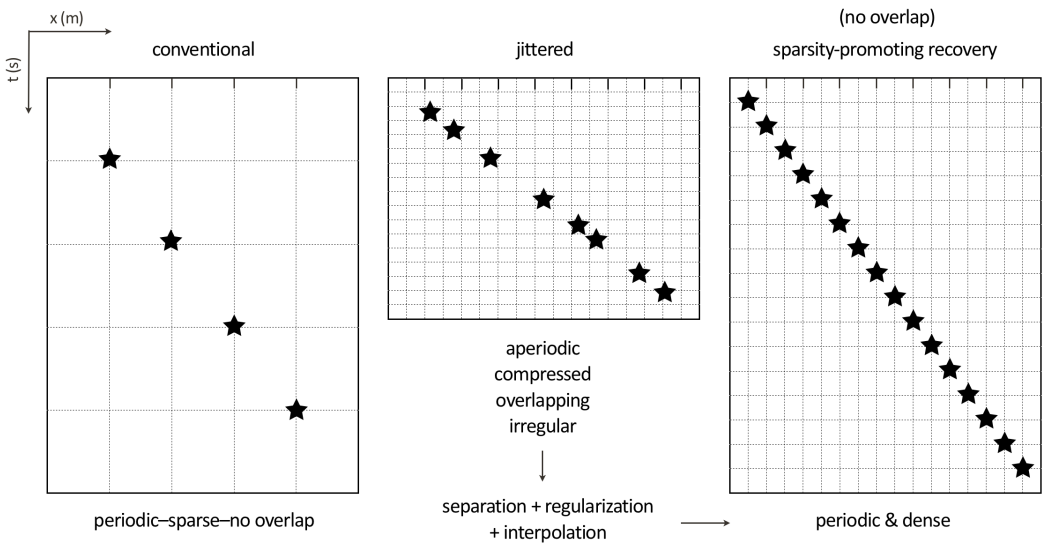

Figure 3.1 Schematic of conventional acquisition and simultaneous, compressed (or time-jittered) acquisition. If the source sampling grid for conventional acquisition is 25.0 m (or 50.0 m for flip-flop acquisition), then the time-jittered acquisition jitters (or perturbs) shot positions on a finer grid, which is 1/4 th of the conventional flip-flop sampling grid, for a single air-gun array. Following the same strategy, adding another air-gun array makes the acquisition simultaneous, and hence results in a compressed data volume with overlapping, irregular shots and missing traces. The sparsity-promoting inversion then aims to recover densely sampled data by separating the overlapping shots, regularizing irregular traces and interpolating missing traces.

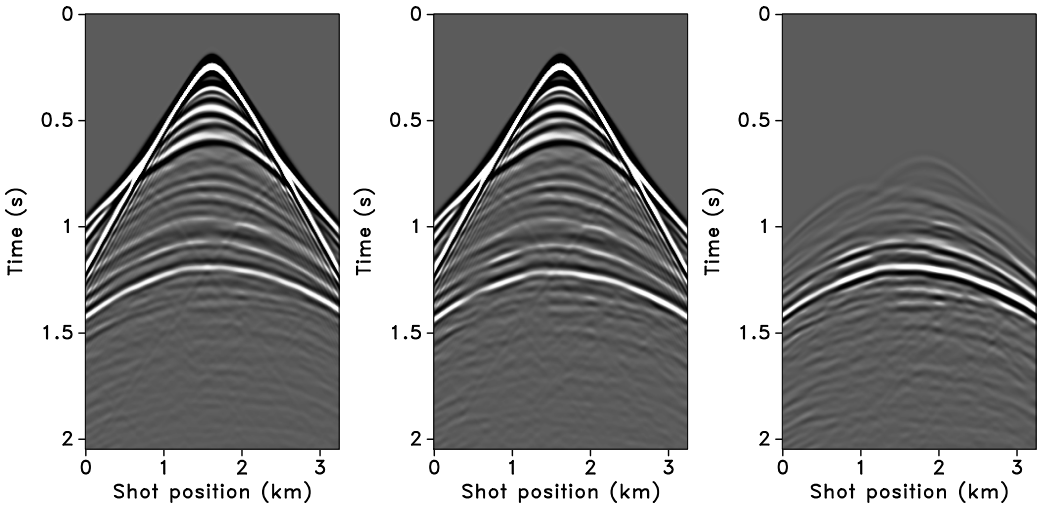

Figure 3.2 Synthetic receiver gathers from a conventional (a) baseline survey, (b) monitor survey. (c) Corresponding time-lapse difference.

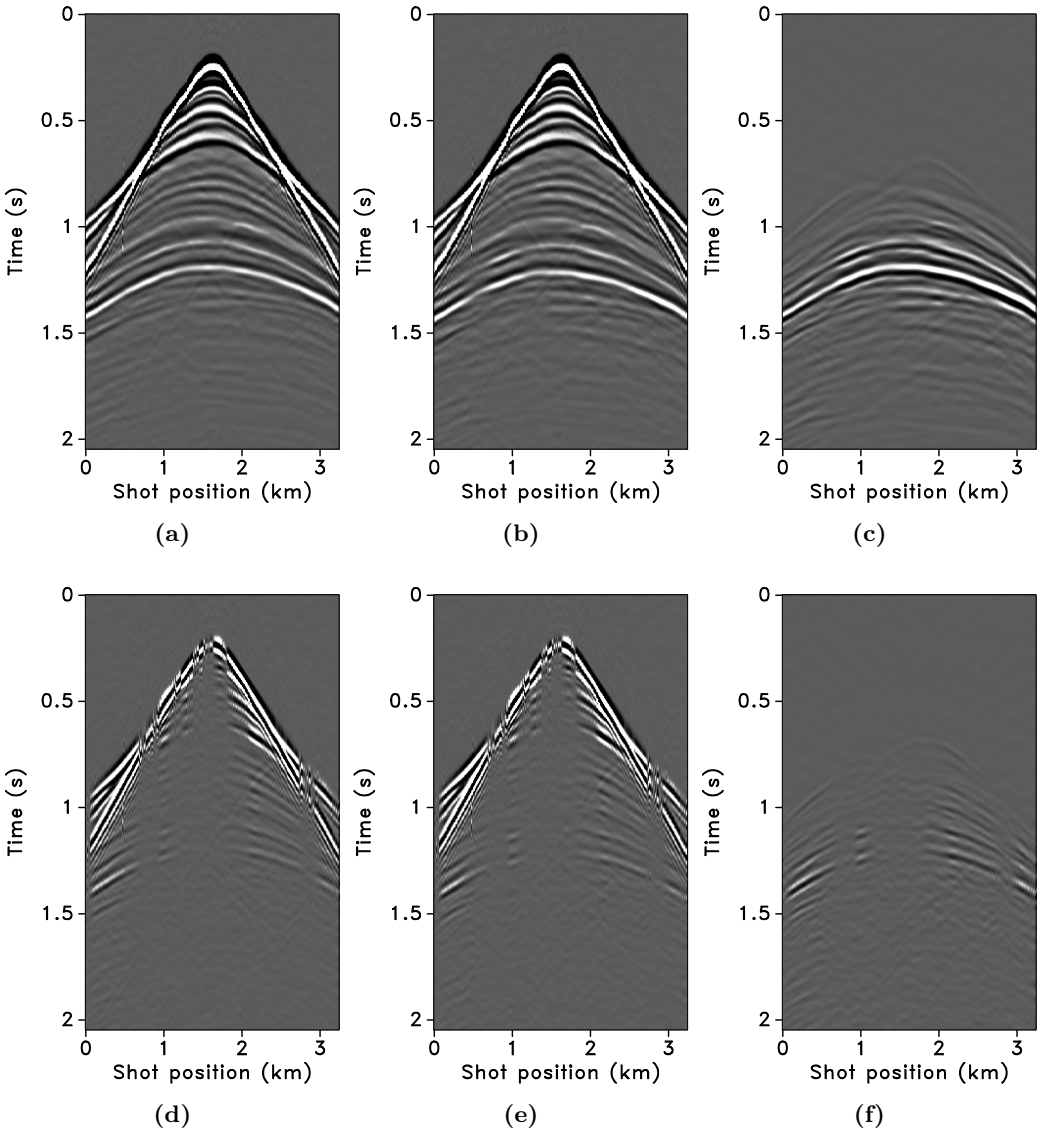

Figure 3.3 Data recovery via the joint recovery method and binning. (a), (b) Binned vintages and (c) corresponding time-lapse difference. (d), (e), (f) Corresponding difference plots.

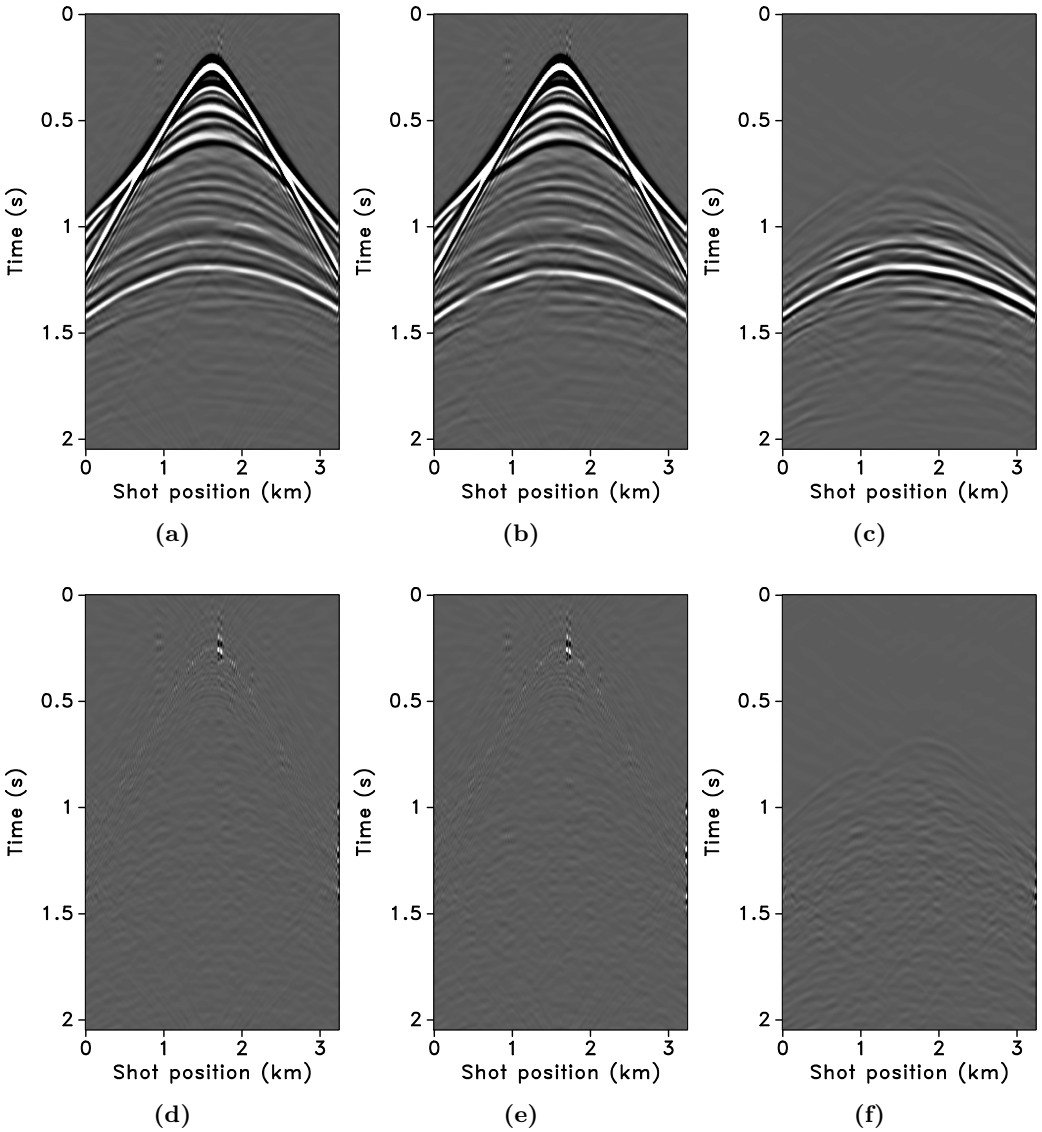

Figure 3.4 Data recovery via the joint recovery method and regularization. (a), (b) Vintages and (c) time-lapse difference recovered via sparsity promotion including regularization of irregular traces. (d), (e), (f) Corresponding difference plots. As illustrated, regularization is imperative for high-quality data recovery.

3.2.2 Contributions

The contributions of this work can be summarized as follows. First, we present an extension of our simultaneous time-jittered marine acquisition for time-lapse surveys by working on more realistic field acquisition scenarios by incorporating irregular spatial grids. Second, we leverage ideas from compressed sensing and

distributed compressed sensing to develop an algorithm that separates simultaneous data, regularizes irregular traces and interpolates missing traces—all at once. Third, through simulated experiments, we show that insistence on replicability of time-lapse surveys can be relaxed since small known deviations in shot positions from a regular grid (or deviations in shot positions of the monitor survey from those in the baseline survey) lead to significant improvements in the recovery of the vintages, without drastic modifications in the recovery of the time-lapse difference.

3.2.3 Outline

The chapter is organized as follows. We begin with the description of the simultaneous time-jittered marine acquisition design, where we explain how subsampled and irregular measurements are generated. Next, we introduce the nonequispaced fast discrete curvelet transform (NFDCT) and its application to recover periodic densely sampled seismic lines from simultaneous and irregular measurements via sparsity-promoting inversion. We then extend this framework to time-lapse surveys where we modify the measurement matrices in the joint recovery method to include the off-the-grid information—i.e., the irregular shot positions and jittered times. Note that we do not describe the independent recovery strategy since it is clear in chapter 2 that the joint recovery method outperforms the former approach. We conduct a series of synthetic seismic experiments with different random realizations of the simultaneous time-jittered marine acquisition to assess the effects (or risks) of irregular sampling in the field on time-lapse data and demonstrate that high-quality data recoveries are the norm and not the exception. We show this by generating 2D seismic lines using two different velocity models—one with simple geology and complex time-lapse difference (BG COMPASS model), and the other with complex geology and complex time-lapse difference (SEAM Phase 1 model with simulated time-lapse difference). Aside from computing signal-to-noise ratios measured with respect to densely sampled true baseline, monitor, and time-lapse differences, we also measure the economic and environmental performance of the proposed acquisition design and recovery strategy by computing the improvement in spatial sampling.

3.3 Time-jittered marine acquisition

The objective of CS is to recover densely sampled data from (randomly) subsampled data by exploiting sparse structure in the data during sparsity-promoting recovery. (Mansour et al., 2012), (Wason and Herrmann, 2013) presented a pragmatic simultaneous marine acquisition scheme, termed as time-jittered marine, that leverages ideas from compressed sensing by invoking randomness and subsampling—i.e., sample randomly with fewer samples than required by Nyquist sampling criteria in the acquisition via random jittering of the source firing times. The success of CS hinges on randomized subsampling since it renders subsampling related artifacts incoherent, and therefore nonsparse, favouring data recovery via structure-promoting

inversion. Consequently, source interferences (in simultaneous acquisition) become incoherent in common-receiver gathers creating a favorable condition for separating simultaneous data into conventional nonsimultaneous data via curvelet-domain sparsity promotion. The CS paradigm, however, assumes signals to be sampled on a periodic discrete grid—i.e., signals with sparse representation in finite discrete dictionaries.

Data volumes collected during seismic acquisition represent discretization of analog finite-energy wavefields in up to five dimensions including time—i.e., we acquire an analog spatiotemporal wavefield $\bar{f}(t,x) \in L^2((0,T] \times [-X,X]^4)$, two dimensions for receivers and two dimensions for sources, with time T in order of seconds and length X in order of kilometers. In an ideal world, signals would perfectly lie on a periodic, regular grid. Hence, with a linear high-resolution analog-to-digital converter $\bar{\Phi}_s$, the discrete signal is represented as $f[q] = \bar{f} \star \bar{\Phi}_s(q)$, for $0 \leq q < N$ (Mallat, 2008), where the samples lie on a grid. Typically, these samples are organized into a vector $\mathbf{f} = f[q]_{q=0,\ldots,N-1} \in \mathbb{R}^N$. Signals we encounter in the real world, however, are usually not uniformly regular and do not lie on a regular grid. Therefore, it is imperative to define an irregular sampling adapted to the local signal regularity (Mallat, 2008). For irregular sampling, the discretized irregular signal is represented as $f[q_n] = \bar{f} \star \bar{\Phi}_s(q_n)$, for $n = 0, ..., M-1$ and $M \leq N$, where q_n are irregular points (or nonequispaced nodes) randomly chosen from the set $\{0, ..., N-1\}$. Its vector representation is $\mathbf{f} = f[q_n]_{n=0,\ldots,M-1}$.

For a signal $\mathbf{f}_0 \in \mathbb{R}^N$ that admits a sparse representation $\mathbf{x}_0$ in some transform domain—i.e., $\mathbf{f}_0$ is sparse with respect to a basis or redundant frame $\mathbf{S} \in \mathbb{C}^{P \times N}$, with $P \geq N$, such that $\mathbf{f}_0 = \mathbf{S}^H \mathbf{x}_0$ ($\mathbf{x}_0$ sparse), where ^{H} denotes the Hermitian transpose—the goal in CS is to reconstruct the signal $\mathbf{f}_0$ from few random linear measurements, $\mathbf{y} = \mathbf{A}\mathbf{f}_0$, where $\mathbf{A}$ is an $n \times N$ measurement matrix with $n \ll N$. Utilizing prior knowledge that $\mathbf{f}_0$ is sparse with respect to a basis or redundant frame $\mathbf{S}$ and assuming the signal to be sampled on a periodic discrete grid, CS aims to find an estimate $\tilde{\mathbf{x}}$ for the underdetermined system of linear equations: $\mathbf{y} = \mathbf{A}\mathbf{f}_0$. This is done by solving the basis pursuit (BP, Candès et al., 2006; Donoho, 2006) convex optimization problem:

$$\tilde{\mathbf{x}} = \underset{\mathbf{x}}{\operatorname{argmin}} \|\mathbf{x}\|_1 := \sum_{i=1}^{N} |x_i| \quad \text{subject to} \quad \mathbf{y} = \mathbf{A}\mathbf{x}. \tag{3.1}$$

In the noise-free case, this problem finds amongst all possible vectors $\mathbf{x}$, the vector that has the smallest ℓ_1-norm and that explains the observed subsampled data.

Mathematically, a seismic line with N_s sources, N_r receivers, and N_t time samples can be reshaped into an N dimensional vector $\mathbf{f}$, where $N = N_s \times N_r \times N_t$. Since real-world signals are not exactly sparse but compressible—i.e., can be well approximated by a sparse signal—a compressible representation, $\mathbf{x}$, of the seismic line in the curvelet domain, $\mathbf{S}$, is represented as $\mathbf{f} = \mathbf{S}^H \mathbf{x}$. Since curvelets are a redundant frame (an over-complete sparsifying dictionary), $\mathbf{S} \in \mathbb{C}^{P \times N}$ with $P > N$, and $\mathbf{x} \in \mathbb{C}^P$. With the inclusion of the sparsifying transform, the measurement ma-

trix $\mathbf{A}$ can be factored into the product of a $n \times N$ (with $n \ll N$) acquisition matrix $\mathbf{M}$ and the synthesis matrix $\mathbf{S}^H$—i.e., $\mathbf{A} = \mathbf{M}\mathbf{S}^H$. For the real-world irregular signals, however, we need to account for the acquired unstructured measurements for high-resolution data recovery. We do this by introducing an operator in the recovery algorithm (by modifying the measurement operator $\mathbf{A}$—see details in the next sections) that acknowledges the irregularity of seismic traces and uses this information to render regularized and interpolated data.

3.3.1 Acquisition geometry

In time-jittered marine acquisition, source vessels map the survey area firing shots at jittered time instances, which translate to jittered shot positions for a given (fixed) speed of the source vessel. The simultaneous data is time compressed, and therefore acquired economically with low environmental imprint. The recovered separated data is periodic and dense. For simplicity, we assume that all shot positions see the same receivers, which makes our method applicable to marine acquisition with ocean bottom cables or nodes (OBC or OBN). The receivers record continuously resulting in simultaneous shot records. Randomization via jittered subsampling offers control over the maximum gap size (on the acquisition grid), which is a practical requirement of wavefield reconstruction with localized sparsifying transforms such as curvelets (Hennenfent and Herrmann, 2008). For simultaneous time-jittered acquisition, parameters such as the minimum distance required between adjacent shots and minimum recharge time for the air guns help in controlling the maximum acquisition gap while maintaining the minimum realistic acquisition gap.

Conventional acquisition with one source vessel and two air-gun arrays where each air-gun array fires at every alternate periodic location is called flip-flop acquisition. If we wish to acquire 10.0 s-long shot records at every 12.5 m, the speed of the source vessel would have to be about 1.25 m/s ($\approx$ 2.5 knots). Figure 3.5a illustrates one such conventional acquisition scheme, where each air-gun array fires every 20.0 s (or 25.0 m) in a flip-flop manner traveling at about 1.25 m/s, resulting in nonoverlapping shot records of 10.0 s every 12.5 m. In time-jittered acquisition, Figures 3.5b and 3.5c, each air-gun array fires on average at every 20.0 s jittered time-instances traveling at about 2.5 m/s ($\approx$ 5.0 knots) with the receivers (OBC/OBN) recording continuously, resulting in overlapping shot records (Figures 3.6a and 3.6b). Note that the acquisition design involves jittered subsampling—i.e., regular decimation of the (fine) interpolation grid and subsequent perturbation of the coarse-grid points completely *off* the fine grid. The idealized discrete jittered subsampling, by contrast, perturbs the coarse-grid points on the fine grid, as presented in chapter 2. The subsampling factor is represented by η. Therefore, the acquired data volume has overlapping shots and missing shots/traces (Figure 3.6a and 3.6b). For this reason, the jittered flip-flop acquisition might not mimic the conventional flip-flop acquisition where air-gun array 1 and 2 fire one after the other—i.e., in the center and right-hand plots of Figure 3.5d a circle (denoting array 1) may be followed by another circle instead of a star (denoting array 2), and vice versa. However, the

minimum interval between the jittered times is maintained at 10.0 s (typical interval required for air-gun recharge), while the maximum interval is 30.0 s. For the speed of 2.5 m/s, this translates to jittering a 50.0 m source grid with a minimum (and maximum) interval of 25.0 m (and 75.0 m) between jittered shots. Both arrays fire at the 50.0 m jittered grid independent of each other.

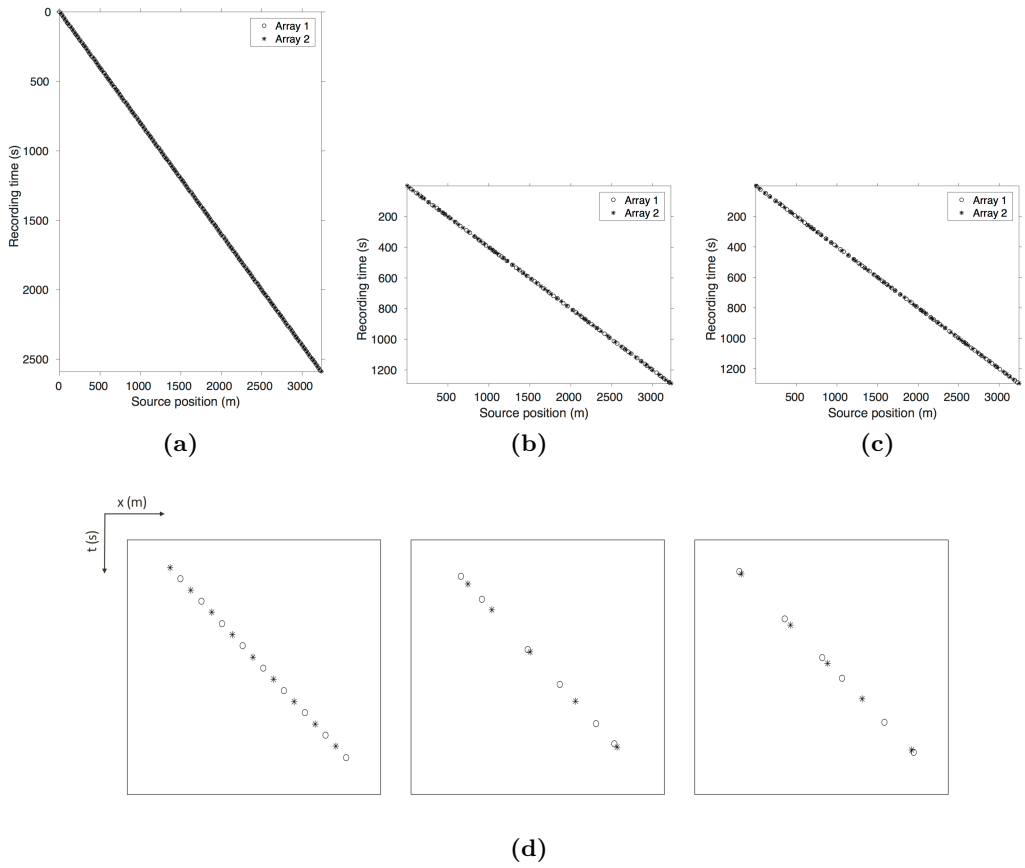

Figure 3.5 Marine acquisition with one source vessel and two air-gun arrays. (a) Conventional flip-flop acquisition. Time-jittered acquisition with a subsampling factor $\eta = 2$ for the (b) baseline and (c) monitor. Note the acquisition speedup during jittered acquisition, where the recording time is reduced to one-half the recording time of the conventional acquisition. (d) Zoomed sections of (a), (b) and (c), respectively.

In time-jittered marine acquisition, the acquisition operator $\mathbf{M}$ is a combined jittered-shot selector and time-shifting operator. Since data is acquired on an irregular grid, it is imperative to incorporate operators in the design of the acquisition matrix $\mathbf{M}$ that account for and hence regularize the irregularity in the data. This is critical to the success of the recovery algorithm. The off-the-grid acquisition design is different from that presented by (Li et al., 2012a), wherein an *interpolated*

restriction operator accounts for irregular points by incorporating Lagrange interpolation into the restriction operator—i.e., the measurements are approximated using a k^{th}-order Lagrange interpolation. In time-jittered acquisition, the jittered time instances are put on a time grid (defined by a time-sampling interval) where each jittered time instance is placed on the point closest to it on the regular time grid. The difference between the true jittered time and the regular grid point, Δt, is corrected by shifting the traces by $e^{-i\omega\Delta t}$, where ω is the angular frequency. The irregularity in the shot positions is corrected by including the nonequispaced fast Fourier transform, NFFT (Potts et al., 2001; Kunis, 2006), in the sparsifying operator $\mathbf{S}$ (Hennenfent and Herrmann, 2006; Hennenfent et al., 2010b), as described in the next section. The NFFT evaluates a Fourier expansion at nonequispaced locations defined by the time-jittered acquisition. Note that in this framework it is also possible to randomly subsample the receivers.

Randomly subsampled and simultaneous measurements for the baseline and monitor surveys are shown in Figures 3.6a and 3.6b, respectively. Note that only 40.0 s of the continuously recorded data is shown. If we simply apply the adjoint of the acquisition operator to the corresponding simultaneous data—i.e., $\mathbf{M}^H\mathbf{y}$—the interferences (or source crosstalk) due to overlapping shots appear as incoherent and nonsparse in the receiver gathers (Figures 3.7a and 3.7b). Moreover, since regularization (and interpolation) is performed by the NFFT inside a nonequispaced curvelet framework (see next section), Figures 3.7a and 3.7b have $\frac{N_s}{\eta}$ irregular traces, where $\eta > 1$ is the subsampling factor. Since the baseline and monitor surveys have different irregular shot positions, the corresponding time-lapse difference cannot be computed unless both time-lapse data are realigned to a common spatal grid. For this purpose, if we apply the adjoint of a 1D NFFT operator $\mathbf{N}$—i.e., $\mathbf{N}^H\mathbf{M}^H\mathbf{y}$—the time-lapse data are realigned to a common fine spatial grid (Figures 3.7c and 3.7d). The corresponding time-lapse difference is shown in Figure 3.7e. As illustrated by these figures, in order to eventually remove the interferences and interpolate missing traces it is important to consider the recovery problem as an inversion problem. Since the time-jittered acquisition generates simultaneous, irregular data with missing traces, the recovery problem becomes a joint source separation, regularization and interpolation problem.

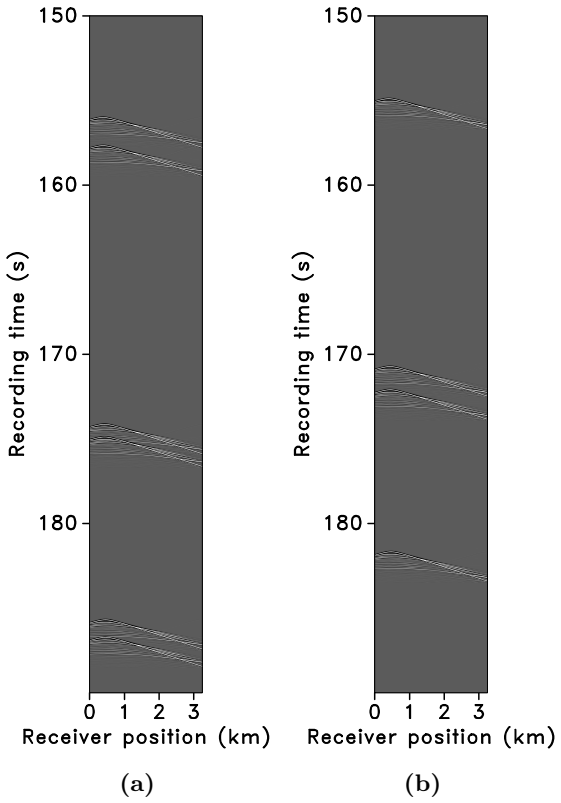

Figure 3.6 Simultaneous data for the (a) baseline and (b) monitor surveys. Only 40.0 s of the full data is shown. Time-jittered acquisition generates a simultaneous data volume with overlapping shots and missing shots.

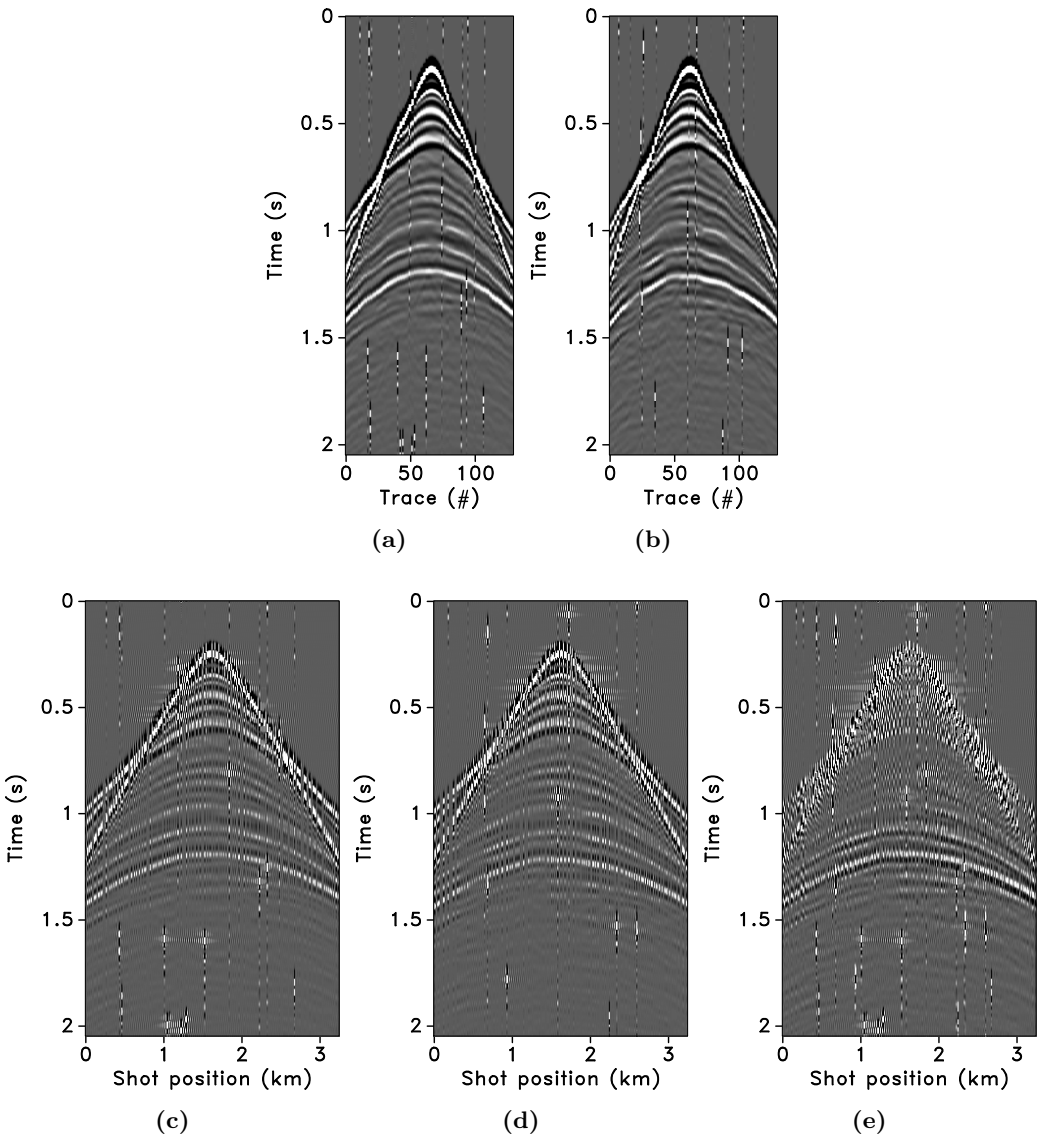

Figure 3.7 Interferences (or source crosstalk) in a common-receiver gather for the (a) baseline and (b) monitor surveys, respectively. Receiver gathers are obtained via $\mathbf{M}^H\mathbf{y}$ for the time-lapse surveys. For a subsampling factor η, (a) and (b) have $\frac{N_s}{\eta}$ irregular traces. (c), (d) Common-receiver gathers for the baseline and monitor surveys, respectively, after applying the adjoint of a 1D NFFT operator to (a) and (b). (e) Corresponding time-lapse difference. As illustrated, the recovery problem needs to be considered as a (sparse) structure-promoting inversion problem, wherein the simultaneous data volume is separated, regularized and interpolated to a finer sampling grid rendering interference-free data.

3.3.2 From discrete to continuous spatial subsampling

Subsampling schemes that are based on an underlying fine interpolation grid incorporate the discrete (spatial) subsampling schemes, since the subsampling is done on the grid. This situation typically occurs when binning continuous randomly-sampled seismic data into small bins that define the fine grid used for interpolation (Hennenfent and Herrmann, 2008). For such cases, the wrapping-based fast discrete curvelet transform, FDCT via wrapping (Candès et al., 2006) can be used to recover the fully sampled data since the inherent fast Fourier transform (FFT) assumes regular sampling along all coordinates. For the interested reader, the curvelet transform is a multiscale, multidirectional, and localized transform that corresponds to a specific tiling of the f-k domain into dyadic annuli based on concentric squares centered around the zero-frequency zero-wavenumber point. Each annulus is subdivided into parabolic angular wedges—i.e., length of wedge $\propto$ width^2 of wedge. The architecture of the analysis operator (or forward operation) of the FDCT via wrapping is as follows: (1) apply the analysis 2D FFT; (2) form the angular wedges; (3) wrap each wedge around the origin; and (4) apply the synthesis 2D FFT to each wedge. The synthesis/adjoint operator—also the inverse owing to the tight-frame property—is computed by reversing these operations (Candès et al., 2006).

Seismic data, however, is usually acquired irregularly, typically nonuniformly sampled along the spatial coordinates. Simultaneous time-jittered marine acquisition, mentioned above, is an instance of acquiring seismic data on irregular spatial grids. Hence, binning can lead to a poorly-jittered subsampling scheme, which will not favor wavefield reconstruction by sparsity-promoting inversion. Moreover, failure to account for the nonuniformly sampled data can adversely affect seismic processing, imaging, etc. Therefore, we should work with an extension to the curvelet transform for irregular grids (Hennenfent et al., 2010b). Using this extension for the simultaneous time-jittered marine acquisition will produce colocated fine-scale time-lapse data. Continuous random sampling typically leads to improved interpolation results because it does not create coherent subsampling artifacts (Xu et al., 2005b).

3.3.3 Nonequispaced fast discrete curvelet transform (NFDCT)

For irregularly acquired seismic data, the (FFT inside) FDCT (Candès et al., 2006) assumes regular sampling along all (spatial) coordinates. Ignoring the nonuniformity of the spatial sampling no longer helps in detecting the wavefronts because of a lack of continuity. (Hennenfent and Herrmann, 2006) addressed this issue by extending the FDCT to nonuniform (or irregular) grids via the nonequispaced fast Fourier transform, NFFT (Potts et al., 2001; Kunis, 2006). The outcome was the 'first generation NFDCT' (nonequispaced fast discrete curvelet transform), which relied on accurate Fourier coefficients obtained by an ℓ_2-regularized inversion of the NFFT.

The NFDCT handles irregular sampling, thus, exploring continuity along the wavefronts by viewing seismic data in a geometrically correct way—typically nonuniformly sampled along the spatial coordinates (source and/or receiver). In (Hennen-

fent et al., 2010b), the authors introduced a 'second generation NFDCT', which is based on a direct, ℓ_1-regularized inversion of the operator that links curvelet coefficients to irregular data. Unlike the first generation NFDCT, the second generation NFDCT is lossless by construction—i.e., the curvelet coefficients explain the data at irregular locations exactly. This property is important for processing irregularly sampled seismic data in the curvelet domain and bringing them back to their irregular recording locations with high fidelity. Note that the second generation NFDCT is lossless for regularization not interpolation. The NFDCT framework as setup in (Hennenfent et al., 2010b) basically involves a Kronecker product ($\otimes$) of a 1D FFT operator $\mathbf{F}_t$, used along the temporal coordinate, and a 1D NFFT operator $\mathbf{N}_x$, used along the spatial coordinate, followed by the application of the curvelet tilling operator $\mathbf{T}$ that maps curvelet coefficients to the Fourier domain—i.e., $\mathbf{B} \stackrel{\text{def}}{=} \mathbf{T}(\mathbf{N}_x \otimes \mathbf{F}_t)$. Therefore, $\mathbf{B}$ is the NFDCT operator that links the curvelet coefficients to nonequispaced traces. The 1D NFFT operator ($\mathbf{N}_x$) replaces the 1D FFT operator ($\mathbf{F}_x$) that acts along the spatial coordinate in FDCT. Note that the NFDCT operator described above is written differently than in (Hennenfent et al., 2010b) because the latter defines the synthesis FFT operator as $\mathbf{F}$, whereas $\mathbf{F}$ is the analysis FFT operator in this chapter. This also ensures consistency of notation and terminology with chapter 2.

For the proposed simultaneous acquisition, the joint problem of source separation, regularization and interpolation is addressed by using a sparsifying operator ($\mathbf{S}$) that handles the multidimensionality of this problem. Therefore, $\mathbf{S} \stackrel{\text{def}}{=} \mathbf{C} \otimes \mathbf{W}$, where $\mathbf{C}$ is a 2D NFDCT operator and $\mathbf{W}$ is a 1D wavelet operator. The NFDCT operator is modified as

$$\mathbf{C} \stackrel{\text{def}}{=} \mathbf{T}(\mathbf{N}_{xs} \otimes \mathbf{F}_{xr}), \tag{3.2}$$

where the 1D NFFT operator $\mathbf{N}_{xs}$ acts along the jittered shot coordinate and the 1D FFT operator $\mathbf{F}_{xr}$ acts along the regular receiver coordinate. The 1D wavelet operator is applied on the time coordinate. As mentioned previously, the measurement matrix $\mathbf{A} = \mathbf{M}\mathbf{S}^H$. From a practical point of view, it is important to note that matrix-vector products with all the matrices are matrix free—i.e., these matrices are operators that define the action of the matrix on a vector, but are never formed explicitly.

In summary, recovery of nonoverlapping, periodic and densely sampled data from simultaneous, irregular and compressed data is achieved by incorporating an NFFT operator inside the curvelet framework that acts along the irregular spatial coordinate(s) and applying time shifts to the traces wherever necessary. Note that the NFFT operator is incorporated in the 2D NFDCT operator $\mathbf{C}$, which is incorporated in the sparsifying operator $\mathbf{S}$, and the time shift Δt is incorporated in the acquisition operator $\mathbf{M}$. The NFFT computes (fine grid) 2D Fourier coefficients by mapping the coarse nonuniform spatial grid to a fine uniform grid. The curvelet coefficients are computed directly from the 2D Fourier coefficients.

3.4 Time-lapse acquisition via jittered sources

In chapter 2, we extended the time-jittered marine acquisition to time-lapse surveys where the shot positions were jittered on a discrete periodic grid. In this chapter, we extend the framework to more realistic field acquisition scenarios by incorporating irregular grids. Figure 3.5a illustrates a conventional marine acquisition scheme and two realizations of the off-the-grid time-jittered marine acquisition are shown in Figures 3.5b and 3.5c, one each for the baseline and the monitor survey. Remember that these surveys generate simultaneous, irregular and subsampled measurements. We assume no significant variations in the water column velocities, wave heights or temperature and salinity profiles, etc., amongst the different surveys. The source signature is also assumed to be the same.

We describe noise-free time-lapse data acquired from a baseline and a monitor survey as $\mathbf{y}_j = \mathbf{A}_j\mathbf{x}_j$ for $j = \{1, 2\}$, where $\mathbf{y}_1$ and $\mathbf{y}_2$ represent the subsampled, simultaneous measurements for the baseline and monitor surveys, respectively; $\mathbf{A}_1$ and $\mathbf{A}_2$ are the corresponding flat ($n \ll N < P$) measurement matrices. Note that both the measurement matrices incorporate the NFDCT operator, as described above, to account and correct for the irregularity in the observed measurements of the baseline ($\mathbf{y_1}$) and monitor surveys ($\mathbf{y_2}$). Recovering densely sampled vintages for each vintage independently (via Equation 3.1) is referred to as the independent recovery strategy (IRS). Since in chapter 2 we demonstrated that recovery via IRS is inferior to recovery via the joint recovery method, we work only with the latter in this chapter.

3.4.1 Joint recovery method

The joint recovery method (JRM) performs a joint inversion by exploiting shared information between the vintages. The joint recovery model is formulated as

$$\begin{bmatrix}\mathbf{y}_1\\ \mathbf{y}_2\end{bmatrix} = \begin{bmatrix}\mathbf{A}_1 & \mathbf{A}_1 & \mathbf{0}\\ \mathbf{A}_2 & \mathbf{0} & \mathbf{A}_2\end{bmatrix}\begin{bmatrix}\mathbf{z}_0\\ \mathbf{z}_1\\ \mathbf{z}_2\end{bmatrix}, \quad \text{or}$$
$$\mathbf{y} = \mathbf{A}\mathbf{z}. \tag{3.3}$$

In this model, the vectors $\mathbf{y}_1$ and $\mathbf{y}_2$ represent observed measurements from the baseline and monitor surveys, respectively. The vectors for the vintages are given by

$$\mathbf{x}_j = \mathbf{z}_0 + \mathbf{z}_j, \qquad j \in 1, 2, \tag{3.4}$$

where the common component is denoted by $\mathbf{z}_0$, and the innovations are denoted by $\mathbf{z}_j$ for $j \in 1, 2$ with respect to this common component that is shared by the vintages. The symbol $\mathbf{A}$ is overloaded to refer to the matrix linking the observations of the time-lapse surveys to the common component and innovations pertaining to

the different vintages. The above joint recovery model can be extended to $J > 2$ surveys, yielding a $J \times$ (number of vintages $+ 1$) system.

Since the vintages share the common component in Equation 3.3, solving

$$\widetilde{\mathbf{z}} = \underset{\mathbf{z}}{\operatorname{argmin}} \|\mathbf{z}\|_1 \quad \text{subject to} \quad \mathbf{y} = \mathbf{A}\mathbf{z}, \tag{3.5}$$

will exploit the correlations amongst the vintages. Equation 3.5 seeks solutions for the common component and innovations that have the smallest ℓ_1-norm such that the observations explain the incomplete recordings for both vintages. The densely sampled vintages are estimated via Equation 5.6 with the recovered $\widetilde{\mathbf{z}}$ and the time-lapse difference is computed via $\widetilde{\mathbf{z}}_1 - \widetilde{\mathbf{z}}_2$.

Given a baseline data vector $\mathbf{f}_1$ and a monitor data vector $\mathbf{f}_2$, $\mathbf{x}_1$ and $\mathbf{x}_2$ are the corresponding sparse representations. Given the measurements $\mathbf{y}_1 = \mathbf{M}_1\mathbf{f}_1$ and $\mathbf{y}_2 = \mathbf{M}_2\mathbf{f}_2$, and $\mathbf{A}_1 = \mathbf{M}_1\mathbf{S}_1^H$, $\mathbf{A}_2 = \mathbf{M}_2\mathbf{S}_2^H$, our aim is to recover the wavefields (or sparse approximations) $\widetilde{\mathbf{f}}_1$ and $\widetilde{\mathbf{f}}_2$ by solving the sparse recovery problem as described above from which the time-lapse signal can be computed. Note that $\mathbf{S} \overset{\text{def}}{=} \mathbf{C} \otimes \mathbf{W}$, where $\mathbf{C}$ is the NFDCT operator (see Equation 3.2) and $\mathbf{W}$ is a 1D wavelet operator. The reconstructed wavefields $\widetilde{\mathbf{f}}_1$ and $\widetilde{\mathbf{f}}_2$ are obtained as: $\widetilde{\mathbf{f}}_1 = \mathbf{S}^H\widetilde{\mathbf{x}}_1$ and $\widetilde{\mathbf{f}}_2 = \mathbf{S}^H\widetilde{\mathbf{x}}_2$, where $\widetilde{\mathbf{x}}_1$ and $\widetilde{\mathbf{x}}_2$ are the recovered sparse representations and the operator $\mathbf{S}$ is re-defined to represent the Kronecker product between the standard FDCT operator and the 1D wavelet operator. The standard FDCT operator is used because the recovered sparse representations $\widetilde{\mathbf{x}}_1$ and $\widetilde{\mathbf{x}}_2$ correspond to the coefficients of the regularized wavefields. Since we are always subsampled in both the baseline and monitor surveys, have irregular traces and cannot exactly repeat, which is inherent of the acquisition design and due to natural environmental constraints, we would like to recover the periodic densely sampled prestack vintages and time-lapse difference. For the given recovery problem, the vintages and time-lapse difference are mapped to one colocated fine regular periodic grid.

3.5 Economic performance indicators

To quantify the cost savings associated with simultaneous acquisition, we measure the performance of the proposed acquisition design and recovery scheme in terms of an improved spatial-sampling ratio (ISSR), defined as

$$\text{ISSR} = \frac{\text{number of shots recovered via sparsity-promoting inversion}}{\text{number of shots in simultaneous acquisition}}. \tag{3.6}$$

For time-jittered marine acquisition, a subsampling factor $\eta = 2, 4, ...,$ etc., implies a gain in the spatial sampling by factor of $2, 4, ...,$ etc. In practice, this corresponds to an improved efficiency of the acquisition by the same factor. Recently, (Mosher et al., 2014) have shown that factors of two or as high as ten in efficiency improvement are achievable in the field.

The survey-time ratio (STR)—a performance indicator proposed by (Berkhout, 2008)—compares the time taken for conventional and simultaneous acquisition:

$$\text{STR} = \frac{\text{time of conventional acquisition}}{\text{time of simultaneous acquisition}}. \tag{3.7}$$

As mentioned previously, if we wish to acquire 10.0 s-long shot records at every 12.5 m, the speed of the source vessel would have to be about 1.25 m/s ($\approx$ 2.5 knots). In simultaneous acquisition, the speed of the source vessel is approximately maintained at (the standard) 2.5 m/s ($\approx$ 5.0 knots). Therefore, for a subsampling factor of $\eta = 2, 4, ...$, etc., there is an implicit reduction in the survey time by $\frac{1}{\eta}$.

3.6 Synthetic seismic case study

To illustrate the performance of our proposed joint recovery method for off-the-grid surveys, we carry out a number of experiments on 2D seismic lines generated from two different velocity models—first, the BG COMPASS model (provided by BG Group) that has simple geology with complex time-lapse difference; and second, the SEAM Phase 1 model (provided by HESS) that has complex geology with complex time-lapse difference due to the complexity of the overburden. Note that for the SEAM model, we generate the time-lapse difference via fluid substitution as shown below. Also, the geology of the BG COMPASS model is relatively simpler than the SEAM model, although it does have vertical and lateral complexity.

3.6.1 BG COMPASS model simple geology, complex time-lapse difference

The synthetic BG COMPASS model has a (relatively) simple geology but a complex time-lapse difference. Figures 3.8a and 3.8b display the baseline and monitor models. Note that this is a subset of the BG COMPASS model, wherein the monitor model includes a gas cloud. The time-lapse difference in Figure 3.8c shows the gas cloud.

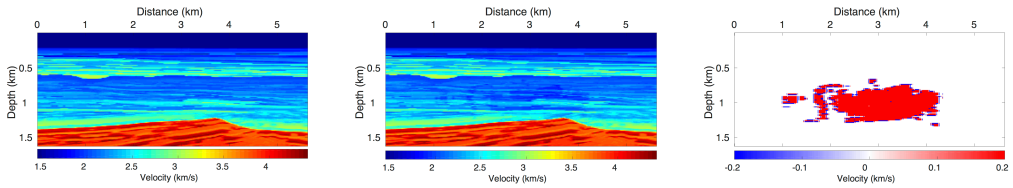

(a) **(b)** **(c)**

Figure 3.8 Subset of the BG COMPASS model. (a) Baseline model; (b) monitor model; (c) difference between (a) and (b) showing the gas cloud.

Using IWAVE (Symes, 2010), a time-stepping simulation software, two acoustic data sets with a conventional source (and receiver) sampling of 12.5 m are generated, one from the baseline model and the other from the monitor model. Each data set has $N_t = 512$ time samples, $N_r = 260$ receivers and $N_s = 260$ sources. The time sampling interval is 0.004 s. Subtracting the two data sets yields the time-lapse difference. Since no noise is added to the data, the time-lapse difference is simply the time-lapse signal. A receiver gather from the simulated baseline data, the monitor data and the corresponding time-lapse difference is shown in Figure 3.2a, 3.2b and 3.2c, respectively. The first shot position in the receiver gathers—labeled as 0 m in the figures—corresponds to 1.5 km in the synthetic velocity model. Given the spatial sampling of 12.5 m, the subsampling factor η for the time-jittered acquisition is 2. Hence, the number of measurements for each experiment is fixed—i.e., $n = N/\eta = N/2$, each for $\mathbf{y}_1$ and $\mathbf{y}_2$. We also conduct experiments for $\eta = 4$.

To reflect current practices in time-lapse acquisition—where people aim to replicate the surveys—we simulate 10 different realizations of the time-jittered marine acquisition with 100% overlap between the baseline and monitor surveys. The term "overlap" refers to the percentage of shot positions from the baseline survey revisited (or replicated exactly) for the monitor survey, and therefore rows in the measurement matrices $\mathbf{A_1}$ and $\mathbf{A_2}$ are exactly the same. Note that these shot positions are irregular, and hence off the grid. However, since exact replication of the surveys in the field is not possible, we conduct experiments to study the impact of deviations in the shot positions that would occur naturally in the field. We introduce small deviations of average $\pm(1, 2, 3)$ m in the shot positions of the baseline surveys to generate the shot positions for the monitor surveys. For instance, given a realization of the time-jittered baseline survey, deviating each shot position by $\approx \pm 1$ m generates shot positions for the corresponding monitor survey. Note that these deviations are average deviations in the sense that for a given realization of the time-jittered baseline survey, the shot positions are deviated by random real numbers resulting in average deviations of ± 1 m, ± 2 m or ± 3 m. One of our aims is to analyze the effects of nonreplication of the time-lapse surveys on time-lapse data—i.e., when $\mathbf{A_1} \neq \mathbf{A_2}$. By virtue of the design of the simultaneous acquisition and based upon the subsampling factor (η), it is not possible to have two completely different (0% overlap) realizations of the time-jittered acquisition. Therefore, we compare recoveries from the above cases with the acquisition scenarios that have least possible (or unavoidable) overlap between the time-lapse surveys. In all cases, we recover periodic densely sampled baseline and monitor data from the simultaneous data $\mathbf{y}_1$ and $\mathbf{y}_2$, respectively, using the joint recovery method (by solving Equation 3.5). The inherent time-lapse difference is computed by subtracting the recovered baseline and monitor data.

We conduct 10 experiments for the baseline measurements, wherein each experiment has a different random realization of the measurement matrix $\mathbf{A_1}$. Then, for each experiment, we fix the baseline measurement and subsequently work with different realizations of the monitor survey generated by introducing small deviations in the shot positions and jittered firing times from the baseline survey, resulting in

slightly different overlaps between the surveys. To get better insight on the effects of nonreplication of the time-lapse surveys, we also conduct experiments for the case of least possible overlap between the surveys. Tables 3.1 and 3.2 summarize the recovery results for the time-lapse data for $\eta = 2$ and 4, respectively, in terms of the signal-to-noise ratio defined as

$$\mathrm{SNR}(\mathbf{f}, \widetilde{\mathbf{f}}) = -20 \log_{10} \frac{\|\mathbf{f} - \widetilde{\mathbf{f}}\|_2}{\|\mathbf{f}\|_2}. \tag{3.8}$$

Each table compares recoveries for different overlaps between the baseline and monitor surveys, with and without position deviations. Each SNR value is an average of 10 experiments including the standard deviation. Note that for time-jittered acquisition with $\eta = 2$, the least possible overlap between the surveys is observed to be greater than 0% and less than 15%. Hence, Table 3.1 shows the SNRs for the overlap of $< 15\%$. Similarly, for time-jittered acquisition with $\eta = 4$, Table 3.2 shows the SNRs for the overlap of $< 5\%$.

We recover periodic densely sampled data from simultaneous, subsampled and irregular data by solving Equation 3.5. The recovered time-lapse data is colocated, regularized and interpolated to a fine uniform grid since both the measurement matrices $\mathbf{A_1}$ and $\mathbf{A_2}$ incorporate a 2D nonequispaced fast discrete curvelet transform that handles irregularity of traces by viewing the observed data in a geometrically correct way. The SNRs of the recovered time-lapse data lead to some interesting observations. First, there is little variability in the recovery of the time-lapse difference from (the ideal) 100% overlap between the surveys to the more realistic scenarios of in-the-field acquisitions that have natural deviations or irregularities in the shot positions. Second, time-lapse difference recovery from the least possible overlap (between the surveys) is similar to the recovery of 100% overlap with and without deviations. This is significant because it indicates a possibility to relax the insistence on replication of the time-lapse surveys, which makes this technology challenging and expensive. The small standard deviations for each case suggest little variability in the recovery for different random realizations. Moreover, the standard deviations are greater for cases other than the minimum overlap. The above observations hold for both subsampling factors, $\eta = 2$ and 4, as illustrated in Figures 3.10 and 3.12.

Third, increasing deviations or irregularities in shot positions improve recovery of the vintages (Figures 3.9c, 3.9e, 3.9g), with the minimum overlap between surveys giving the best recovery (Figure 3.9i). This is due to the (partial) independence of the measurement matrices that contribute additional information via the first column of $\mathbf{A}$ in Equation 3.3 connecting the common component to observations of both vintages—i.e., for time-lapse seismic, independent surveys give additional structural information leading to improved recovery quality of the vintages. The improvement in the recoveries is better visible through the corresponding difference plots in Figures 3.9d, 3.9f, 3.9h, 3.9j. This observation is important because, as mentioned previously, time-lapse differences are often studied via differences in certain poststack attributes computed from the (recovered) prestack vintages. Hence, as

the quality of the recovered prestack vintages improves with decrease in the overlap, they serve as better input to extract the poststack attributes. Moreover, the small standard deviations for each overlap indicate little variability in the recovery from one random realization to another. This is desirable since it offers a possibility to relax the insistence on replication of the time-lapse surveys along with embracing the naturally occurring random deviations in the field. The standard deviations for different overlaps also do not fluctuate as much as compared to those of the time-lapse difference. Recovery of the vintages and the corresponding difference plots for a subsampling of $\eta = 4$ are shown in Figure 3.11.

An increase in the subsampling factor leads to decrease in the SNRs of the recovered time-lapse data, however, the recoveries are reasonable as shown in Figures 3.11 and 3.12. This observation is in accordance with the CS theory wherein the recovery quality decreases for increased subsampling. Note that recovery of weak late-arriving events can be further improved by rerunning the recovery algorithm using the residual as input, using weighted one-norm minimization that exploits correlations between locations of significant transform-domain coefficients of different partitions—e.g., shot records, common-offset gathers, or frequency slices—of the acquired data (Mansour et al., 2013), etc. This needs to be carefully investigated. Remember that for a given subsampling factor the number of measurements is the same for all experiments and the observed differences can be fully attributed to the performance of the joint recovery method in relation to the overlap between the two surveys encoded in the measurement matrices. Also, given the context of randomized subsampling and irregularity of the observed data, it is important to recover the densely sampled vintages and then the time-lapse difference. Moreover, as mentioned previously, while we do not insist that we actually visit predesigned irregular (or off-the-grid) shot positions for the time-lapse surveys, however, it is important to know these positions to sufficient accuracy after acquisition for high-quality data recovery. This can be achieved in practice as shown by (Mosher et al., 2014).

Overlap ± avg. deviation	Baseline	Monitor	4D signal
100%	19.8 ± 1.0	19.7 ± 1.0	11.3 ± 2.2
100% ± 1.0 m	19.7 ± 1.0	19.6 ± 1.0	10.3 ± 1.5
100% ± 2.0 m	20.3 ± 1.1	20.2 ± 1.0	10.7 ± 1.1
100% ± 3.0 m	20.8 ± 1.2	20.7 ± 1.1	11.0 ± 1.4
< 15%	23.8 ± 1.4	23.6 ± 1.4	10.2 ± 1.2

Table 3.1 Summary of recoveries in terms of SNR (dB) for data recovered via JRM for a subsampling factor $\eta = 2$. The SNRs show little variability in the time-lapse difference recovery for different overlaps between the surveys offering a possibility to relax insistence on replicability of time-lapse surveys. This is supported by the improved recovery of the vintages as the overlap decreases. Note that the deviations are average deviations over many experiments.

Overlap ± avg. deviation	Baseline	Monitor	4D signal
100%	14.3 ± 0.6	14.2 ± 0.6	6.4 ± 0.7
100% ± 1.0 m	14.9 ± 0.8	14.8 ± 0.8	6.5 ± 1.0
100% ± 2.0 m	15.6 ± 1.0	15.5 ± 1.0	6.4 ± 1.3
100% ± 3.0 m	16.4 ± 0.9	16.3 ± 0.9	6.4 ± 0.7
$< 5\%$	18.4 ± 0.7	18.2 ± 0.7	5.8 ± 0.4

Table 3.2 Summary of recoveries in terms of SNR (dB) for data recovered via JRM for a subsampling factor $\eta = 4$. The SNRs show little variability in the time-lapse difference recovery for different overlaps between the surveys offering a possibility to relax insistence on replicability of time-lapse surveys. This is supported by the improved recovery of the vintages as the overlap decreases. Note that the deviations are average deviations over many experiments.

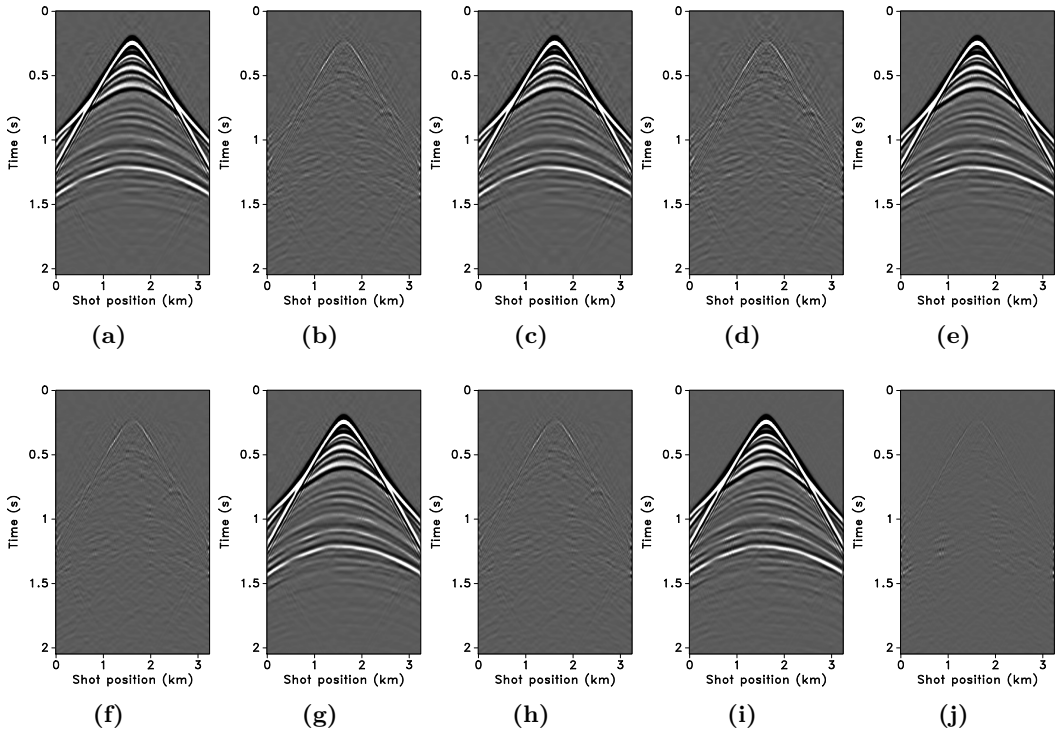

Figure 3.9 JRM recovered monitor receiver gathers from the BG COMPASS model for a subsampling factor $\eta = 2$. Recovered monitor data and residual with (a,b) 100% overlap in the measurement matrices ($\mathbf{A_1}$ and $\mathbf{A_2}$); (c,d) 100% overlap and average shot-position deviation of 1 m; (e,f) 100% overlap and average shot-position deviation of 2 m; (g,h) 100% overlap and average shot-position deviation of 3 m; (i,j) $< 15\%$ overlap, respectively.

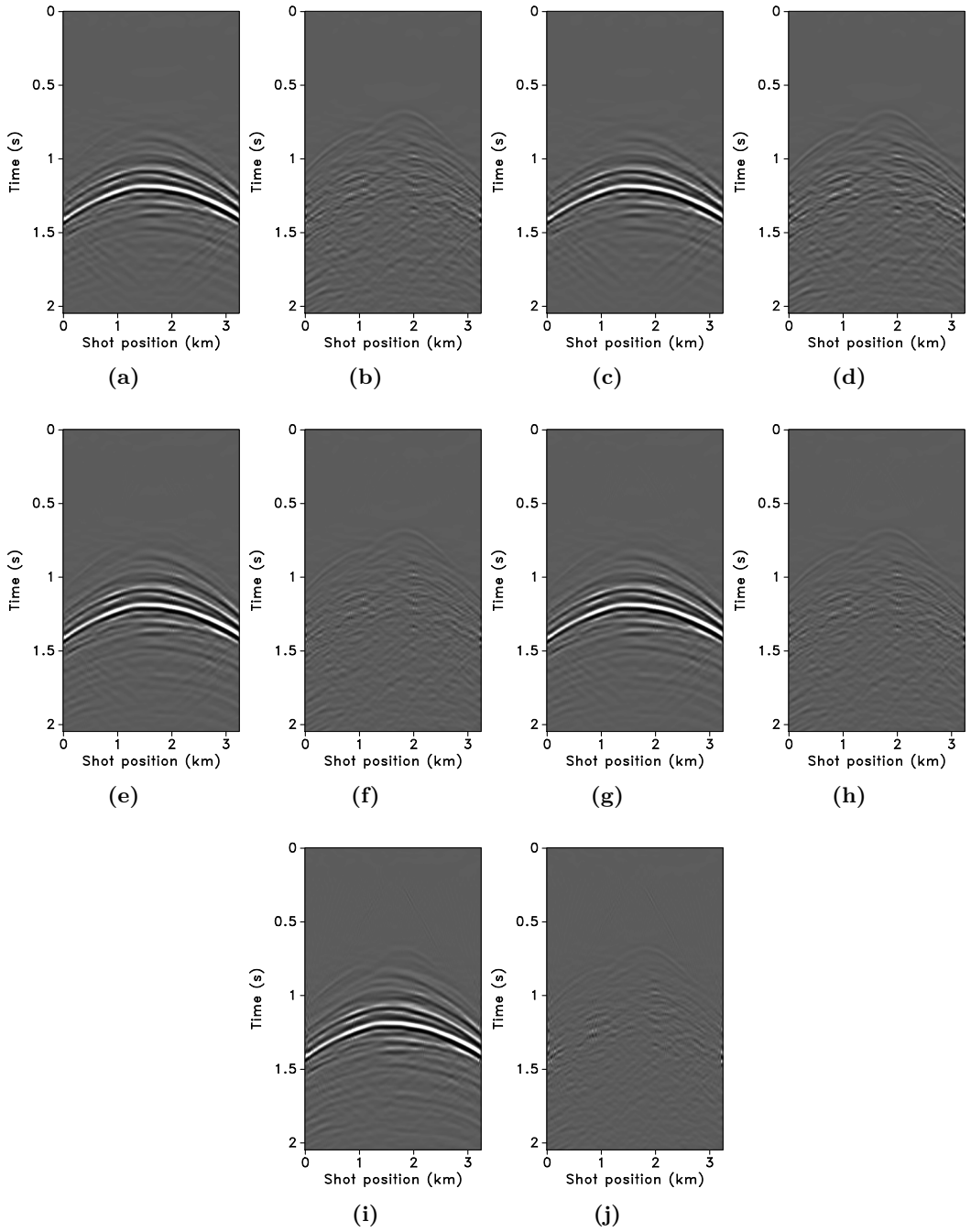

Figure 3.10 JRM recovered time-lapse difference receiver gathers from the BG COMPASS model for a subsampling factor $\eta = 2$. Recovered time-lapse difference and residual with (a,b) 100% overlap in the measurement matrices ($\mathbf{A_1}$ and $\mathbf{A_2}$); (c,d) 100% overlap and average shot-position deviation of 1 m; (e,f) 100% overlap and average shot-position deviation of 2 m; (g,h) 100% overlap and average shot-position deviation of 3 m; (i,j) $< 15\%$ overlap, respectively.

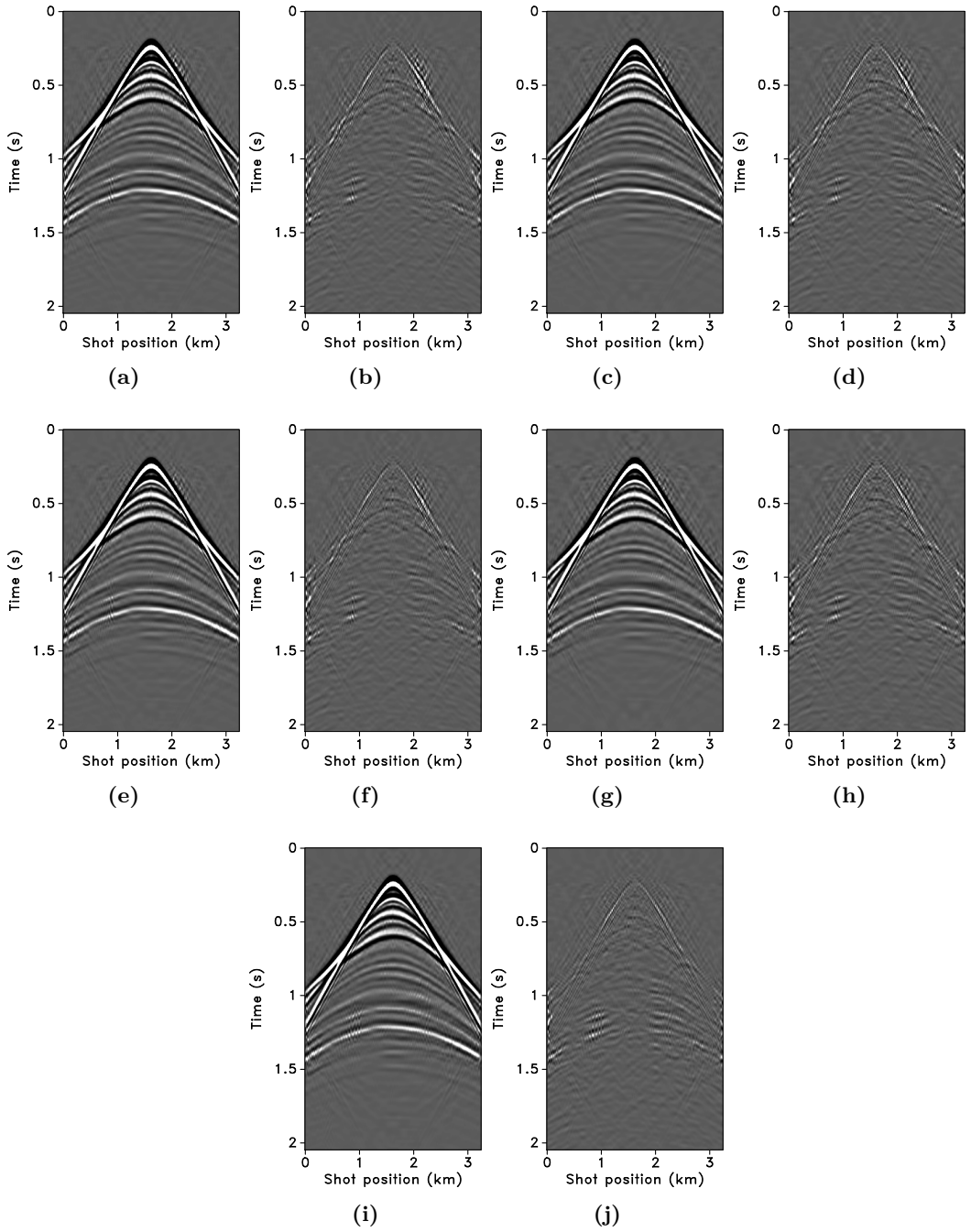

Figure 3.11 JRM recovered monitor receiver gathers from the BG COMPASS model for a subsampling factor $\eta = 4$. Recovered monitor data and residual with (a,b) 100% overlap in the measurement matrices ($\mathbf{A_1}$ and $\mathbf{A_2}$); (c,d) 100% overlap and average shot-position deviation of 1 m; (e,f) 100% overlap and average shot-position deviation of 2 m; (g,h) 100% overlap and average shot-position deviation of 3 m; (i,j) $< 5\%$ overlap, respectively.

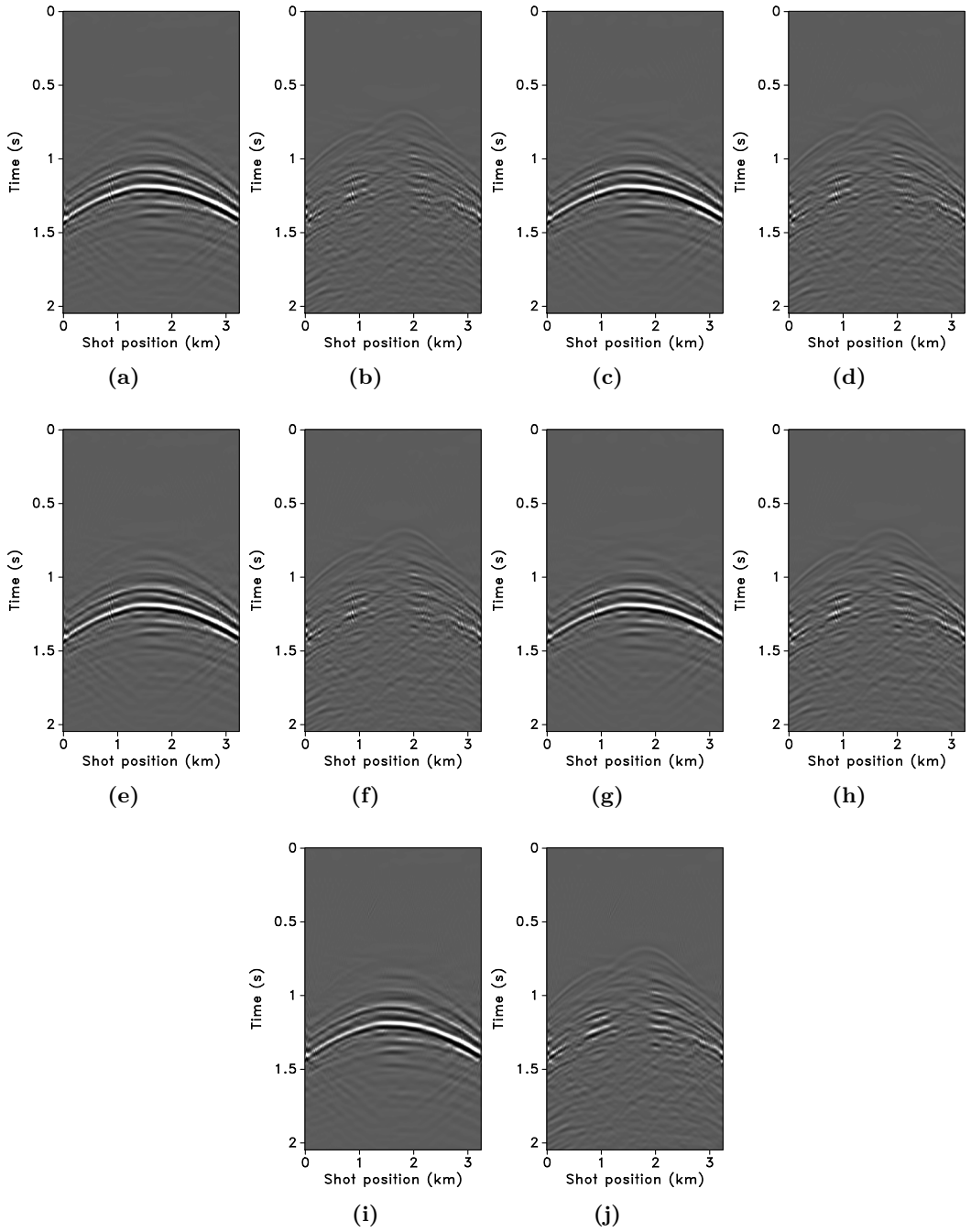

Figure 3.12 JRM recovered time-lapse difference receiver gathers from the BG COMPASS model for a subsampling factor $\eta = 4$. Recovered time-lapse difference and residual with (a,b) 100% overlap in the measurement matrices ($\mathbf{A_1}$ and $\mathbf{A_2}$); (c,d) 100% overlap and average shot-position deviation of 1 m; (e,f) 100% overlap and average shot-position deviation of 2 m; (g,h) 100% overlap and average shot-position deviation of 3 m; (i,j) $< 5\%$ overlap, respectively.

3.6.2 SEAM Phase 1 model complex geology, complex time-lapse difference

The SEAM model is a 3D deepwater subsalt earth model that includes a complex salt intrusive in a folded Tertiary basin. We select a 2D slice from the 3D model to generate a seismic line. Figure 3.13a shows a subset of the 2D slice used as the baseline model. We define the monitor model, Figure 3.13b, from the baseline model via fluid substitution resulting in a time-lapse difference under the overburden as shown in Figure 3.13c.

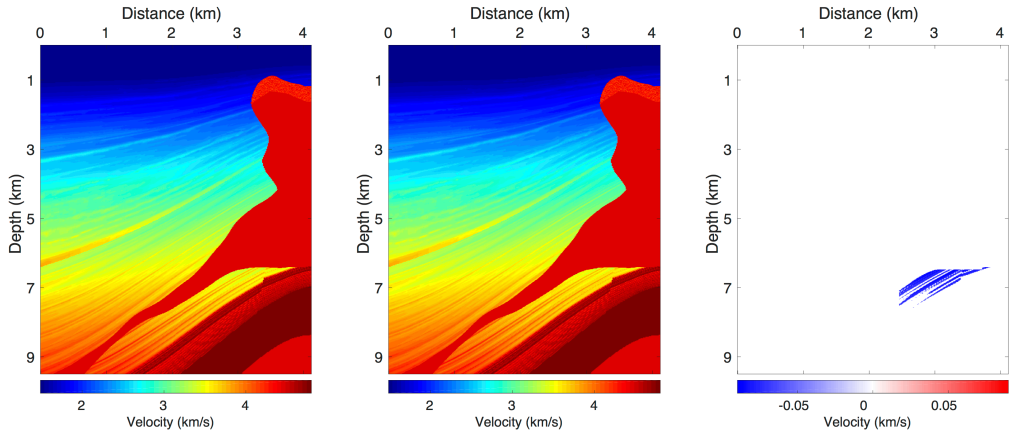

(a) **(b)** **(c)**

Figure 3.13 Subset of the SEAM model. (a) Baseline model; (b) monitor model; (c) difference between (a) and (b) showing the time-lapse difference.

Using IWAVE (Symes, 2010), two acoustic data sets with a conventional source (and receiver) sampling of 12.5 m are generated, one from the baseline model and the other from the monitor model. Each data set has $N_t = 2048$ time samples, $N_r = 320$ receivers and $N_s = 320$ sources. The time sampling interval is 0.004 s. Subtracting the two data sets yields the time-lapse difference. Since no noise is added to the data, the time-lapse difference is simply the time-lapse signal. A receiver gather from the simulated baseline data, the monitor data and the corresponding time-lapse difference is shown in Figures 3.14a, 3.14b and 3.14c, respectively. Note that the amplitude of the time-lapse difference is one-tenth the amplitude of the baseline and monitor data. Therefore, in order to make the time-lapse difference visible, the color axis for the figures showing the time-lapse difference is one-tenth the color axis for the figures showing the baseline and monitor data. This colormap applies for the remainder of the chapter. Given the spatial sampling of 12.5 m, the subsampling factor η for the time-jittered acquisition is 2. The number of measurements for each experiment is fixed—i.e., $n = N/\eta = N/2$, each for $\mathbf{y}_1$ and $\mathbf{y}_2$.

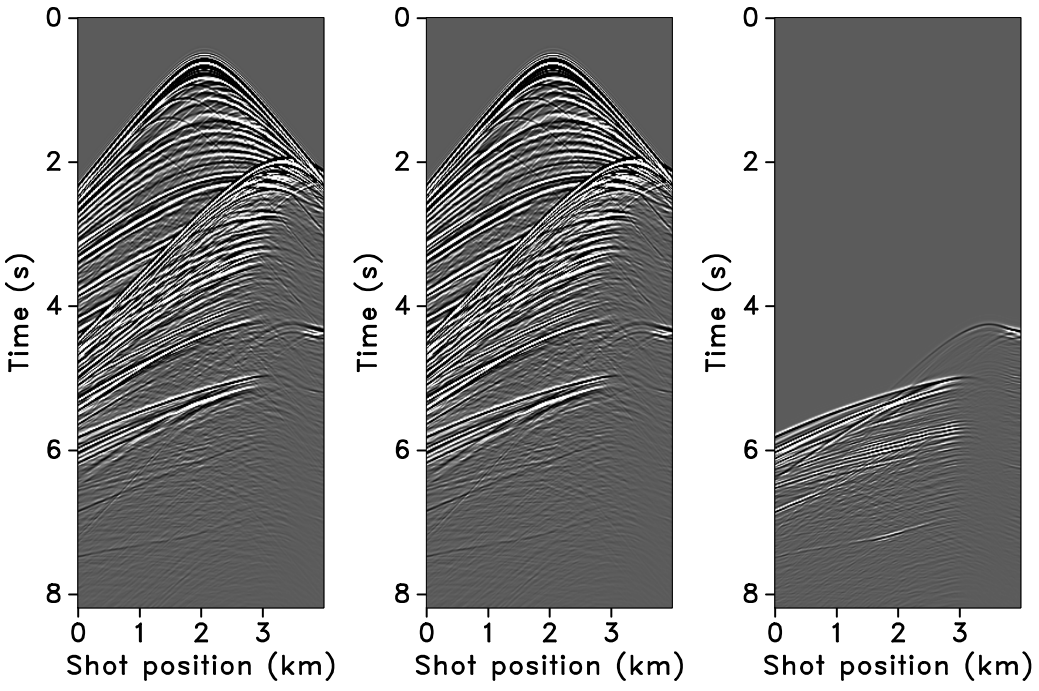

Figure 3.14 Synthetic receiver gathers from the conventional SEAM (a) baseline survey, (b) monitor survey. (c) Corresponding time-lapse difference. The amplitude of the time-lapse difference is one-tenth the amplitude of the baseline and monitor data.

We simulate a realization of the time-jittered marine acquisition with 100% overlap between the baseline and monitor surveys. Since our main aim is to analyze the effects of nonreplication of the time-lapse surveys on time-lapse data—i.e., when $\mathbf{A_1} \neq \mathbf{A_2}$—we compare recovery from the above case with the acquisition scenario that has least possible (or unavoidable) overlap between the time-lapse surveys only. Given the bigger size of the data set and limited computational resources, we restrict ourselves to one experiment for each case and a subsampling of $\eta = 2$. Periodic densely sampled baseline and monitor data is recovered from the simultaneous data $\mathbf{y}_1$ and $\mathbf{y}_2$, respectively, by solving Equation 3.5. The inherent time-lapse difference is computed by subtracting the recovered baseline and monitor data.

The recovered time-lapse data is colocated, regularized and interpolated to a fine uniform grid. We note that all the observations made for the BG COMPASS model, which is a relatively simpler model, hold true for the more complex SEAM model. Minimum overlap (or nonreplication) between time-lapse surveys improves recovery of the vintages since independent surveys give additional structural information. Hence, they serve as better input to extract certain poststack attributes used to study time-lapse differences. Figures 3.15a, 3.15b, 3.15c and 3.15d show

the corresponding monitor data recovery. The SNR for the vintage recovery for minimum overlap between the surveys is 30.2 dB—a significant improvement from the 19.5 dB recovery for 100% overlap between the surveys. Moreover, as seen in Figures 3.15e, 3.15f, 3.15g and 3.15h, there is little variability in the recovery of the time-lapse difference from (the ideal) 100% overlap between the surveys to the more realistic almost nonreplicated surveys. The corresponding SNRs for the recovered time-lapse difference are 9.6 dB for 100% overlap and 4.1 dB for minimum overlap between the surveys. We note that the SNR for the minimum overlap between the surveys is biased due the presence of incoherent noise—between 3.5 s to 5.0 s—above the main time-lapse difference. If we compute the SNRs for the lower-half of the data that contains the time-lapse difference—i.e., after 4.5 s—the SNR for minimum overlap between the surveys increases to 6.8 dB. More importantly, if we look at the plots themselves, we see that there is not much difference in the two recoveries. We are able to recover the primary arrivals and some reverberations below. Recall that the amplitude of the time-lapse difference is one-tenth the amplitude of the vintages. It is quite remarkable that we get good results given the complexity of the model and the low amplitude of the time-lapse difference. Recovery of the vintages and the time-lapse difference for a subsampling of $\eta = 4$ follows the same trend as above.

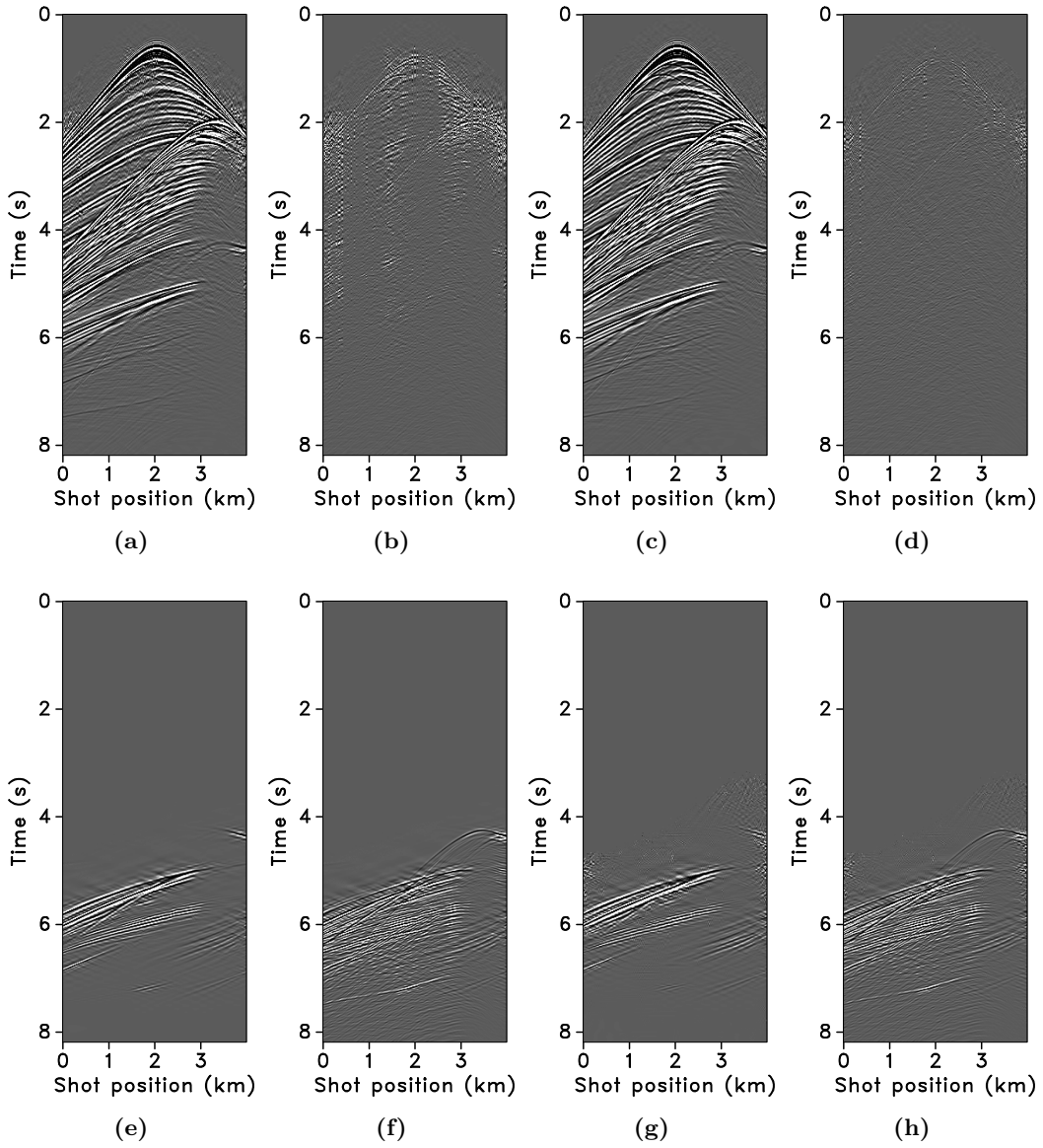

Figure 3.15 JRM recovered monitor and time-lapse difference receiver gathers from the SEAM model for a subsampling factor $\eta = 2$. Recovered monitor data and residual with (a,b) 100% overlap in the measurement matrices ($\mathbf{A_1}$ and $\mathbf{A_2}$); (c,d) $< 15\%$ overlap, respectively. Recovered time-lapse difference and residual with (e,f) 100% overlap in the measurement matrices; (g,h) $< 15\%$ overlap, respectively. Note that the amplitude of the time-lapse difference is one-tenth the amplitude of the monitor data.

3.7 Discussion

Realistic field seismic acquisitions suffer, amongst other possibly detrimental external factors, from irregular spatial sampling of sources and receivers. This poses technical challenges for the time-lapse seismic technology that currently aims to replicate densely sampled surveys for monitoring changes due to production. The experiments and synthetic results shown in the previous sections demonstrate favourable effects of irregular sampling and nonreplication of surveys on time-lapse data—i.e., decrease in replicability of the surveys leads to improved recovery of the vintages with little variability in the recovery of the time-lapse difference itself—while unraveling overlapping shot records. Note that we do not insist on replicating the irregular spatial positions in the field, however, the above observations hold as long as we know the irregular sampling positions after acquisition to a sufficient degree of accuracy, which is attainable in practice (see e.g., Mosher et al., 2014). Furthermore, we assume that there are no significant variations in the water column velocities, wave heights or temperature and salinity profiles amongst the different surveys while the source signature is also assumed to be the same. As long as these physical changes can be modeled, we do not foresee major problems. For instance, we expect that our approach can relatively easily be combined with source equalization (see e.g., Rickett and Lumley, 2001) and curvelet-domain matched filtering techniques (Beyreuther et al., 2005; Tegtmeier-Last and Hennenfent, 2013).

The proposed methodology involves a combination of economical randomized samplings with low environmental imprint and sparsity-promoting data recovery that aims to reduce cost of surveys and improve quality of the prestack time-lapse data without relying on expensive dense sampling and high degrees of replicability of the surveys. The combined operation of source separation, regularization and interpolation renders periodic densely sampled time-lapse data from time-compressed, and therefore economical, simultaneous, subsampled and irregular data. While the simultaneous data are separated reasonably well, recovery of the weak late-arriving events can be further improved by rerunning the recovery algorithm using the residual as input, using weighted one-norm minimization that exploits correlations between locations of significant transform-domain coefficients of different partitions—e.g., shot records, common-offset gathers, or frequency slices—of the acquired data (Mansour et al., 2013), etc. This needs to be examined in detail. Effects of noise and other physical changes in the environment also need to be carefully investigated. Nevertheless, as expected using standard CS, our recovery method should be stable with respect to noise (Candès et al., 2006). Moreover, recent successes in the application of compressed sensing to land and marine field data acquisition (see e.g., Mosher et al., 2014) support the fact that technical challenges with noise and calibration can be overcome in practice.

3.8 Conclusions

We present an extension of our simultaneous time-jittered marine acquisition to time-lapse surveys for realistic, off-the-grid acquisitions where the sample points are known but do not coincide with a regular periodic grid. We conduct a series of synthetic seismic experiments with different random realizations of the simultaneous time-jittered marine acquisition to assess the effects of irregular sampling in the field on time-lapse data and demonstrate that dense, high-quality data recoveries are the norm and not the exception. We achieve this by adapting our proposed joint recovery method—a new and economic approach to randomized simultaneous time-lapse data acquisition that exploits transform-domain sparsity and shared information among different time-lapse recordings—to incorporate a regularization operator that maps traces from an irregular grid to a regular periodic grid. The recovery method is a combined operation of source separation, regularization and interpolation, wherein periodic densely sampled and colocated prestack data is recovered from time-compressed, and therefore economical, simultaneous, subsampled and irregular data.

We observe that with decrease in replication between the surveys—i.e., shot points are not replicated amongst the vintages—recovery of time-lapse data improve significantly (about 4dB gain) with little (about 0.5dB) variability in recovery of the time-lapse difference itself. We make this observation assuming source equalization and no significant changes in wave heights, water column velocities or temperature and salinity profiles, etc., amongst the different surveys. We also demonstrate the delicate reliance on exact replicability (between surveys) by showing that known deviations as small as average $\pm(1, 2, 3)$ m in shot positions of the monitor surveys from the baseline surveys vary recovery quality of the time-lapse difference—expressed as slight decrease or increase in the signal-to-noise ratios—and hence negate the efforts to replicate. Therefore, it would be better to focus on knowing what the shot positions were (post acquisition) than aiming to replicate. Moreover, since irregular spatial sampling is inevitable in the real world, the requirement for replicability in time-lapse surveys can perhaps be relaxed by embracing or better purposefully randomizing the acquisitions to maximize collection of information by effectively doubling the number of measurements for the common component, leading to surveys acquired at low cost and environmental imprint.

Chapter 4

Highly repeatable time-lapse seismic with distributed Compressive Sensing—mitigating effects of calibration errors

4.1 Summary

In chapters 2 and 3, we demonstrated that combining joint recovery with low-cost non-replicated randomized sampling tailored to time-lapse seismic can give us access to high fidelity, highly repeatable, dense prestack vintages, and high-grade time-lapse. To arrive at this result, we assumed well-calibrated surveys—i.e., we presumed accurate post-plot source/receiver positions. Unfortunately, in practice seismic surveys are prone to calibration errors, which are unknown deviations between actual and post-plot acquisition geometry. By means of synthetic experiments, we analyze the possible impact of these errors on vintages and on time-lapse data obtained with our joint recovery model from compressively sampled surveys. Supported by these experiments, we demonstrate that highly repeatable time-lapse vintages are attainable despite the presence of unknown calibration errors in the positions of the shots. We assess the repeatability quantitatively for two scenarios by studying the impact of calibration errors on conventional dense but irregularly sampled surveys and on low-cost compressed surveys. To separate time-lapse effects from calibration issues, we consider the idealized case where the subsurface remains unchanged and the practical situation where time-lapse changes are restricted to a subset of the data. In both cases, the quality of the recovered vintages and time-lapse decreases gracefully for low-cost compressed surveys with increasing calibration errors. Conversely, the quality of vintages from expensive densely periodically sampled surveys decreases more rapidly as unknown and difficult to control calibration errors increase.

4.2 Introduction

The current paradigm in time-lapse (4D) seismic necessitates expensive replication of the baseline during the monitor survey to attain high degrees of repeatability (Eiken et al., 2003; Brown and Paulsen, 2011). In contrast, motivated by the successful field application of randomized Compressive Sensing surveys (Mosher et al., 2014) and academic contributions (see e.g. Herrmann, 2010, and references therein), our recent findings (Oghenekohwo et al., 2017; Wason et al., 2017) — described in chapters 2 and 3 — suggest that one does not need to replicate subsampled randomized time-lapse surveys to get equivalent and acceptable levels of repeatability. While these results are encouraging, our findings relied on two critical assumptions, namely we ignored noise and assumed calibrated surveys. Although our randomized time-lapse acquisition does not insist on exact replication in the field — allowing for deviations between planned (pre-plot) and actual survey geometries — reconstruction of the vintages towards a common fine periodic grid from the randomized samplings relies on accurate knowledge of the actual acquisition parameters. Thus, we ignore possible unknown calibration errors defined as differences between the actual (true) and observed (recorded) post-plot geometries.

Since these calibration errors are unavoidable in practice, we study the performance of our approach, namely, compressed time-lapse acquisition with calibration errors and subsequent recovery with our joint recovery model (JRM), via a series of experiments designed to measure attainable degrees of repeatability. As before, key to our success is the sparse recovery of the component common to the vintages, and "innovations" with respect to this component that sparsely encode the differences between the vintages. Because the common component is sensed by all time-lapse surveys, recovery with the JRM leads to improved quality of the vintages when the surveys are not replicated as we confirmed with a specific compressive sensing-inspired acquisition design (time-jittered sources in marine by (Wason and Herrmann, 2013)).

There have been earlier attempts (Eggenberger et al., 2014), with sparsity promotion to recover more repeatable time-lapse surveys but these also relied on having well-calibrated surveys. Albeit these approaches do not exploit the possible advantages distributed compressive sensing (DCS, Baron et al., 2009b) has to offer but instead rely on having access to multiple periodically but coarsely sampled wavefield components for their reconstruction. By combining random subsampling and joint recovery, we are able to obtain high-quality repeatable vintages from significantly fewer calibrated measurements (Oghenekohwo et al., 2017; Wason et al., 2017).

Practitioners of time-lapse seismic studies often use the normalized root mean square (NRMS, Kragh and Christie, 2002) to quantify the degree of repeatability in 4D seismic. Repeatability, which measures similarity between vintages, depends on several factors including unknown positioning errors for each survey (Schisselé et al., 2009), differences in noise, and processing workflows (Rickett and Lumley, 2001; Hicks et al., 2014) that aim to preserve the 4D signal. The smaller the NRMS

value, the less likely it is that the 4D signal is due to differences amongst the surveys or environment (currents, wave heights, etc.) the surveys were acquired in.

Our main contribution is to demonstrate that high quality and highly repeatable surveys are attainable with our JRM despite the presence of unknown calibration errors. We substantiate this claim by measuring the recovery quality and repeatability in terms of signal-to-noise ratios (S/N) and NRMS values for a series of carefully designed idealized — ignoring noise and environmental changes — randomized time-lapse surveys for which *(i)* there are no time-lapse changes present so worsening recovery quality and repeatability can solely be attributed to calibration errors and *(ii)* time-lapse changes are confined to subsets of the data.

We first describe a primer on how compressive sensing can be setup in marine acquisition before presenting the main aspects of the chapter. The rest of this chapter is organized as follows. First, we present the theoretical framework for low-cost randomized time-lapse subsampled data acquisition and recovery with the JRM. Next, we introduce the NRMS in the two settings where either the earth model remains unchanged or where there is a time-lapse signal present in a subset of the data. We conclude by a series of numerical experiments that reflect these two scenarios and that allow us to analyze the possible impact of unknown calibration errors.

4.3 Primer on Compressive Sensing in marine acquisition

To obtain high resolution images of the Earth subsurface, marine seismic surveys require dense sampling that can become prohibitively expensive especially when time-lapse is of interest. To address this issue in seismic data acquisition, (Hennenfent and Herrmann, 2008), (Herrmann, 2010), (Mansour et al., 2012), and (Mosher et al., 2014) adapted ideas from Compressive Sensing (CS, Donoho, 2006; Candès et al., 2006), whereby cost of surveys depends on our ability to leverage certain inherent structure in seismic data rather than on the sample rate and size of the survey area. In seismic applications, adherence to three + one key principles of (distributed) CS are critical, namely we need to
(i) find a compressible representation, e.g. via transform-domain sparsity; *(ii)* design a physically realizable randomized subsampling scheme, which turns subsampling related artifacts into incoherent noise that is not compressible; *(iii)* restore densely sampled data by promoting structure—i.e., by mapping incoherent artifacts to coherent signal; *(iv)* exploit information shared amongst time-lapse vintages during the recovery, which allows us to maximally benefit from randomized sampling without insisting on replicating the surveys.

A physically realizable way to render marine acquisition more economically viable is to fire airgun sources at random time-jittered compressed-in-time firing times (Wason and Herrmann, 2013). Depending on whether we work with dynamic towed

arrays or static receivers (OBNs or OBCs), the variability in jittered shot firing times can either be small or large. For towed arrays, because the sources and receivers are in motion, we can only permit a small variability so that the array records information from the pair of airgun sources. In the case of static receivers, we can permit low to high variability. We include Figure 4.1 to illustrate the difference between periodic sampling (resulting in non-overlapping records) and randomized sampling (resulting in overlapping shots) in two acquisition settings.

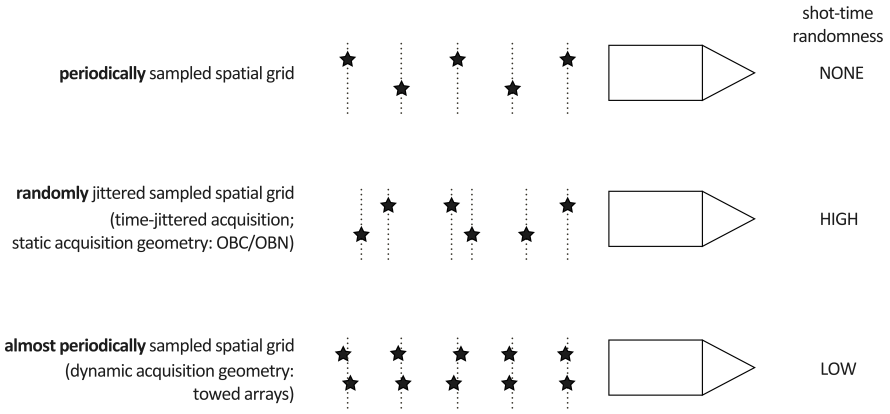

Figure 4.1 Periodic versus randomized (jittered) marine survey showing scenarios for low and high variability in shot firing times.

Conventional acquisition involves firing shots at regular time intervals resulting in non-overlapping regularly sampled shots (first column of Figure 4.2). In processing, we typically interpolate the regularly sampled shots onto a finer grid (third column of Figure 4.2) to increase the source sampling. For our compressive sensing based marine acquisition, we consider the more favorable case of large variability in shot firing times, for which good recovery results have been reported in the literature (Mansour et al., 2012; Wason and Herrmann, 2013) from surveys with overlapping shot records and coarse source sampling. The second column of Figure 4.2 illustrates how our scheme compresses the survey time compared to the conventional approach, and how we aim to reconstruct the wavefield onto a fine periodic grid with increased source sampling. Both the conventional and jittered scheme sample data on different spatial grids covering the same length of the seismic line but with reduction in survey time via the jittered scheme. Because our jittered sampling scheme compresses the acquisition time and recovers densely sampled data, our acquisition is more economic.

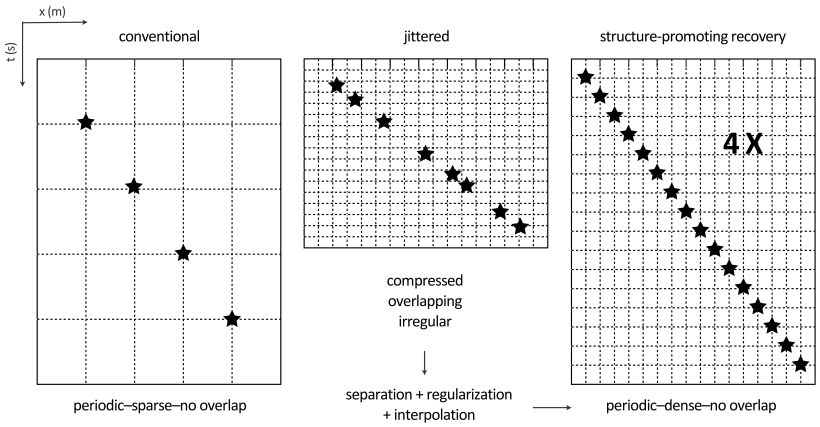

Figure 4.2 Schematic of sampling schemes and recovery. Left: conventional survey with non-overlapping shots. Middle: compressed survey time with overlapping shots. Right: recovery of non-overlapping dense periodic shots with improved source sampling. [Adapted from (Wason et al., 2017)]

When provided with time-jittered surveys that are sufficiently calibrated, we can expect good recovery results (Oghenekohwo et al., 2017; Wason et al., 2017). However, as we mentioned in the Introduction of this chapter, 3D and 4D seismic surveys are both susceptible to calibration errors, which are by definition unknown deviations between actual (true) and observed (post-plot) coordinates of sources/receivers. Figure 4.3 illustrates an example of our randomized and compressed time-lapse surveys where observed shot positions differ from the truth. The purpose of this work is to investigate the possible impact of these calibration errors on the recovered vintages and the time-lapse difference after reconstructing the surveys onto one and same fine periodic dense grid using our joint recovery model.

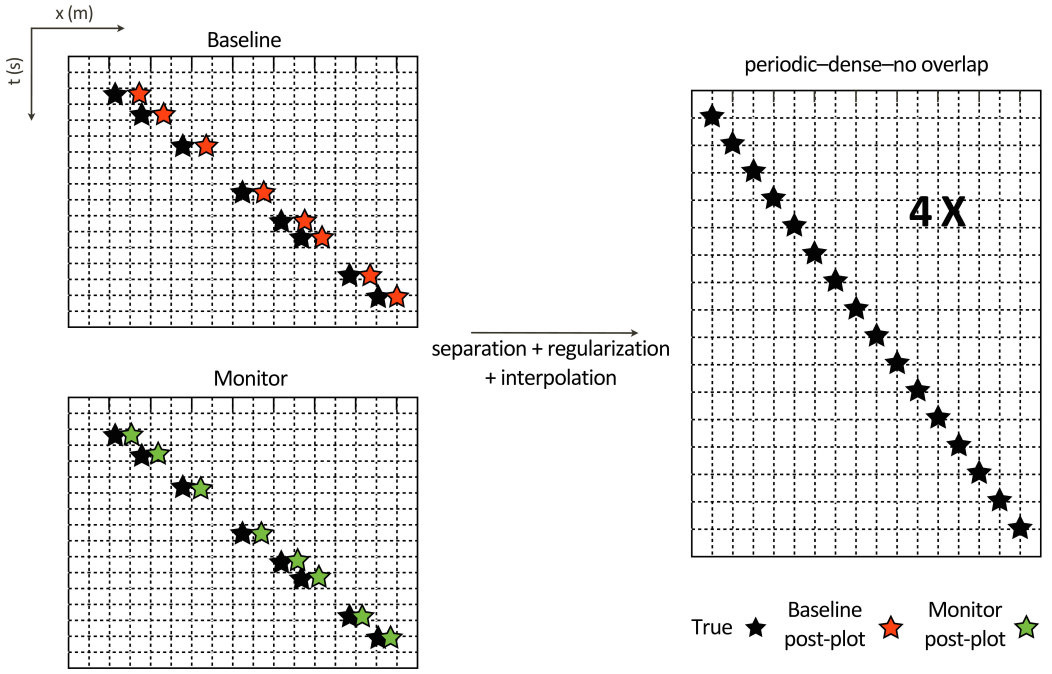

Figure 4.3 Illustration of compressive time-lapse jittered surveys with calibration errors as deviations between true and observed post-plot shot positions. The calibration errors are not the same for the baseline and monitor. Notice the compression in acquisition time for the time-jittered surveys, the difference in acquisition geometry, and the mapping of the vintages to one and the same fine-grained source grid.

4.4 Methodology

Before we conduct experiments to quantify the degree of repeatability of randomized time-lapse surveys with calibration errors, let us first briefly review the joint recovery model and the NRMS. Without loss of generality, we consider the case of two time-lapse surveys only.

4.4.1 Compressive time-lapse acquisition

Let us denote baseline surveys with the index $j = 1$ and monitor surveys with the index $j = 2$. Following ideas from compressive sensing, we model data acquired with these two surveys by: $\mathbf{y}_j = \mathbf{A}_j \mathbf{x}_j$ for $j = \{1, 2\}$, where $\mathbf{y}_j$ are the usually observed randomly under-sampled data for each survey. As described in (Hennenfent and Herrmann, 2008), (Herrmann, 2010), and (Mansour et al., 2012), the matrices $\mathbf{A}_j$ encapsulate specifics on the survey geometry for each vintage and the sparsifying transform used during the recovery. The task of the time-lapse seismic practitioner now is to recover the coefficient vectors $\widetilde{\mathbf{x}}_j$'s from sparse randomly under-sampled

$\mathbf{y}_j$'s from which estimates for densely sampled vintages $\widetilde{\mathbf{d}}_j$, that live on one and the same fine periodic grid can be derived. However, rather than recovering each vintage separately, by solving

$$\widetilde{\mathbf{x}}_j = \arg\min_{\mathbf{x}_j} \|\mathbf{x}_j\|_1 \quad \text{subject to} \quad \mathbf{y}_j = \mathbf{A}_j\mathbf{x}_j,\ j = 1, 2, \tag{4.1}$$

we solve

$$\widetilde{\mathbf{z}} = \arg\min_{\mathbf{z}} \|\mathbf{z}\|_1 \quad \text{subject to} \quad \mathbf{y} = \mathbf{A}\mathbf{z} \tag{4.2}$$

with

$$\underbrace{\begin{bmatrix}\mathbf{y}_1\\ \mathbf{y}_2\end{bmatrix}}_{\mathbf{y}} = \underbrace{\begin{bmatrix}\mathbf{A}_1 & \mathbf{A}_1 & \mathbf{0}\\ \mathbf{A}_2 & \mathbf{0} & \mathbf{A}_2\end{bmatrix}}_{\mathbf{A}} \underbrace{\begin{bmatrix}\mathbf{z}_0\\ \mathbf{z}_1\\ \mathbf{z}_2\end{bmatrix}}_{\mathbf{z}} \tag{4.3}$$

instead. Compared to recovering the vintages separately as in Equation 4.2, the joint recovery model inverts for the coefficient vectors of the common component ($\widetilde{\mathbf{z}}_0$) and *innovations* ($\widetilde{\mathbf{z}}_j$) that encode the time-lapse. By construction, the common component of JRM benefits from sensing by both surveys (first column of $\mathbf{A}$). This can lead to markedly improved recoveries of densely periodically sampled vintages $\widetilde{\mathbf{d}}_j$ derived from $\widetilde{\mathbf{z}}_0$ and $\widetilde{\mathbf{z}}_j$, without insisting on replicating the surveys as recently reported by (Oghenekohwo et al., 2017) and (Wason et al., 2017).

While the combination of randomized subsampling and the JRM offers unprecedented flexibility in cost-effective time-lapse acquisition, the recovery of densely sampled time-lapse data is built on the premise that reliable information on the actual acquisition geometry is available. This is to ensure that the modelling matrices ($\mathbf{A}_j$'s) accurately mimic the time-lapse measurements in the field. This reliance on accurate knowledge on the acquisition geometry raises some concern because in practice there will always be unknown calibration errors between observed and actual acquisition parameters.

To quantify the impact of these calibration errors, we will first consider the special case where $\mathbf{x}_1 = \mathbf{x}_2$— i.e., there is no time-lapse, but the randomized acquisitions differ ($\mathbf{A}_1 \neq \mathbf{A}_2$) and where there are differences between actual and observed post-plot acquisition parameters. In this situation and in the practical situation where time-lapse changes are localized, we still hope to attain high quality recovery and repeatability despite the presence of calibration errors.

4.4.2 NRMS a measure for 4D repeatability

Common practice in time-lapse seismic processing is to measure the degree of repeatability of observed and processed data at each consecutive processing step (Ross et al., 1997; Harris and Veritas, 2005; Houck, 2007). This degree of repeatability

measures the similarity between two time-lapse data sets, for example the recovered baseline ($\widetilde{\mathbf{d}}_1$) and monitor ($\widetilde{\mathbf{d}}_2$) surveys. As described by (Kragh and Christie, 2002), we quantify the degree of repeatability of the two vintages defined as the RMS of the difference between the two vintages divided by the average RMS of these two vintages—i.e., we have

$$\text{NRMS}(\widetilde{\mathbf{d}}_1, \widetilde{\mathbf{d}}_2) = \frac{200 \times \text{RMS}(\widetilde{\mathbf{d}}_1 - \widetilde{\mathbf{d}}_2)}{\text{RMS}(\widetilde{\mathbf{d}}_1) + \text{RMS}(\widetilde{\mathbf{d}}_2)},$$

with

$$\text{RMS}(\mathbf{d}) = \sqrt{\frac{\sum_{t=t_1}^{t_2} (\mathbf{d}[t])^2}{N}},$$

where N is the number of samples in the interval t_1 to t_2 and $\mathbf{d}[t]$ refers to a sample recorded at "time" t. By virtue of this definition, NRMS values range between 0 and 200 as percentages. The smaller the percentage, the more repeatable the vintages are. In practice, NRMS values are computed using seismic traces extracted from the data in a common time window and frequency band where there are no time-lapse changes. According to today's best 4D practices, NRMS values less than 10% are considered acceptable and in some cases, excellent.

4.5 Numerical experiments

To demonstrate the impact of calibration errors, we conduct a series of synthetic experiments involving non-replicated 2-D marine (ocean bottom cable) time-lapse surveys with unknown calibration errors only in the source positions. Recall that these errors are unknown deviations between the actual (true) and observed post-plot positions. For reference, we simulate idealized densely and regularly (periodic) sampled shots at 12.5m interval on a realistic synthetic earth model (see Figure 4.4a) with laterally varying densities and velocities, provided to us by the BG group.

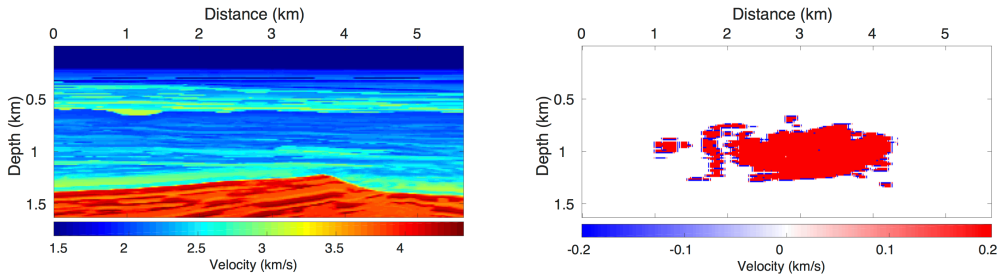

(a) **(b)**

Figure 4.4 The BG model. (a) Subset of the baseline velocity model (b) The difference between the baseline and monitor model (not shown here) revealing a gas cloud.

Our experiments compare a conventional dense survey, sampled irregularly with on average the same 12.5m shot interval, and simultaneous source (randomly time-jittered) surveys acquired with our low-cost subsampling scheme (Wason and Herrmann, 2013). The latter entails a 4× speed-up in acquisition time resulting in overlapping shot records at irregular positions, sampled at an average coarse shot interval of 50m. To mimic observed data with unknown calibration errors, we add random perturbations from a uniform distribution to the actual shot locations. As Table 4.1 shows, while we only need to regularize the conventional data since it is densely sampled, we process the low-cost data via shot separation, interpolation, and regularization. These experiments allow us to assess the repeatability quantitatively for the idealized case where the subsurface does not change and the practical situation where time-lapse changes are confined to a subset of the data.

	Conventional dense survey	Low-cost (4× compressed) survey
Shot geometry	Flip-flop irregular shot sampling	2 Sim. source (time-jittered sources)
Receiver geometry	OBC	OBC
Number of shots	450	100
Shot interval	12.5m	50m
Number of receivers	450	450
Receiver interval	12.5m	12.5m
Recovery (Processing)	Regularization	Shot separation, Interpolation, Regularization

Table 4.1 Experiment details including acquisition information and processing steps both for conventional (dense) and low-cost (compressed) random time-jittered surveys.

4.5.1 Idealized case no time-lapse

To separate the possible impact of calibration errors from the time-lapse signal itself, we first consider the case where the earth model does not change between time-lapse surveys but where both the known survey parameters and unknown calibration errors differ. In this case, differences in the vintages can be attributed to differences in the surveys. For the densely but irregularly sampled data, we recover regularly sampled vintages via regularization of the observed data $\mathbf{y}_j$ by directly computing the pseudo inverse $\mathbf{A}_j^{\dagger}\mathbf{y}_j$, where the modelling matrices ($\mathbf{A}_j$'s) encapsulate the irregular shot geometry up to calibration errors that increase from 0 to 50% of the 12.5m shot interval. We collect low-cost data by firing more often with *jittering* yielding fewer but irregular source locations that also contain calibration errors between 0 to 50% of the original 12.5m shot interval. The nominal shot sampling interval in our low-cost survey is about 50m. We introduce calibration errors in our measurements by adding random perturbations from a uniform distribution to the actual shot locations. In principle, we could also add such perturbations to the receiver locations.

We recover these randomly subsampled datasets via independent and joint recovery (cf. Equation 4.1 and 4.2). We examine the quality of the recovered vintages in terms of S/N, and compute repeatability in terms of NRMS, for the conventional and low-cost acquisition as a function of the relative calibration errors. As we can see from Figure 4.5, recovery with JRM (third column) attains a relatively high S/N and greatly improved NRMS compared to the results from conventional acquisition (first column) and independent recovery (middle column), despite unknown calibration errors up to 20% of the interpolated shot interval.

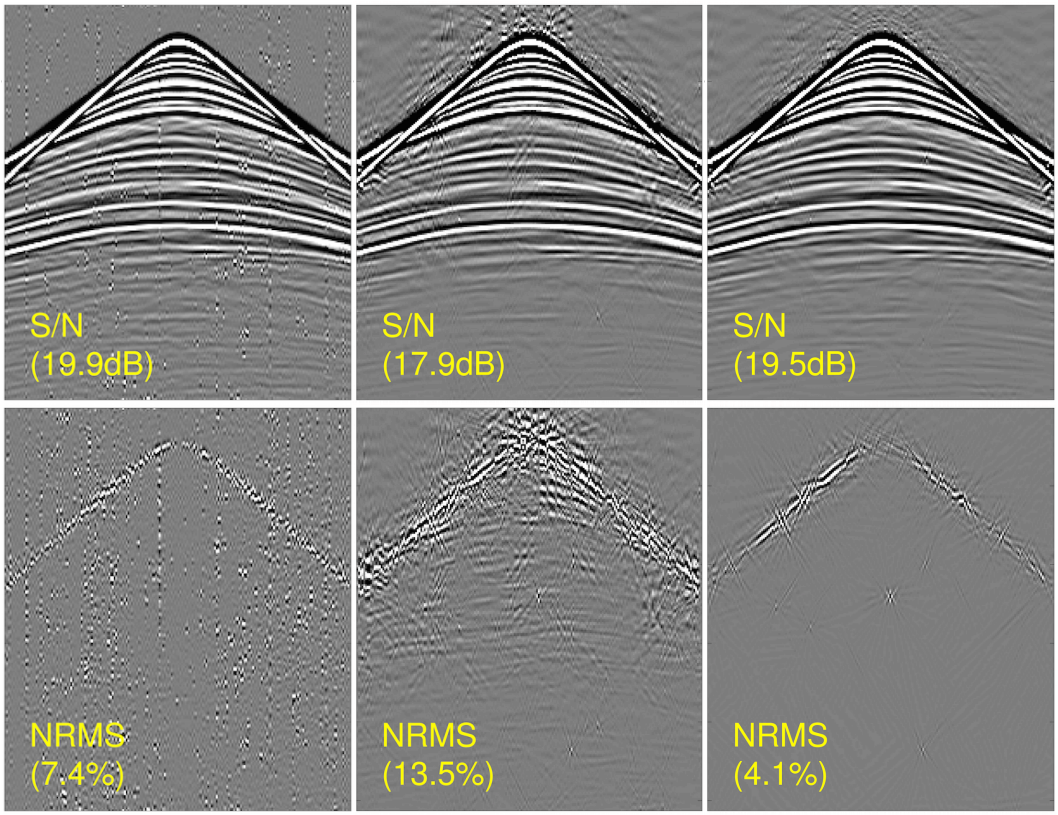

Figure 4.5 Idealized case (no time-lapse) - A receiver gather extracted from recovered vintage (top) and difference (bottom) between vintages obtained from surveys, each with calibration errors up to 2.5m, i.e. 20% of the interpolated shot interval (12.5m). Notice the improved repeatability using our joint recovery model.

Furthermore, to get more reliable estimates (mean and standard deviation) of the S/N and NRMS for increasing calibration errors, we repeat the experiments for 10 independent random realizations of the pairs of modelling matrices. Figures 4.6a and 4.6b show the results of this exercise, which allow us to make the following observations: *(i)* expectedly, calibrated surveys yield highest-quality vintages in terms

of S/N compared to surveys that are not calibrated — this is because the modelling matrix for calibrated surveys correctly maps the observed data to the actual shot points whereas uncalibrated surveys violate this mapping; *(ii)* the quality of the vintages decreases gradually for the low-cost compressed surveys with increasing calibration errors. Conversely, the quality of conventional irregular dense surveys decreases rapidly for increasing calibration errors — this is because errors arising from uncalibrated dense surveys behave like noise whose magnitude grows with the number of shots; *(iii)* for surveys with large ($> 40\%$) calibration errors, our low-cost sampling scheme with JRM is on par with the dense surveys regarding the recovery quality but relatively better in repeatability — the NRMS values for the low-cost acquisitions remain acceptable. These observations are consistent with our earlier findings on calibrated low-cost acquisitions (Oghenekohwo et al., 2017; Wason et al., 2017), again owing to making the common component shared by the the vintages explicit in the recovery.

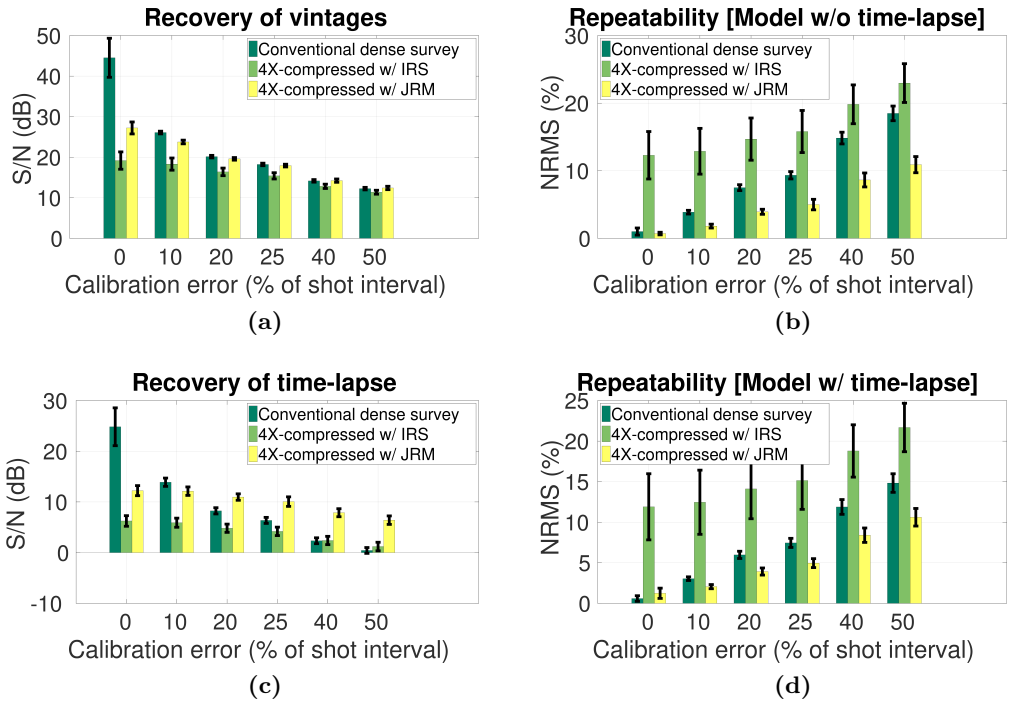

Figure 4.6 Top: Idealized case (no time-lapse). (a) Recovery quality and (b) repeatability of vintages, from conventional dense and low-cost surveys with calibration errors. Bottom: Practical case (localized 4D). (c) Recovery quality of 4D signal and (d) repeatability of vintages. Note the NRMS in (d) is computed outside the 4D signal window.

4.5.2 Practical case localized time-lapse

While the previous experiments demonstrate the impact of calibration errors on the vintages and the difference, we cannot guarantee that the effect of these errors will not propagate to the time-lapse signal in situations where the earth actually changes. Therefore, we conduct experiments on a synthetic time-lapse earth model (Figure 4.4) with localized changes in both density and velocity. We compute the prestack localized 4D signal via subtraction of the two vintages after recovery towards a common grid. We now measure the recovery quality of the 4D signal and the repeatability of the vintages in presence of calibration errors, both for the conventional and low-cost acquisitions.

After data simulation and recovery as done previously, we perform repeatability analysis—compute the NRMS—outside the 4D signal window, and compute the S/N of the recovered prestack 4D signal only in the window where the 4D signal resides. We present the result of this experiment in Figures 4.6c and 4.6d. Despite the fact that the earth changes, the NRMS values behave more or less the same as in Figure 4.6b. This means that high degrees of repeatability are achievable with S/Ns that decrease gracefully compared to the conventional sampling and independent recovery. This experiment clearly shows that the uplift of costly dense sampling may be negated by the presence of relatively small (10% $\approx$ 1.25 m) calibration errors.

4.6 Discussion

We also investigated the impact of timing errors on acquisition and on time-lapse repeatability and we found that repeatability is more sensitive to small errors in firing times (as small as 1ms). This underscores the need for GPS recordings of shot firing times to be highly accurate for our shot separation algorithm to work in practice. As we have seen with experiments on calibration errors in the source positions, relatively small calibration errors (up to about 25% of the interpolated shot interval) in the actual visited shot positions can still yield highly repeatable data (i.e., NRMS $\leq$ 10%) for densely sampled surveys but this comes at a high cost. However, as soon as the errors are 25% or more, the repeatability deteriorates and is even worse than the NRMS value for the data recovered from compressively sampled surveys with the JRM. This trend continues for even larger errors—i.e., we still have a NRMS value close 10% for calibration errors of up to 40%. This indicates that our algorithm is relatively robust to calibration errors.

4.7 Conclusions

Errors in acquisition parameters unbeknown to subsequent seismic data processing, including regularization and shot separation, can have detrimental effects on the

quality and repeatability in particular when mapping time-lapse seismic surveys to a common densely sampled periodic grid. For the case of post-plot calibration errors in the source locations, we were able to demonstrate that high quality and highly repeatable vintages and time-lapse data are attainable in the presence of source position errors that are of order of $20-25\%$ of the interpolated shot sample interval. As expected, high-cost densely sampled acquisitions may indeed lead to the best quality and repeatability in the absence of calibration errors. However, the quality and repeatability of these expensive densely sampled surveys decays very rapidly in the presence of even relatively small (10% of the shot sample interval) calibration errors. Understandably, the quality and repeatability of four times cost-reduced compressive acquisitions is also affected by calibration errors but this deterioration is much more modest for vintages and time lapse data obtained with our joint recovery model. This result holds for both the idealized situation where the subsurface does not change and where differences in the vintages and time-lapse data are due to both differences in the surveys and (uncontrollable) calibration errors, or for the realistic situation where time-lapse changes in the subsurface are confined to subsets of the data. Either way, the performance of the joint recovery model for acquisitions with unknown calibration errors is remarkable and can be explained by the fact that our approach leverages information that is common amongst the vintages explicitly. With these observations, we are confident that economic time-lapse surveys with Compressive Sensing are indeed feasible and ready to be conducted in the field.

Chapter 5

Time-lapse seismic imaging with distributed compressive sensing

This chapter comprises two broad sections. The first titled "Randomized sampling without repetition in time-lapse seismic surveys" is an inversion framework using the joint recovery model that produces images as stacked sections from randomly undersampled prestack data volumes. The second titled "Using common information in compressive time-lapse full-waveform inversion" describes an implementation of full-waveform inversion of time-lapse data using the joint recovery model.

5.1 Randomized sampling without repetition in time-lapse seismic surveys

5.1.1 Summary

Vouching for higher levels of repeatability in acquisition and processing of time-lapse (4D) seismic data has become the standard with oil and gas contractor companies, with significant investment in the design of acquisition systems and processing algorithms that attempt to address some of the current 4D challenges, in particular, imaging weak 4D signals. Recent developments from the field of compressive sensing have shown the benefits of variants of randomized sampling in marine seismic acquisition and its impact for the future of seismic exploration. Following these developments, we show that the requirement for accurate survey repetition in time-lapse seismic data acquisition can be waived provided we solve a sparsity-promoting convex optimization program that makes use of the shared component between the baseline and monitor data. By setting up a framework for inversion of the stacked sections of a time-lapse data, given the pre-stack data volumes, we are able to extract 4D signals with relatively high-fidelity from significant sub-samplings.

Our formulation is applied to time-lapse data that has been acquired with different source/receiver geometries, paving the way for an efficient approach to dealing with time-lapse data acquired with initially poor repeatability levels, provided the survey geometry details are known afterwards.

5.1.2 Introduction

Repeatability in acquisition and processing ranks highest among the technical challenges faced with time-lapse seismic studies (Lumley and Behrens, 1998) and researchers continue to develop methods that will address these challenges. Computing weak 4-D signals pose another significant challenge the industry currently faces as the signal is below the non-repeatable noise introduced during acquisition or processing. Therefore, many studies have been focused on improving repeatability levels of acquired and processed time-lapse data (Porter-Hirsche and Hirsche, 1998; Landrø, 1999; Eiken et al., 2003). Recently, permanent monitoring systems have been used to acquire multiple time-lapse data and automated systems are being designed to improve the accuracy and repeatability of time-lapse surveys (Brown and Paulsen, 2011; Eggenberger et al., 2014). Although these systems improve the repeatability levels of the time-lapse data, they are very expensive to maintain and enormous effort is required for their operation. In our recent study (Oghenekohwo et al., 2014b), we show how the concern for repeatability can be relaxed provided we randomly sample the shots during the time-lapse surveys. Consequently, we solve an inverse problem, exploiting the shared information in the baseline and monitor data, to recover a densely sampled time-lapse data from the measured randomized data. The net result was a high-fidelity 4D signal in the data domain.

Few studies involving a joint processing or inversion scheme for imaging time-lapse data have been conducted. (Rickett and Lumley, 2001) proposed a cross-equalization data processing flow where data repeatability is matched at each processing step, while (Ayeni et al., 2009) imaged time-lapse data acquired from simultaneous source (or blended acquisition) which is a variant of randomized marine acquisition. However, while the cross-equalization approach does not address data which has been randomly sampled without repetition, and the inversion scheme does not account for the shared information in the data sets, we exploit both requirements in our formulation to improve the 4D signal recovery quality.

In this paper, we extend our independent and joint recovery methods to the computation of time-lapse images using our randomized sampling scheme without repetition, having observed its' efficacy to recover reliable 4D signals in the data domain. For simplicity, we show the computation of time-lapse stacked sections including 4D difference stacked sections, from randomized, subsampled baseline and monitor data.

5.1.3 Methodology

Given an earth model $\mathbf{m}$, the conventional approach to modeling seismic data $\mathbf{y}$ from a modeling operator $\mathbf{F}$ is:

$$\mathbf{Fm} = \mathbf{y}. \tag{5.1}$$

Ideally, $\mathbf{F}$ is either an elastic or acoustic wave-equation operator, however, for simplicity (but without generality), we redefine $\mathbf{F} = \mathbf{M^H N^H S^H}$ as a linear operator mapping a stacked time section to a pre-stack seismic data volume. Here, $\mathbf{M}$ is the midpoint-offset to source-receiver operator, and $\mathbf{S}$ is the stacking operator. This linear mapping relies on the prior knowledge of the stacking velocities. This is required for constructing the normal move-out (NMO) operator $\mathbf{N}$. This velocity requirement is true with any imaging or stacking algorithm. Incorrect background velocity model or stacking velocities can lead to significant misalignments of reflectors in a migrated image or stacked section respectively, therefore it is important to have an accurate estimate of the velocity. The earth model can also be represented as $\mathbf{m} = \mathbf{C^H x}$, where $\mathbf{x}$ is the sparse representation of $\mathbf{m}$, and $\mathbf{C^H}$ is the synthesis curvelet operator linking the model to the curvelet coefficients. Taking $\mathbf{m}$ to be the stacked time section, and combining the curvelet representation of the model with the redefined modeling operator $\mathbf{F}$, equation (5.1) can be recast as :

$$\mathbf{Ax} = \mathbf{F}\mathrm{C}^{\mathbf{H}}\mathbf{x} = \mathbf{y}. \tag{5.2}$$

Clearly, this formulation gives rise to an over-determined system of equations, where the observed data $\mathbf{y}$ has a higher dimension compared to the model $\mathbf{m}$. An inversion approach is typically required to find an estimate $\tilde{\mathbf{m}}$ of the true model $\mathbf{m}$, given the observed data. Inversion for the stacked section of a seismic data is a viable approach as it affords us to sample as little as possible since the number of unknowns in our linear system of equations is small. Furthermore, we note that the estimation of the stacked sections from the observed data is significantly less computationally expensive than recovering the complete wavefield. The inversion can be done in several ways and in consistency with our previous work, we will adopt the ℓ_1 inversion procedure where we promote sparsity in $\mathbf{x}$ by solving the convex optimization problem:

$$\tilde{\mathbf{x}} = \arg\min_{\mathbf{x}} \|\mathbf{x}\|_1 \quad \text{subject to} \quad \mathbf{y} = \mathbf{Ax}.$$

For time-lapse studies, where we have at least a baseline pre-stack data $\mathbf{y}_1$ and a monitor pre-stack data $\mathbf{y}_2$, we can do several things including (1) inversion of the data sets to obtain an estimate of the stacked section for the baseline $\tilde{\mathbf{m}}_1 = \mathbf{C^H}\tilde{\mathbf{x}}_1$, the monitor $\tilde{\mathbf{m}}_2 = \mathbf{C^H}\tilde{\mathbf{x}}_2$, and finally differencing the two stacked sections; (2) inversion of the difference between the pre-stack baseline and monitor data (provided the data are matched to a common computational grid), to obtain the time-lapse stacked section; (3) joint inversion for both the "static" and "changing" parts of the stack sections. The problem formulation allows us to employ our independent recovery strategy (IRS) and joint recovery method (JRM), discussed in (Oghenekohwo et al., 2014b), to estimate the individual stacked sections and the corresponding

4D stacked sections. The IRS simply inverts for the baseline and monitor stacked sections independently, by solving the following problems

$$\begin{aligned}\tilde{\mathbf{x}}_1 = &\quad \arg\min_{\mathbf{x}_2} \|\mathbf{x}_1\|_1 \quad \text{subject to} \quad \mathbf{y}_1 = \mathbf{A}_1\mathbf{x}_1 \\ \tilde{\mathbf{x}}_2 = &\quad \arg\min_{\mathbf{x}_2} \|\mathbf{x}_2\|_1 \quad \text{subject to} \quad \mathbf{y}_2 = \mathbf{A}_2\mathbf{x}_2\end{aligned}$$

On the other hand, the JRM performs a joint inversion by taking into account the shared information (Baron et al., 2005) between the time-lapse data. We let $\mathbf{x}_1 = \mathbf{z}_0 + \mathbf{z}_1$ and $\mathbf{x}_2 = \mathbf{z}_0 + \mathbf{z}_2$ where $\mathbf{z}_0$ srepresents the common part of the baseline and monitor models, whereas $\mathbf{z}_1$ and $\mathbf{z}_2$ are the parts contributing to the differences in the models. Therefore, we solve the following problem:

$$\tilde{\mathbf{z}} = \arg\min_{\mathbf{z}} \|\mathbf{z}\|_1 \quad \text{subject to} \quad \mathbf{y} = \mathbf{A}\mathbf{z}.$$

where $\mathbf{A} = \begin{bmatrix} \mathbf{A}_1 & \mathbf{A}_1 & \mathbf{0} \\ \mathbf{A}_2 & \mathbf{0} & \mathbf{A}_2 \end{bmatrix}$, $\mathbf{z} = \begin{bmatrix} \mathbf{z}_0 \\ \mathbf{z}_1 \\ \mathbf{z}_2 \end{bmatrix}$, and $\mathbf{y} = \begin{bmatrix} \mathbf{y}_1 \\ \mathbf{y}_2 \end{bmatrix}$.

From $\tilde{\mathbf{z}}$, we can compute an estimate of the individual stacked sections and the differences between the stacks.

5.1.4 Numerical Experiments

We model a fixed-spread acquisition configuration by simulating densely sampled synthetic time-lapse data comprising a baseline data set and a monitor data set $\mathbf{y}_2$ using $\mathbf{F}$ while keeping the acquisition geometries same . An example of the synthetic seismic data is shown in Figure 5.1.

In an effort to justify the need to relax time-lapse seismic data acquisition repeatability, we randomly subsample the idealized pre-stack synthetic baseline data by reducing the shot interval, simulating a baseline acquisition with several shots missing at random locations. Similarly, a different randomized subsampling of the monitor data was performed to represent randomized monitor survey with a different set of shot locations missing, independent of the baseline survey.

Figure 5.2 shows an example of the observed common midpoint (CMP) gather indicating missing shots in the data. Although we have only simulated data with missing shots between the vintages, this can equally be extended to missing receivers or missing shots and receivers. This experiment produces time-lapse data from different acquisition geometries, resulting in different sets of shot data and missing traces. In addition, we can also extend this experiment to simultaneous marine acquisition where seismic sources fire at randomly dithered times (Wason and Herrmann, 2013).

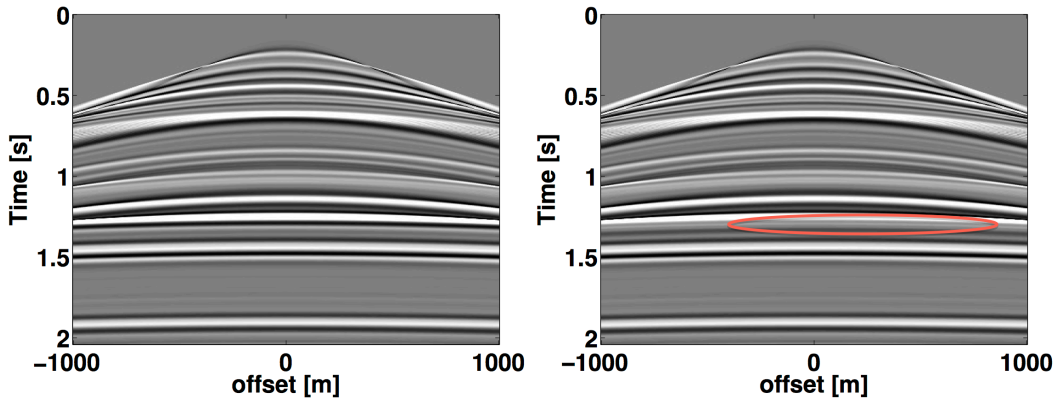

Figure 5.1 Densely sampled time-lapse data with repetition. (a) baseline data, (b) monitor data. The ellipse indicates the time-lapse change zone.

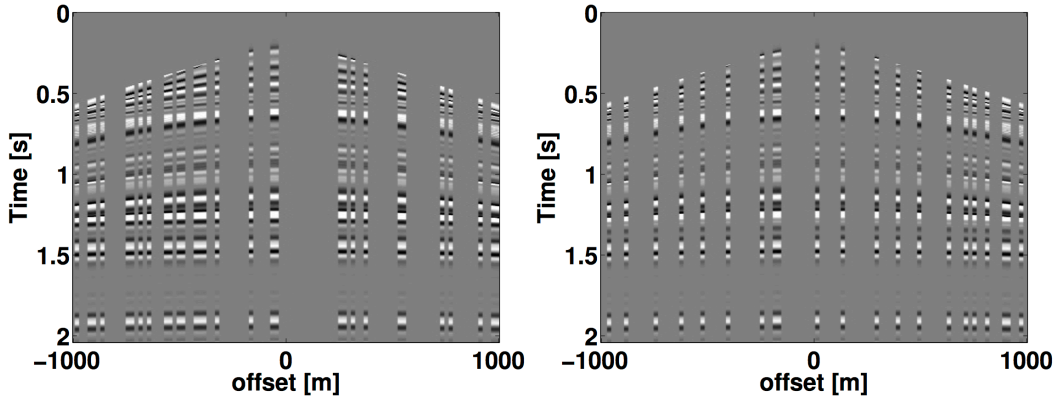

Figure 5.2 Observed randomly sampled time-lapse data without repetition. (a) baseline data, (b) monitor data. Note the missing shots in the data due to the randomized sampling without repetition.

Conventional processing involving NMO and stacking was applied to the densely sampled idealized data sets and this produced a baseline stacked section and monitor stacked section respectively. Figure 5.3 shows the true (idealized) stacked sections. These served as a benchmark for the rest of our experiment. The stacked section shows the complexity of the model with an indication of strong impedance contrast at different time depths. The time-lapse signal is at a time-depth of between 1.2s and 1.4s and varies laterally over a range of approximately 1km.

To establish the effects of randomized time-lapse survey without repetition and with different subsampling ratios, as it relates to inversion for the stacked sections,

we performed experiments for different subsampling ratios. We investigated the inversion results using IRS and JRM, when we have severely subsampled data (1% data) and when the data is less subsampled (5% data). The signal-to-noise ratio (SNR) of our results were also computed, since we know the true time-lapse signal. The percentage subsampling we have considered is permissible since we are in an idealized setting, and they do illustrate the potential uplift of what happens when the wave propagation effects are completely accounted for or when the physics is right.

The top row of Figure 5.4 shows the estimated difference time-lapse stacked sections when the acquired data is just 1% of the idealized densely sampled pre-stack data. In comparison with the ideal stacked sections, we notice a poor match using the IRS (SNR = 0.27dB) and good recovery using the JRM (SNR = 6.28dB). The artifacts observed in the difference stacked sections using the IRS poses a significant problem for interpreters especially when the time-lapse signal is very weak. Such a weak signal will be lost in field data having considerable amount of non-repeatable noise. We have modeled a strong time-lapse signal, so we can still delineate signals from artifacts. We also note that the joint recovery approach benefits more in recovering the 4D difference than the independent recovery strategy.

The next experiment is an inversion for the time-lapse stacked sections using randomly selected 5% of the shots from the densely sampled data, again without repetition. In line with our observation from using 1% of the data, we noticed a significant increase (5.03dB for IRS and 8.36dB for JRM) in the SNR levels of the estimated stacked sections. Consequently, the artifacts level in the difference section is reduced and the resolution of the recovered time-lapse signal is increased as shown in the bottom row of Figure 5.4. In both subsampling cases, the joint recovery method performs significantly better than the independent recovery method because it exploits the shared information between the observed time-lapse data.

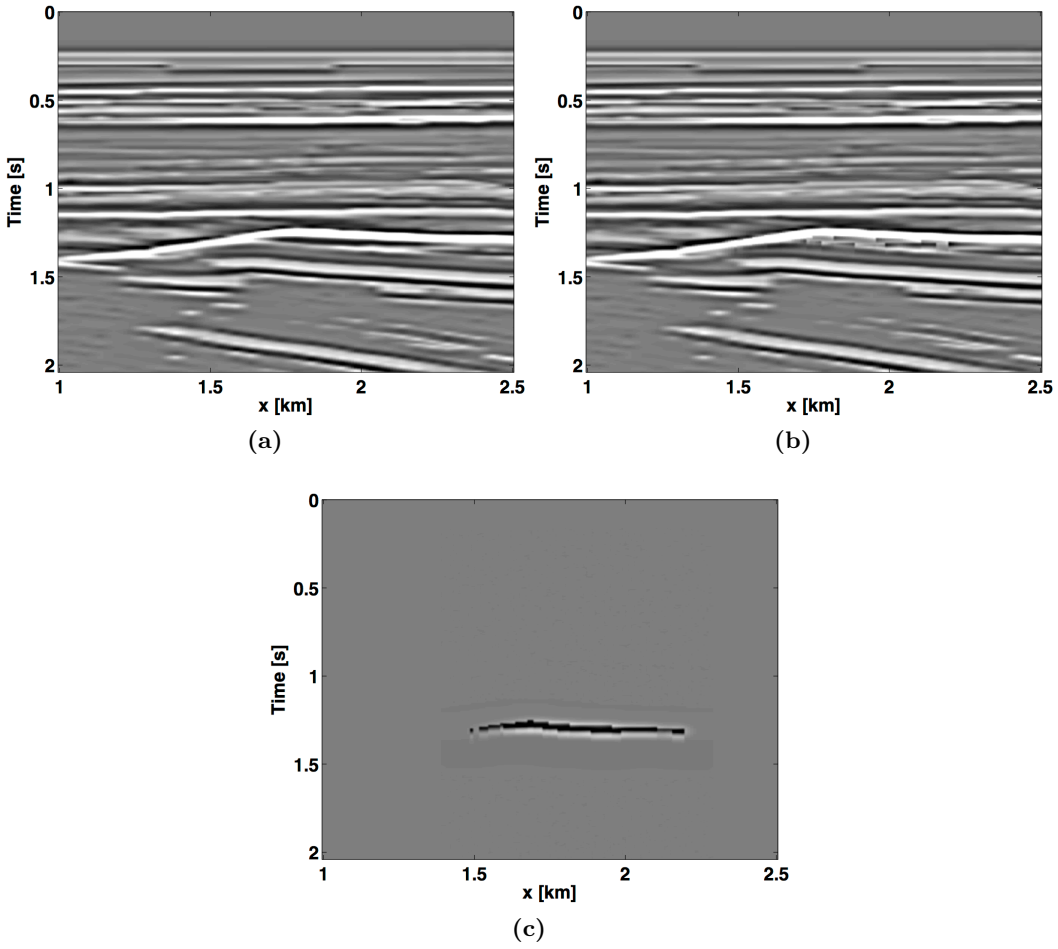

Figure 5.3 Stacked sections of the densely sampled time-lapse data with repetition. (a) baseline, (b) monitor, (c) 4D difference between baseline and monitor.

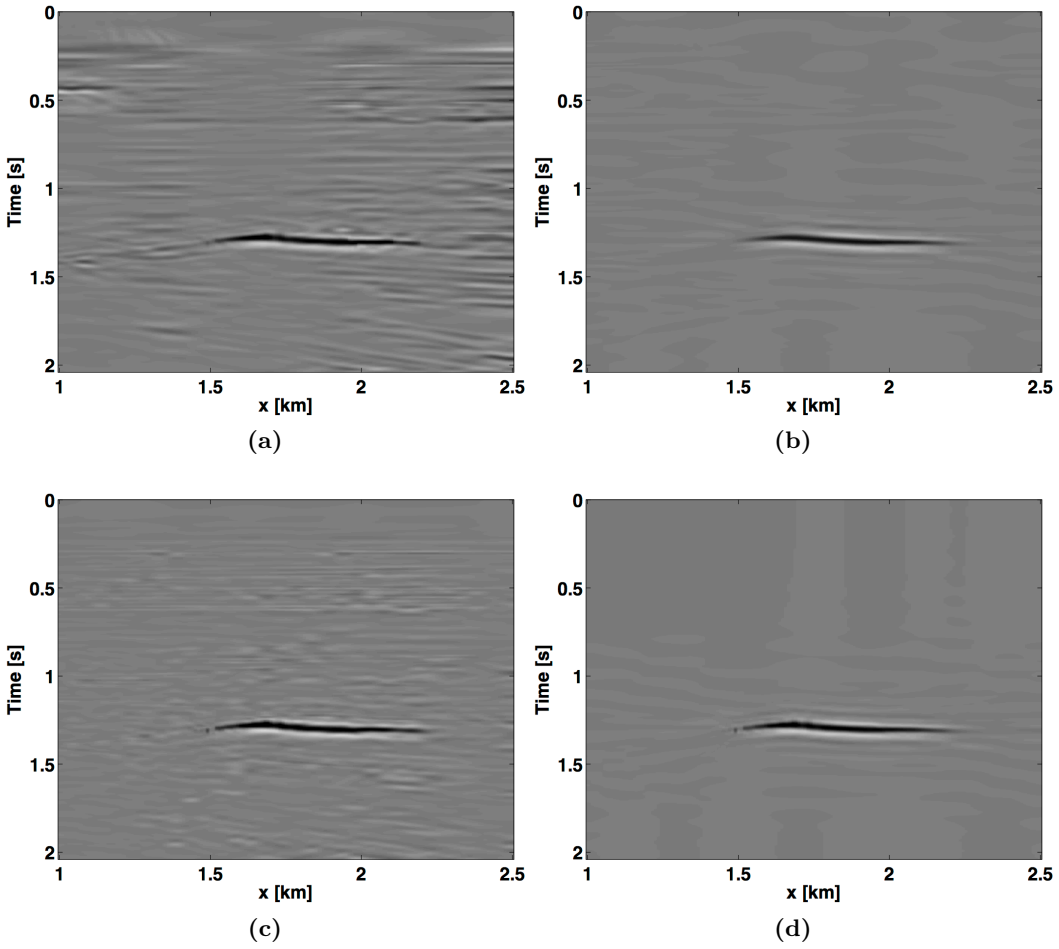

Figure 5.4 4D difference stacked sections from randomly sampled time-lapse data without repetition (top row) using 1% of fully sampled data , (bottom row) 5% of fully sampled data. (a,c) using independent recovery approach, (b,d) using joint recovery method. Note the poor recovery quality using the independent recovery approach which does not account for the shared information between the two datasets.

5.1.5 Discussion and Conclusions

The synthetic study is idealistic in that it uses the same forward modeling operator in the inversion scheme. This is necessary for the inversion to be stable, as we require our data to be in the range of the modeling operator. In other words, it is very crucial to account for the physics of the wave propagation in the forward modeling operator. We have also worked with noiseless synthetic data, although we do not expect a poor performace of our methods in such case. Despite our study being idealistic, it is proof of concept of a potential formulation for analysis of 4D signals in the image domain where we have randomized and subsampled measurements

from a baseline survey and monitor survey. We have investigated the performance of the recovery algorithms as a function of subsampling ratio and have studied the results for few subsampling ratios . We applied the independent recovery approach and the joint recovery method, and recovered the stacked sections as well as the 4D stacked sections. We observed that extension of our algorithm to recovery of time-lapse stacked section is not as computationally expensive as its application to the recovery of the densely sampled wavefields. In addition, this formulation is not limited to analysis of just two vintages of time-lapse data. It can be applied to multiple time-lapse data which have been acquired with different source/receivers missing.

In conclusion, we have presented an extension of our randomized sampling strategy for time-lapse data acquisition, to estimation of stacked sections. We show that imaging of time-lapse data and stacking are two related phenomena and both follow the same inversion procedure. We present 2D inversion results for a synthetic model illustrating the feasibility of randomized sampling for time-lapse studies, and the results demonstrate the usefulness of the joint recovery method for extracting 4D signals from significantly subsampled time-lapse data. We claim that time-lapse data acquired without repetition, can be processed to obtain stacked sections which reveal high-fidelity 4D difference provided we carry out a sparsity-promoting inversion program. In addition, we distinguish between two recovery algorithms that can both handle the measured data while delineating between the efficiency of the methods when the data are severely and less subsampled. The next step in our study is to extend this methodology to realistic wave equation based inversion of seismic data from time-lapse surveys without repetition, and produce migrated images in depth.

5.2 Using common information in compressive time-lapse full-waveform inversion

5.2.1 Summary

The use of time-lapse seismic data to monitor changes in the subsurface has become standard practice in industry. In addition, full-waveform inversion has also been extended to time-lapse seismic to obtain useful time-lapse information. The computational cost of this method are becoming more pronounced as the volume of data increases. Therefore, it is necessary to develop fast inversion algorithms that can also give improved time-lapse results. Rather than following existing joint inversion algorithms, we are motivated by a joint recovery model which exploits the common information among the baseline and monitor data. We propose a joint inversion framework, leveraging ideas from distributed compressive sensing and the modified Gauss-Newton method for full-waveform inversion, by using the shared information in the time-lapse data. Our results on a realistic synthetic example highlight the benefits of our joint inversion approach over a parallel inversion method that does not exploit the shared information. Preliminary results also indicate that our formulation can address time-lapse data with inconsistent acquisition geometries.

5.2.2 Introduction

Full-waveform inversion (FWI) is a nonlinear problem that finds the model parameters that characterize the earth from measured seismic data (Virieux and Operto, 2009). Time-lapse seismic data can be used to provide information about changes in the subsurface over a period of time (Lumley, 2001). As an example, full-waveform inversion of time-lapse seismic data has been applied to storage and monitoring of CO_2 (Queißer and Singh, 2013). While there have been a few attempts to apply FWI to time-lapse seismic data (Raknes et al., 2013; Asnaashari et al., 2014; Maharramov and Biondi, 2014; Yang et al., 2014), some of the challenges of processing time-lapse data still persist. Issues such as differences in geometry, weak 4-D signals below the level of inversion or migration artifacts pose a challenge to the inversion algorithms (Lumley et al., 1997).

To address some of the challenges of processing time-lapse data, a few inversion methods (Denli and Huang, 2009; Shragge and Lumley, 2013; Yang et al., 2014; Maharramov and Biondi, 2014; Yang et al., 2015; Maharramov et al., 2016) have been proposed. One common idea in these methods is to use a prior information in the baseline inversion for the monitor inversion (see e.g. (Asnaashari et al., 2014)). Another approach is a joint or simultaneous inversion of the baseline and monitor data (see e.g. (Yang et al., 2015); (Maharramov et al., 2016); (Kamei and Lumley, 2017)). Both strategies are used in order to extract better time-lapse difference models that are obtained by subtracting the baseline and monitor inversion results. A common approach in these methods is to use the common information between the

time-lapse vintages in different ways. In this work, we propose a novel joint inversion algorithm where we exploit the shared information between the baseline and monitor data explicitly in an alternative way from previous approaches. Leveraging ideas from distributed compressed sensing (Baron et al., 2009b), and stochastic optimization, we present an inversion framework that is fast, and gives a better time-lapse difference model compared to a similar independent or parallel inversion approach that doesn't exploit the shared information in the data. Our algorithm combines our earlier work on joint recovery from subsampled time-lapse data (Oghenekohwo et al., 2014a; Wason et al., 2014) and the modified Gauss-Newton inversion strategy proposed by (Li et al., 2012b). The efficacy of our proposed method is demonstrated on a realistic synthetic velocity model, which shows the imprint of a gas cloud in the time-lapse difference model.

5.2.3 Methodology

To arrive at an inversion formulation for time-lapse seismic data, we describe FWI on baseline ($j = 1$) and monitor ($j = 2$) data as the solution to the following problem:

$$\tilde{\mathbf{m}}_j = \underset{\mathbf{m}_j}{\operatorname{argmin}} \|\mathbf{d}_j - \mathcal{F}(\mathbf{m}_j)\|_2^2 \qquad \text{for} \quad j = \{1, 2\}, \tag{5.3}$$

where $\mathcal{F}$ represents the operator generating synthetic data from time-lapse model parameters $\mathbf{m}$, and $\mathbf{d}$ is the measured field data. In this formulation, $\tilde{\mathbf{m}}_1$ and $\tilde{\mathbf{m}}_2$ represent the final inversion results of the baseline and monitor, respectively. Constrained Gauss-Newton (GN) subproblems involve the pseudo-inverse of the reduced Hessian, computed from the Jacobian operator $\nabla\mathcal{F}(\mathbf{m}^k)$. The subproblems can be used to set up a GN update ($\delta\mathbf{m}^k$) for FWI at the $k-$th iteration. For time-lapse inversion, this translates to updates of the models via the following step:

$$\mathbf{m}_j^{k+1} = \mathbf{m}_j^k + \delta\mathbf{m}_j^k. \tag{5.4}$$

(Li et al., 2012b)] showed that the GN updates are sparse,-i.e. $\delta\mathbf{m}_j = \mathbf{S}^H\mathbf{x}_j$; where $\mathbf{S}^H$ is the conjugate transpose of a sparsifying transform $\mathbf{S}$ and $\mathbf{x}_j$ is a vector of transform coefficients. By linearizing the objective function of Equation 5.3 and promoting sparsity of the GN updates, the time-lapse FWI problem in Equation 5.3 becomes:

$$\tilde{\mathbf{x}}_j^k = \underset{\mathbf{x}_j}{\operatorname{argmin}} \frac{1}{2}\|\mathbf{d}_j^k - \mathcal{F}(\mathbf{m}_j^k) - \nabla\mathcal{F}(\mathbf{m}_j^k)\mathbf{S}^H\mathbf{x}_j\|_2^2 \quad \text{subject to } \|\mathbf{x}_j\|_1 < \tau_j^k \quad \text{for} \quad j = \{1, 2\}. \tag{5.5}$$

To choose τ_j^k, we follow the modified Gauss-Newton(mGN) strategy by (Li et al., 2012b). In fact, Equation 5.5 gives parallel inversion results for the baseline and monitor data. Naively inverting for the baseline model and monitor model independently does not account for the shared information in the data. In our recent work (Oghenekohwo et al., 2014a) on time-lapse seismic data recovery from subsampled data, we presented a joint recovery method (JRM) that exploits the shared

information in the time-lapse vintages. Our method recovered time-lapse vintages and differences that are better than the estimates from parallel or independent processing. Incidentally, the mGN updates in Equation 5.5 look very much like the problems we solve using the JRM. Therefore, this motivates the extension of the JRM to inversion of time-lapse seismic data.

5.2.4 Inversion with JRM

We consider two signals $\mathbf{x}_1$ and $\mathbf{x}_2$ representing the mGN updates for baseline and monitor inversion, respectively. These signals share a common component $\mathbf{z}_0$ while each individual signal has an innovation component $\mathbf{z}_j$. Therefore, each signal can be written as

$$\mathbf{x}_j = \mathbf{z}_0 + \mathbf{z}_j, \qquad j \in 1, 2. \tag{5.6}$$

Using this model, we define for the $k-$th iteration of mGN for time-lapse FWI

$$\mathbf{b}^k = \begin{bmatrix} \mathbf{d}_1^k - \mathcal{F}(\mathbf{m}_1^k) \\ \mathbf{d}_2^k - \mathcal{F}(\mathbf{m}_2^k) \end{bmatrix}, \quad \mathbf{A}^k = \begin{bmatrix} \nabla\mathcal{F}(\mathbf{m}_1^k)\mathbf{S}^H & \nabla\mathcal{F}(\mathbf{m}_1^k)\mathbf{S}^H & \mathbf{0} \\ \nabla\mathcal{F}(\mathbf{m}_2^k)\mathbf{S}^H & \mathbf{0} & \nabla\mathcal{F}(\mathbf{m}_2^k)\mathbf{S}^H \end{bmatrix}, \mathbf{z}^k = \begin{bmatrix} \mathbf{z}_0^k \\ \mathbf{z}_1^k \\ \mathbf{z}_2^k \end{bmatrix}.$$

Contrary to the independent approach, which solves separate inversion problems for the vintages, without exploiting their correlations, the JRM exploits these correlations by solving one GN problem at the $k-$th iteration:

$$\tilde{\mathbf{z}}^k = \underset{\mathbf{z}^k}{\operatorname{argmin}} \frac{1}{2}\|\mathbf{b}^k - \mathbf{A}^k\mathbf{z}^k\|_F^2 \quad \text{subject to } \|\mathbf{z}^k\|_1 < \tau^k. \tag{5.7}$$

Equation 5.7 summarizes our proposed joint inversion scheme using the MGN algorithm. As stated previously, we refer to (Li et al., 2012b) regarding the selection of τ^k. The model updates from the above optimization problem for the baseline and monitor models are

$$\mathbf{m}_j^{k+1} = \mathbf{m}_j^k + \mathbf{S}^H(\tilde{\mathbf{z}}_0^k + \tilde{\mathbf{z}}_j^k). \tag{5.8}$$

In the next section, we illustrate the performance of this method by means of a synthetic example that characterize realistic time-lapse scenarios.

5.2.5 BG Compass time-lapse model

We study our formulation by means of synthetic experiments on the BG Compass time-lapse velocity model (Figure 5.5), showing the baseline, and the time-lapse difference anomaly obtained by subtracting the baseline and monitor (not shown). All the inversion results were obtained using a good initial model and the same starting model was used for the baseline and monitor inversion. All synthetic data are generated using a finite-difference acoustic modeling engine based on the constant density acoustic wave equation in the frequency domain. The range of velocities in

the baseline and monitor models is between 1480m/s and 4500m/s (Figure 5.5a), while the time-lapse difference is plotted on a color scale of -100m/s to 150m/s. The inversion results are also displayed using the same color scale.

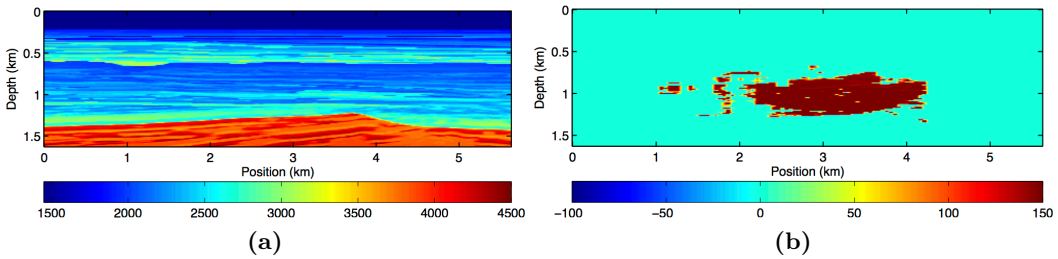

Figure 5.5 Time-lapse models (a) baseline (b) time-lapse difference.

Using a Ricker wavelet with central frequency of 12Hz, 226 receivers sampled at 25m interval, and 112 shots sampled at 50m interval, a dense baseline data was generated. Two sets of dense monitor data were generated with similar receiver geometry. However, in the first set, the source acquisition geometry was exactly the same for the baseline but in the second set, same number of sequential shots were acquired by shifting the original source locations by 12.5m. This second monitor acquisition serves as a proxy for time-lapse data acquisition with non-repeated or inconsistent acquisition geometry.

The inversion procedure is based on a rerandomization procedure which entails the use of simultaneous shots as part of each mGN subproblem. The rerandomization corresponds to giving the sequentially sampled shots a different set of random weights at every step of the inversion. Details of this technique have been published by (Li et al., 2012b) and it's beyond the scope of this work. The main idea is to use only a subset of the total data during every step of the inversion. This approach has been shown to reduce the computational cost required for the inversion and this efficiency motivates the adaptation of the method to our experiments on time-lapse FWI. Using simultaneous shots from the baseline and monitor data, we perform the independent or parallel inversion (Equation 5.5) and compare the results with the inversion with JRM (Equation 5.7).

5.2.6 Experiments

We conduct four experiments spanning the range of possible acquisition and processing scenario, namely, *(i)* Repeat acquisition and processing, *(ii)* Repeat acquisition with different processing, *(iii)* Different acquisition but same processing, *(iv)* Different acquisition with different processing. In these experiments, repeated processing means we are using the same random weights to generate the simultaneous shots. In all cases, we compare parallel inversion with joint inversion using JRM. We find, judging from the signal-to-noise ratio (SNR), that the third scenario gave the best

time-lapse inversion results for the parallel (SNR = 4.4dB) and joint (SNR = 6.0dB) methods. Figure 5.6 shows the inversion results for the monitor and time-lapse signal in this scenario–i.e. different acquisition and same processing. In addition, we observe the results of inversion with JRM to be better than the parallel inversion in all the scenarios.

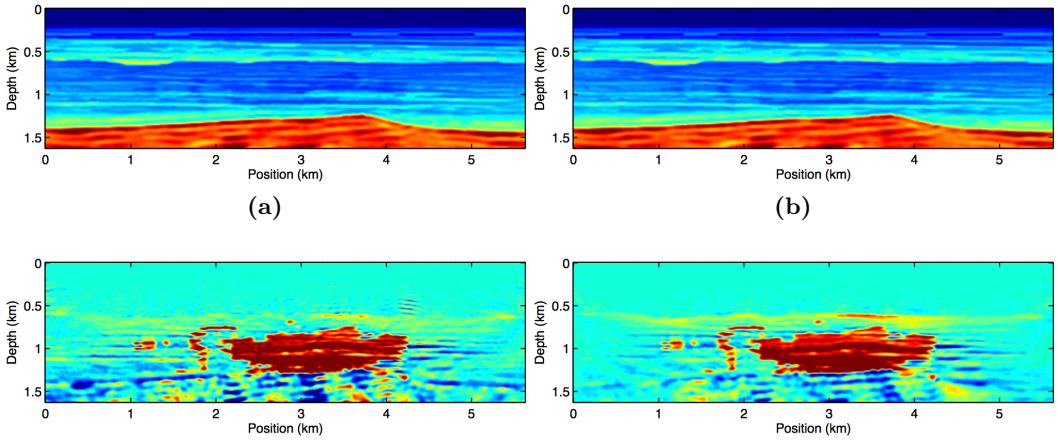

Figure 5.6 Monitor inversion results using (a) Parallel method (b) Joint method. Time-lapse inversion results using (c) Parallel method (d) Joint method. Notice the attenuation of the artifacts with the joint inversion compared to the parallel inversion.

5.2.7 Discussion

The results we have shown indicate the benefits of our joint inversion algorithm over the independent or parallel inversion method. In both methods, we used a starting model close to the true baseline model in order to mitigate some common FWI problems such as local minima. We also used a common source signature for both inversions to reduce any repeatability effects in the data arising from different source functions. Although we expect our method to be able to address such effects in the data, that will be a subject of future research. Both the independent and joint FWI approaches were able to detect the time-lapse anomaly. However, we see less artifacts in the latter method (Figure 5.6d) compared to the former (Figure 5.6c). This improvement is due to the shared information between the baseline and monitor data, which the joint inversion method exploits but the independent inversion doesn't. We also expect our observations to remain consistent in cases where the observed data is noisy since our method is able to handle non-sparse changes. Preliminary findings from our experiments further indicate that our joint inversion method is robust when time-lapse data is acquired with similar or different geometries. This further distinguishes our method from other inversion approaches that are based on a data difference idea, where the sources and receivers location must be exactly the

same between the time-lapse surveys. More detailed comparison to other existing time-lapse inversion approaches will be the subject of future research.

5.2.8 Conclusions

We have presented a joint full-waveform inversion technique which is based on using the shared information between the baseline and monitor data. By using compressively sampled shots to speed up the inversion procedure, we find that our technique can significantly reduce time-lapse artifacts that mask true time-lapse signals. In addition, we have shown that our method is better than an independent inversion approach since it detects the true time-lapse anomaly while removing any unwanted artifacts.

Chapter 6

Conclusions

Time-lapse seismic has been used for more than a decade to monitor subsurface reservoir changes. However, its reliance on repeated surveys and dedicated processing algorithms makes it a technically challenging practice. In addition, requirements for dense sampling of time-lapse wavefields makes it prohibitively expensive to execute. Randomized surveys based on compressive sensing ideas demonstrate an order of acquisition cost reduction and thereby creates an avenue to address some current challenges faced with time-lapse seismic acquisition. By performing experiments that investigates the feasibility of conducting randomized time-lapse surveys in the field, we confirm that the challenging strict requirement to replicate time-lapse surveys can be relaxed. Our findings stem from leveraging ideas from the field of distributed compressive sensing (DCS) and a joint recovery model (JRM) that allows us access to high-fidelity time-lapse data volumes recovered from surveys acquired with randomized sampling techniques, which are based on ideas from compressive sensing. The main conclusions of this thesis are summarized below in three broad categories.

6.1 Relax randomized time-lapse survey replication

Time-lapse survey replication entails making the baseline and monitor(s) survey geometries as similar as possible. The current practice requires dense sampling of sources/receivers and strict survey replication to maximize repeatability, which is a term that describes the similarity of time-lapse vintages. Since surveys based on randomized subsampling have been shown to be economical, we investigate the implications of such surveys — and the consequences of not replicating the surveys — for time-lapse studies particularly with regards to attainable degrees of repeatability measured in terms of normalized root mean square (NRMS). To this end, we considered the situation of recovering time-lapse data from randomly subsam-

pled surveys wherein the shot locations differ amongst the baseline and monitor surveys but with control on actual source/receiver positions post plot (to some accuracy). By ignoring factors such as tidal differences, we found that it is better not to replicate the shot locations amongst the surveys when recovery of the vintages is paramount. This observation is a direct consequence of introducing a common component, which contains information shared amongst the vintages, as part of our proposed joint recovery model.

To our knowledge, we are the first to address time-lapse seismic problems in which the common component amongst vintages—and "innovations" with respect to this shared component—is made explicit. In other words, we are the first to categorize time-lapse differences as "innovations" and to use the JRM to exploit this, thereby distinguishing our formulation from other approaches that equally use the common information in time-lapse vintages. Because we do not replicate the randomly subsampled time-lapse surveys, yet obtain high-quality vintages with our JRM, our findings suggests that the current practice necessitating strict replication of dense time-lapse surveys may be relaxed when conducting randomized time-lapse acquisitions.

We compare recovery results obtained with the JRM to results obtained from independently processing the vintages, and demonstrate that the former approach significantly outperforms the latter in terms of recovery quality of vintages and data repeatability. Our findings remain consistent both for experiments where our observed data are recorded on a discrete grid (Chapter 2), and in the more practical scenario where our data do not lie on the grid (Chapter 3) but where the post plot shot positions are known. In both cases, we assert that the high-fidelity of the recovered vintages makes them credible candidates for algorithms or processes that extract poststack time-lapse attributes, from which subsurface reservoir changes can be deduced. These findings coupled with recent field implementation of actual compressive sensing type surveys (Mosher et al., 2014) in both land and marine, suggest that we can translate empirical simulation studies regarding sampling efficiency to real field efficiency.

6.2 Repeatability in presence of calibration errors

Conventional processing of seismic data relies on having access to accurate information about the acquisition parameters including shot firing times and spatial positions of both sources and receivers. Unfortunately, recorded postplots may differ from actual field measurements, which can cause problems when ignored in seismic processing. This reliance on accurate information is also critical to successful recovery of signals acquired with compressive sensing—i.e., CS relies on accurate operators. For time-lapse seismic, these deviations between actual and postplot positions, hereafter referred to as calibration errors, can have detrimental effects on the quality and repeatability of vintages, if unaccounted for during processing. Therefore we investigate the sensitivity of these errors during regularization of conventional dense

surveys. We also examine the impact of these calibration errors on low cost surveys acquired with compressive sensing and recovered by independently processing the observed subsampled data. We juxtapose the results with vintages recovered with our JRM and evaluate how the JRM behaves as a function of increasing calibration errors.

In Chapter 4, we demonstrate that high quality and highly repeatable vintages and time-lapse data are possible for an ocean bottom survey in the presence of source position errors that are of order of $20 - 25\%$ of the interpolated shot sample interval. This result holds both for randomly subsampled (or compressively sampled) surveys recovered with our proposed JRM and for conventional densely sampled surveys albeit at a high cost. However, as soon as the errors are 25% or more, the repeatability deteriorates and is even worse than the NRMS value for the data recovered from compressively sampled surveys with the JRM. We processed the densely sampled surveys conventionally, by taking the pseudo inverse of the regularization operator, and show that repeatability degrades quite rapidly in the presence of even relatively small (10% of the shot sample interval) calibration errors. In contrast, we observe a modest decay in repeatability as calibration errors increase, for vintages acquired with our low-cost randomized surveys and processed with our joint recovery model. The performance of the joint recovery model for acquisitions with unknown calibration errors is remarkable and can be explained by the fact that our approach leverages information that is common amongst the vintages explicitly. We established these results in the case where the subsurface remains unchanged but the randomized surveys and calibration errors differ, and in the realistic scenario where time-lapse changes are confined to subsets of the data. Our findings support our previous claims that economic time-lapse surveys based on randomized sampling and compressive sensing are ready to be implemented in the field.

6.3 Relevance for randomized time-lapse seismic imaging

To understand the benefits of randomized sampling coupled with the joint recovery model in time-lapse seismic imaging, we investigate a direct extension of the JRM to two problems related to 4D seismic imaging of prestack wavefields. First, we consider an idealized experiment involving stacking of randomly subsampled prestack time-lapse data, by incorporating a normal move out (NMO) and summation operator in the forward model. We cast recovery of the time-lapse stacked sections as a linear inverse problem. Using the joint recovery model in the inversion, we obtain high-quality stacked sections and differences from significantly few non-replicated randomly subsampled baseline and monitor measurements. The stacked sections obtained via independent inversions, however, are not as good as the former (especially for higher subsampling ratios). The findings from this study is proof of concept of an immediate extension of our methodology to wave-equation based lin-

earized inversions such as sparsity-promoting imaging (Herrmann and Li, 2012; Tu and Herrmann, 2015).

In the second part, we consider the problem of time-lapse full-waveform inversion (FWI). Because this study only explores the inherent benefits of extending our joint recovery model to time-lapse FWI, we consider situations and examples that ignore some challenges to FWI. For instance, we use a good initial model in order to mitigate problems such as cycle skipping, and we assume knowledge of the common source wavelets for the time-lapse surveys. We demonstrate that independent inversions of time-lapse vintages obtained from non-replicated surveys are not as good as inversions performed using our joint recovery model. We observe improved repeatability in the inverted models using our joint recovery model and clear delineation of the true time-lapse changes after subtracting the baseline and monitor inverted models. Independent inversions create artifacts in the time-lapse model difference between the baseline and monitor while inversion with JRM attenuates these artifacts. This suggests that we can minimize the risk of construing false time-lapse changes as actual subsurface changes by performing inversions that adapt the joint recovery model. Furthermore, we show that the quality of our inversion results obtained with the JRM do not degrade for data acquired with different survey geometries. This finding sets our method apart from other inversion approaches (e.g. double difference) that relies on exact replication of the time-lapse survey geometries.

As with our conclusions on recovery of prestack time-lapse vintages in the previous sections, the key to our results on time-lapse seismic is in exploiting the common information shared amongst time-lapse vintages and images. Finally, we note that our methodology is not limited to analysis of just two vintages of time-lapse data. According to the theory of DCS, we expect the quality of the vintages and images to improve further as multiple time-lapse measurements are collected.

6.4 Limitations

Some limitations of the work presented in this thesis are as follows :

1. We show the feasibility of our methodology on 2-D time-lapse seismic with fixed receiver configurations, where replication on the receiver side is fairly accurate; however, we do not expect major drawbacks when our methodology is applied to 2-D or 3-D surveys with towed arrays. Initial findings recently reported in an article titled "Highly repeatable 3D compressive full-azimuth towed-streamer time-lapse acquisition — a numerical feasibility study at scale," by Rajiv Kumar, Haneet Wason, Shashin Sharan, and Felix J. Herrmann, confirm our expectation of a large scale 3D implementation of our methodology. In addition, findings by Mosher et al. (2014)'s makes us confident in a straightforward extension of our approach to real field 3-D surveys, perhaps with a bit of tuning.

2. Theoretical validations for solving problems with the joint recovery model requires a numerical search for the most preferred weights $(\gamma_0, \gamma_1, \gamma_2)$ for each of the components — common $(\mathbf{z}_0)$ and innovations $(\mathbf{z}_1, \mathbf{z}_2)$— followed by a *$\gamma$-weighted ℓ_1-norm minimization* (DCS, Baron et al. (2009a)):

$$\widetilde{\mathbf{z}} = \underset{\mathbf{z}}{\operatorname{argmin}}\, \gamma_0||\mathbf{z_0}||_1 + \gamma_1||\mathbf{z_1}||_1 + \gamma_2||\mathbf{z_2}||_1 \quad \text{subject to} \quad \mathbf{y} = \mathbf{Az}.$$

In our work that is void of any analysis of the weights, without loss of generality, we choose $\gamma_0 = \gamma_1 = \gamma_2 = 1$, which may be not be the most preferred weights for seismic applications. Theoretical analysis of a weighted ℓ_1-norm minimization by Li (2015) provide conditions for stable and robust recovery of signals in the DCS framework using the joint recovery model.

3. An essential aspect of seismic acquisition is the impact of various types of noise on seismic data. Differences in the noise generated from baseline and monitor surveys can have detrimental effects on repeatability. So far, we have ignored ambient noise, swell noise etc. that can impact repeatability. However, we are optimistic about the stability of our recovery since theoretical analysis on CS provides stable recovery with respect to noise (Candes et al., 2006). In addition, because we showed robust recovery in presence of unknown calibration errors that behave like noise, we are confident that our method will be suitable for noisy data.

4. From a computational perspective, because of the ambient dimension of the vector $(\mathbf{z})$ recovered using the joint recovery model, we would typically require more iterations during the sparse recovery step compared to an independent recovery approach. However, in this work, we have kept the iterations fixed when comparing both recovery strategies. This is also linked to the second point regarding weights of the common part and innovations; the magnitude of the common part is up to ten times (or more) greater than the innovations.

6.5 Future work

Some considerations for future work are as follows:

1. Examine the results of asymmetric randomized sampling whereby we acquire more for the baseline and less for the monitor and vice-versa. According to Baron et al. (2009a), there is a direct relation between the requisite number of measurements (measurement rates) for each survey and recovery probability with the joint recovery model. Therefore, studying asymmetric sampling is important especially when planning a time-lapse acquisition project that requires at least two monitor surveys. So, it may be necessary to allocate an "optimal" acquisition budget to a specific survey.

2. Verify any opportunities or benefits of implementing the actual γ-*weighted* ℓ_1-*norm minimization* strategy described in the previous section, for seismic problems. As suggested by Li (2015), the weighted ℓ_1-norm minimization approach can potentially lead to higher-quality time-lapse signals and vintages with improved repeatability.

3. Another important factor that affects repeatability is overburden complexity (Misaghi et al., 2007), especially when analyses is carried out on the time-lapse images. In this work, we have restricted our studies to a geological setting with relatively simple overburden. It will be worthwhile to investigate how our results could be impacted when these surveys are conducted in an area with complex overburden such as a salt dome. The sensitivity of our joint recovery model to unknown calibration errors in this setting is also worth looking into.

4. Prestack time-lapse wavefield recovery is incomplete without accounting for time-shifts between the vintages. These time-shifts may arise as a result of differences in the source wavelet between surveys or variations in the processing algorithms applied to the data. In this work, we have ignored such differences. Therefore, it would be worthwhile to examine how this problem can be modeled mathematically and integrated in the existing framework.

5. The imaging work presented in Chapter 5 of this thesis is by no means extensive, and can be considered as "testing the waters" for the potential application of the joint recovery model to wave-equation based inversion of time-lapse seismic data. An array of extensions abound in this direction including directly imaging compressively sampled data to delineate subtle time-lapse changes below complex overburdens. Other related ideas (Ayeni and Biondi, 2010; Qu and Verschuur, 2016) demonstrate the benefits of joint inversion for imaging time-lapse data but none of these methods makes the common part explicit in their approach as we do.

Bibliography

Abma, R., A. Ford, N. Rose-Innes, H. Mannaerts-Drew, and J. Kommedal, 2013, Continued development of simultaneous source acquisition for ocean bottom surveys: Presented at the 75th EAGE Conference and Exhibition. → pages 5, 42

Asnaashari, A., R. Brossier, S. Garambois, F. Audebert, P. Thore, and J. Virieux, 2014, Time-lapse seismic imaging using regularized full-waveform inversion with a prior model: which strategy?: Geophysical Prospecting. → pages 96

———, 2015, Time-lapse seismic imaging using regularized full-waveform inversion with a prior model: which strategy?: Geophysical Prospecting, **63**, 78–98. → pages 16, 40

Ayeni, G., and B. Biondi, 2010, Target-oriented joint least-squares migration/inversion of time-lapse seismic data sets: Geophysics. → pages 107

Ayeni, G., Y. Tang, B. Biondi, et al., 2009, Joint preconditioned least-squares inversion of simultaneous source time-lapse seismic data sets: Presented at the 2009 SEG Annual Meeting, Society of Exploration Geophysicists. → pages 88

Baron, D., M. F. Duarte, S. Sarvotham, M. B. Wakin, and R. G. Baraniuk, 2005, An information-theoretic approach to distributed compressed sensing: Presented at the Proc. 45rd Conference on Communication, Control, and Computing. → pages 90

Baron, D., M. F. Duarte, M. B. Wakin, S. Sarvotham, and R. G. Baraniuk, 2009a, Distributed compressive sensing: CoRR, **abs/0901.3403**. → pages 9, 15, 18, 39, 106

———, 2009b, Distributed compressive sensing: CoRR, **abs/0901.3403**. → pages 75, 97

Beasley, C. J., 2008, A new look at marine simultaneous sources: The Leading Edge, **27**, 914–917. → pages 5, 42

Beasley, C. J., R. E. Chambers, and Z. Jiang, 1998, A new look at simultaneous sources: SEG Technical Program Expanded Abstracts, **17**, 133–135. → pages 5

Beasley, C. J., R. E. Chambers, R. L. Workman, K. L. Craft, and L. J. Meister, 1997, Repeatability of 3-d ocean-bottom cable seismic surveys: The Leading Edge, **16**, 1281–1286. → pages 5, 15

Berkhout, A. J., 2008, Changing the mindset in seismic data acquisition: The Leading Edge, **27**, 924–938. → pages 5, 42, 60

Beyreuther, M., J. Cristall, and F. J. Herrmann, 2005, Computation of time-lapse differences with 3-D directional frames: SEG Technical Program Expanded

Abstracts, 2488–2491. → pages 15, 72
Brown, G., and J. Paulsen, 2011, Improved marine 4d repeatability using an automated vessel, source and receiver positioning system: first break, **29**, 49–58. → pages 5, 15, 75, 88
Candes, E., L. Demanet, D. Donoho, and L. Ying, 2006, Fast discrete curvelet transforms: Multiscale Modeling & Simulation, **5**, 861–899. → pages 8
Candès, E. J., L. Demanet, D. Donoho, and L. Ying, 2006, Fast discrete curvelet transforms: Multiscale Modeling & Simulation, **5**, 861–899. → pages 56
Candès, E. J., J. Romberg, and T. Tao, 2006, Robust uncertainty principles: Exact signal reconstruction from highly incomplete frequency information: IEEE Transactions on information theory, **52**, 489–509. → pages 76
———, 2006, Stable signal recovery from incomplete and inaccurate measurements: Communications on Pure and Applied Mathematics, **59**, 1207–1223. → pages 42, 50, 72
Candes, E. J., J. K. Romberg, and T. Tao, 2006, Stable signal recovery from incomplete and inaccurate measurements: Communications on pure and applied mathematics, **59**, 1207–1223. → pages 39, 106
Candes, E. J., and T. Tao, 2006, Near-optimal signal recovery from random projections: Universal encoding strategies: Information Theory, IEEE Transactions on, **52**, 5406–5425. → pages 4, 6, 15, 17
Candès, E. J., and M. B. Wakin, 2008, An introduction to compressive sampling: Signal Processing Magazine, IEEE, **25**, 21–30. → pages 17
Chadwick, A., G. Williams, N. Delepine, V. Clochard, K. Labat, S. Sturton, M.-L. Buddensiek, M. Dillen, M. Nickel, A. L. Lima, et al., 2010, Quantitative analysis of time-lapse seismic monitoring data at the sleipner co 2 storage operation: The Leading Edge, **29**, 170–177. → pages 1
Day, A., M. Widmaier, T. Høy, and B. Osnes, 2010, Time-lapse acquisition with a dual-sensor streamer over a conventional baseline survey: Presented at the 72nd EAGE Conference and Exhibition incorporating SPE EUROPEC 2010. → pages 5
de Kok, R., and D. Gillespie, 2002, A universal simultaneous shooting technique: Presented at the 64th EAGE Conference and Exhibition. → pages 5, 42
Demanet, L., and L. Ying, 2007, Wave atoms and sparsity of oscillatory patterns: Applied and Computational Harmonic Analysis, **23**, 368–387. → pages 8
Denli, H., and L. Huang, 2009, Double-difference elastic waveform tomography in the time domain, *in* SEG Technical Program Expanded Abstracts 2009: Society of Exploration Geophysicists, 2302–2306. → pages 96
Donoho, D. L., 2006, Compressed sensing: Information Theory, IEEE Transactions on, **52**, 1289–1306. → pages 4, 6, 15, 17, 42, 50, 76
Eggenberger, K., P. Christie, D.-J. van Manen, and M. Vassallo, 2014, Multisensor streamer recording and its implications for time-lapse seismic and repeatability: The Leading Edge, **33**, 150–162. → pages 5, 15, 75, 88
Eiken, O., G. U. Haugen, M. Schonewille, and A. Duijndam, 2003, A proven method for acquiring highly repeatable towed streamer seismic data: Geophysics, **68**, 1303–1309. → pages 5, 15, 75, 88

Fanchi, J. R., 2001, Time-lapse seismic monitoring in reservoir management: The Leading Edge, **20**, 1140–1147. → pages 1, 15

Hampson, G., J. Stefani, and F. Herkenhoff, 2008a, Acquisition using simultaneous sources: The Leading Edge, **27**, 918–923. → pages 5

———, 2008b, Acquisition using simultaneous sources: The Leading Edge, **27**, 918–923. → pages 42

Harris, P., and D. Veritas, 2005, Prestack repeatability of time-lapse seismic data: SEG Technical Program Expanded Abstracts, 2410–2413. → pages 80

Hennenfent, G., L. Fenelon, and F. J. Herrmann, 2010a, Nonequispaced curvelet transform for seismic data reconstruction: A sparsity-promoting approach: Geophysics, **75**, WB203–WB210. → pages 8

———, 2010b, Nonequispaced curvelet transform for seismic data reconstruction: a sparsity-promoting approach: Geophysics, **75**, WB203–WB210. → pages 53, 56, 57

Hennenfent, G., and F. J. Herrmann, 2006, Seismic denoising with non-uniformly sampled curvelets: Computing in Science and Engineering, **8**, 16–25. → pages 53, 56

———, 2008, Simply denoise: wavefield reconstruction via jittered undersampling: Geophysics, **73**, V19–V28. → pages 4, 9, 15, 27, 51, 56, 76, 79

Herrmann, F. J., 2010, Randomized sampling and sparsity: Getting more information from fewer samples: Geophysics, **75**, WB173–WB187. → pages 4, 8, 9, 15, 32, 75, 76, 79

Herrmann, F. J., and G. Hennenfent, 2008, Non-parametric seismic data recovery with curvelet frames: Geophysical Journal International, **173**, 233–248. → pages 17

Herrmann, F. J., and X. Li, 2012, Efficient least-squares imaging with sparsity promotion and compressive sensing: Geophysical Prospecting, **60**, 696–712. → pages 13, 40, 105

Herrmann, F. J., P. Moghaddam, and C. C. Stolk, 2008, Sparsity-and continuity-promoting seismic image recovery with curvelet frames: Applied and Computational Harmonic Analysis, **24**, 150–173. → pages 8, 17

Hicks, E., H. Hoeber, G. Poole, and B. King, 2014, An efficient 4d processing flow for variable-depth streamer data: The Leading Edge, **33**, 172–180. → pages 75

Houck, R. T., 2007, Time-lapse seismic repeatability—how much is enough?: The Leading Edge, **26**, 828–834. → pages 80

Johnston, D. H., 2013, Practical applications of time-lapse seismic data: Society of Exploration Geophysicists. → pages 5

Kamei, R., and D. Lumley, 2017, Full waveform inversion of repeating seismic events to estimate time-lapse velocity changes: Geophysical Journal International, **209**, 1239–1264. → pages 16, 40, 96

Koster, K., P. Gabriels, M. Hartung, J. Verbeek, G. Deinum, and R. Staples, 2000, Time-lapse seismic surveys in the north sea and their business impact: The Leading Edge, **19**, 286–293. → pages 1, 15

Kragh, E., and P. Christie, 2002, Seismic repeatability, normalized rms, and predictability: The Leading Edge, **21**, 640–647. → pages 16, 33, 75, 81

Kumar, R., H. Wason, and F. J. Herrmann, 2015, Source separation for simultaneous towed-streamer marine acquisition — a compressed sensing approach: Geophysics, **80**, WD73–WD88. → pages 42

Kunis, S., 2006, Nonequispaced FFT: generalisation and inversion: PhD thesis, Lübeck University. → pages 53, 56

Landrø, M., 1999, Repeatability issues of 3-d vsp data: Geophysics, **64**, 1673–1679. → pages 5, 88

———, 2001, Discrimination between pressure and fluid saturation changes from time-lapse seismic data: Geophysics, **66**, 836–844. → pages 16, 43

———, 2008, The effect of noise generated by previous shots on seismic reflection data: Geophysics, **73**, Q9–Q17. → pages 5

Li, C., C. C. Mosher, and S. T. Kaplan, 2012a, Interpolated compressive sensing for seismic data reconstruction: SEG Technical Program Expanded Abstracts, 1–6. → pages 52

Li, X., 2015, A weighted ℓ_1-minimization for distributed compressive sensing: Master's thesis, The University of British Columbia, Vancouver. ((MSc)). → pages 20, 106, 107

Li, X., A. Y. Aravkin, T. van Leeuwen, and F. J. Herrmann, 2012b, Fast randomized full-waveform inversion with compressive sensing: Geophysics, **77**, A13–A17. → pages 13, 97, 98, 99

Lumley, D., 2010, 4d seismic monitoring of co 2 sequestration: The Leading Edge, **29**, 150–155. → pages 1, 15

Lumley, D., D. C. Adams, M. Meadows, S. Cole, and R. Wright, 2003, 4d seismic data processing issues and examples, *in* SEG Technical Program Expanded Abstracts 2003: Society of Exploration Geophysicists, 1394–1397. → pages 5

Lumley, D., and R. Behrens, 1998, Practical issues of 4d seismic reservoir monitoring: What an engineer needs to know: SPE Reservoir Evaluation & Engineering, **1**, 528–538. → pages 15, 42, 88

Lumley, D. E., 2001, Time-lapse seismic reservoir monitoring: Geophysics, **66**, 50–53. → pages 1, 15, 16, 96

Lumley, D. E., R. A. Behrens, and Z. Wang, 1997, Assessing the technical risk of a 4-d seismic project: The Leading Edge, **16**, 1287–1292. → pages 5, 96

Maharramov, M., and B. Biondi, 2014, Robust joint full-waveform inversion of time-lapse seismic data sets with total-variation regularization: arXiv preprint arXiv:1408.0645. → pages 40, 96

Maharramov, M., B. L. Biondi, and M. A. Meadows, 2016, Time-lapse inverse theory with applications: Geophysics. → pages 16, 40, 96

Mallat, S., 2008, A wavelet tour of signal processing: the sparse way: Academic press. → pages 50

Mansour, H., F. J. Herrmann, and O. Yilmaz, 2013, Improved wavefield reconstruction from randomized sampling via weighted one-norm minimization: Geophysics, **78**, V193–V206. → pages 63, 72

Mansour, H., H. Wason, T. T. Lin, and F. J. Herrmann, 2012, Randomized marine acquisition with compressive sampling matrices: Geophysical Prospecting, **60**, 648–662. → pages 4, 6, 8, 9, 15, 17, 42, 49, 76, 77, 79

Misaghi, A., M. Landrø, and S. A. Petersen, 2007, Overburden complexity and repeatability of seismic data: Impacts of positioning errors at the oseberg field, north sea: Geophysical prospecting, **55**, 365–379. → pages 107

Moldoveanu, N., L. Combee, P. Van Baaren, D. Addessi, and L. Stubbington, 1996, Repeatability of the seismic experiments for 4d seismic in transition zone surveys, *in* SEG Technical Program Expanded Abstracts 1996: Society of Exploration Geophysicists, 5–8. → pages 5

Moldoveanu, N., et al., 2010, Random sampling: A new strategy for marine acquisition: Presented at the 2010 SEG Annual Meeting, Society of Exploration Geophysicists. → pages 5

Moldoveanu, N., and J. Quigley, 2011, Random sampling for seismic acquisition: Presented at the 73rd EAGE Conference & Exhibition. → pages 42

Mosher, C., C. Li, L. Morley, Y. Ji, F. Janiszewski, R. Olson, and J. Brewer, 2014, Increasing the efficiency of seismic data acquisition via compressive sensing: The Leading Edge, **33**, 386–391. → pages 4, 5, 6, 8, 15, 17, 30, 39, 42, 43, 59, 63, 72, 75, 76, 103, 105

Oghenekohwo, F., E. Esser, and F. Herrmann, 2014a, Time-lapse seismic without repetition-reaping the benefits from randomized sampling and joint recovery: Presented at the 76th EAGE Conference and Exhibition 2014. → pages 97

Oghenekohwo, F., E. Esser, and F. J. Herrmann, 2014b, Time-lapse seismic without repetition: reaping the benefits from randomized sampling and joint recovery: Presented at the EAGE, UBC, UBC. → pages 88, 89

Oghenekohwo, F., R. Kumar, E. Esser, and F. J. Herrmann, 2015, Using common information in compressive time-lapse full-waveform inversion: Presented at the 77th EAGE Conference and Exhibition 2015. → pages 16, 40

Oghenekohwo, F., H. Wason, E. Esser, and F. J. Herrmann, 2017, Low-cost time-lapse seismic with distributed Compressive Sensing——part 1: Exploiting common information among the vintages: Geophysics, **82**, P1–P13. → pages 75, 78, 80, 84

Porter-Hirsche, J., and K. Hirsche, 1998, Repeatability study of land data aquisition and processing for time lapse seismic. → pages 15, 88

Potts, D., G. Steidl, and M. Tasche, 2001, Modern Sampling Theory: Mathematics and Applications: 249–274. → pages 53, 56

Qu, S., and D. Verschuur, 2016, Simultaneous time-lapse imaging via joint migration and inversion: Presented at the 78th EAGE Conference and Exhibition 2016. → pages 107

Queißer, M., and S. C. Singh, 2013, Full waveform inversion in the time lapse mode applied to co2 storage at sleipner: Geophysical Prospecting, **61**, 537–555. → pages 96

Raknes, E. B., W. Weibull, B. Arntsen, et al., 2013, Time-lapse full waveform inversion: Synthetic and real data examples: Presented at the 2013 SEG Annual Meeting, Society of Exploration Geophysicists. → pages 96

Rickett, J., and D. Lumley, 2001, Cross-equalization data processing for time-lapse seismic reservoir monitoring: A case study from the gulf of mexico: Geophysics, **66**, 1015–1025. → pages 15, 72, 75, 88

Roach, L. A., D. White*, and B. Roberts, 2014, An assessment of the time-lapse seismic repeatability using a permanent array for reservoir monitoring at the aquistore co2 storage site, saskatchewan, canada, *in* SEG Technical Program Expanded Abstracts 2014: Society of Exploration Geophysicists, 4924–4929. → pages 5

Ross, C. P., and M. S. Altan, 1997, Time-lapse seismic monitoring: Some shortcomings in nonuniform processing: The Leading Edge, **16**, 931–937. → pages 5, 15

Ross, C. P., S. Altan, et al., 1997, Time-lapse seismic monitoring: Repeatability processing tests: Presented at the Offshore Technology Conference, Offshore Technology Conference. → pages 80

Schisselé, E., E. Forgues, J. Echappé, J. Meunier, O. De Pellegars, and C. Hubans, 2009, Seismic repeatability–is there a limit?: Presented at the 71st EAGE Conference & Exhibition. → pages 75

Schonewille, M., A. Klaedtke, A. Vigner, J. Brittan, and T. Martin, 2009, Seismic data regularization with the anti-alias anti-leakage fourier transform: First Break, **27**. → pages 17

Shragge, J., and D. Lumley, 2013, Time-lapse wave-equation migration velocity analysis: Geophysics, **78**, S69–S79. → pages 96

Shulakova, V., R. Pevzner, J. Christian Dupuis, M. Urosevic, K. Tertyshnikov, D. E. Lumley, and B. Gurevich, 2015, Burying receivers for improved time-lapse seismic repeatability: Co2crc otway field experiment: Geophysical Prospecting, **63**, 55–69. → pages 5

Spetzler, J., and Ø. Kvam, 2006, Discrimination between phase and amplitude attributes in time-lapse seismic streamer data: Geophysics, **71**, O9–O19. → pages 16, 43

Symes, W. W., 2010, IWAVE: a framework for wave simulation. → pages 26, 61, 68

Tegtmeier-Last, S., and G. Hennenfent, 2013, System and method for processing 4D seismic data. (US Patent App. 13/804,029). → pages 15, 72

Tu, N., and F. J. Herrmann, 2015, Fast imaging with surface-related multiples by sparse inversion: Geophysical Journal International, **201**, 304–317. → pages 13, 105

Tu, N., T. T. Lin, and F. J. Herrmann, 2011, Sparsity-promoting migration with surface-related multiples: Presented at the EAGE, EAGE, EAGE. → pages 40

Van Den Berg, E., and M. P. Friedlander, 2008, Probing the pareto frontier for basis pursuit solutions: SIAM Journal on Scientific Computing, **31**, 890–912. → pages 17

Virieux, J., and S. Operto, 2009, An overview of full-waveform inversion in exploration geophysics: Geophysics, **74**, WCC1–WCC26. → pages 13, 96

Wang, D., R. Saab, Ö. Yilmaz, and F. J. Herrmann, 2008, Bayesian wavefield separation by transform-domain sparsity promotion: Geophysics, **73**, A33–A38. → pages 33

Wason, H., and F. J. Herrmann, 2013, Time-jittered ocean bottom seismic acquisition: SEG Technical Program Expanded Abstracts, 1–6. → pages 4, 6, 8, 15, 16, 17, 26, 42, 49, 75, 76, 77, 82, 90

Wason, H., F. Oghenekohwo, and F. J. Herrmann, 2015, Compressed sensing in 4-d marine-recovery of dense time-lapse data from subsampled data without repetition: Presented at the 77th EAGE Conference and Exhibition 2015. → pages 17

———, 2017, Low-cost time-lapse seismic with distributed Compressive Sensing—part 2: Impact on repeatability: Geophysics, **82**, P15–P30. → pages x, xiv, 7, 75, 78, 80, 84

Wason, H., F. Oghenekohwo, F. J. Herrmann, et al., 2014, Randomization and repeatability in time-lapse marine acquisition: Presented at the 2014 SEG Annual Meeting, Society of Exploration Geophysicists. → pages 97

White, D. J., L. A. Roach, and B. Roberts, 2015, Time-lapse seismic performance of a sparse permanent array: Experience from the aquistore co2 storage site: Geophysics, **80**, WA35–WA48. → pages 5

Xiong, Z., A. D. Liveris, and S. Cheng, 2004, Distributed source coding for sensor networks: Signal Processing Magazine, IEEE, **21**, 80–94. → pages 18

Xu, S., Y. Zhang, D. Pham, and G. Lambaré, 2005a, Antileakage fourier transform for seismic data regularization: Geophysics, **70**, V87–V95. → pages 17

———, 2005b, Antileakage Fourier transform for seismic data regularization: Geophysics, **70**, V87 – V95. → pages 56

Yang, D., A. Malcolm, M. Fehler, and L. Huang, 2014, Time-lapse walkaway vertical seismic profile monitoring for co2 injection at the sacroc enhanced oil recovery field: A case study: Geophysics. → pages 16, 40, 96

Yang, D., M. Meadows, P. Inderwiesen, J. Landa, A. Malcolm, and M. Fehler, 2015, Double-difference waveform inversion: Feasibility and robustness study with pressure data: Geophysics, **80**, M129–M141. → pages 16, 40, 96